GENETIC AND MOLECULAR ANALYSES OF TURKISH PATIENTS WITH PELIZAEUS-MERZBACHER DISEASE

by

Birdal Bilir

B.S., Molecular Biology and Genetics, Boğaziçi University, 1999

M.S., Molecular Biology and Genetics, Boğaziçi University, 2001

Submitted to the Institute for Graduate Studies in
Science and Engineering in partial fulfillment of
the requirements for the degree of
Doctor of Philosophy

Graduate Program in Molecular Biology and Genetics

Boğaziçi University

2007

To my beloved family

ACKNOWLEDGMENTS

The research presented in this thesis was carried out at the Department of Molecular Biology and Genetics at Boğaziçi University, except the part of *in vitro* studies which was performed at the Center for Molecular Medicine and Genetics at Wayne State University School of Medicine, Detroit, Michigan. This work was supported by Boğaziçi University Scientific Research Fund and TÜBİTAK-BİDEB.

I would like to express my sincere gratitude to my thesis supervisor Dr. Esra Battaloğlu for her invaluable guidance, strong encouragement and crucial criticisms throughout my studies.

My appreciation is also extended to the members of my thesis committee, Dr. A. Nazlı Başak, Dr. Kuyaş Buğra, Dr. Nihan Ünaltuna and Dr. Zuhal Yapıcı, for allocating their time to evaluate this work.

I would like to thank Dr. Zuhal Yapıcı and Dr. Cengiz Yalçınkaya at İstanbul University, İstanbul University Medical School and Cerrahpaşa Medical Faculty, Department of Neurology for clinical evaluation of the patients included in this study, and for providing the blood samples.

I am very grateful to Dr. Alexander Gow and Dr. Garbern for giving me the chance of working at their lab at Wayne State University School of Medicine. I would also like to express my special thanks to Dr. Ömer Küçük and Hüseyin Akbay for their valuable friendship and help during my stay in Detroit.

I would like to thank the academic staff of the Department of Molecular Biology and Genetics at Boğaziçi University for improving my knowledge.

I would like to extend my thanks to all my dear friends for their precious friendship, support and help, among whom I would like to mention especially Sibel Aylin Uğur,

İbrahim Barış, Cihan Erkut, Rezan Fahrioğlu, Demet Candaş, Kader Çavuşoğlu, İnanç Fidancı, Özlem Yalçın, Renin Hazan, Yeşim Özmen, Ergül Berber and Elif Çağlar.

I am grateful to my beloved mother, father and brothers for their endless love, support and patience.

ABSTRACT

GENETIC AND MOLECULAR ANALYSES OF TURKISH PATIENTS WITH PELIZAEUS-MERZBACHER DISEASE

Pelizaeus-Merzbacher disease (PMD) is a type of leukodystrophy, affecting the formation of the myelin sheath in the central nervous system. PMD is a rare inherited disorder with X-linked recessive segregation, mostly affecting males. The clinical severity and age of onset vary widely among the PMD patients, but common characteristics include nystagmus, ataxia, stridor, spasticity, and mental retardation. About 80 per cent of patients, clinically diagnosed as PMD, have been associated with mutations of the proteolipid protein 1 (*PLP1*) gene on chromosome Xq21.3-Xq22, encoding two proteins, PLP1 and DM20, expressed abundantly in oligodendrocytes. Mutations in the gap junction protein α12 (*GJA12*) gene on chromosome 1q41-42 are responsible for at least some of the PMD cases with autosomal recessive inheritance which are known to be associated with Pelizaeus-Merzbacher-like disease (PMLD).

In the framework of this study, the molecular basis of PMD was investigated in a cohort of 21 Turkish families with PMD. Linkage analysis excluded the *PLP1* locus in three familial cases. In total, pathogenic mutations were identified in 57 per cent of the families, 19 per cent of which were due to *PLP1* duplications, and nine and 29 per cent were due to mutations in the *PLP1* and *GJA12* genes, respectively. The distribution of the mutations associated with the PMD phenotype in our cohort of patients were different from those reported in the literature, which may result due to the high frequency of consanguinity and autosomal recessive cases in our population. Absence of mutations in *PLP1* or *GJA12* genes in 43 per cent of the cases analyzed suggests presence of further genetic heterogeneity in PMD. In order to characterize the effects of two *PLP1* mutations identified in our cohort, *in vitro* immunocytochemical assays were performed. Accumulation of mutant proteins in the endoplasmic reticulum, leading to unfolded protein response (UPR) activation and subsequent apoptosis were observed for the mutant

proteins. However, one of the mutations showed a different pattern of localization for DM20 isoform. Since patients present similar clinical features, the results implicate that PLP1 and DM20 may have different roles in myelin.

ÖZET

TÜRK PELIZAEUS-MERZBACHER HASTALARINDA GENETİK VE MOLEKÜLER ANALİZLER

Pelizaeus-Merzbacher hastalığı (PMD) merkezi sinir sistemi miyelin kılıfının oluşumunu etkileyen bir tür lökodistrofidir. PMD, X kromozomuna bağlı ve çekinik seyreden, çoğunlukla erkekleri etkileyen ender rastlanan kalıtsal bir hastalıktır. Klinik şiddet ve başlama yaşı geniş ölçüde değişkenlik göstermektedir, ancak sıklıkla rastlanan özellikleri arasında nistagmus, ataksi, nefes alma bozukluğu, spastizm ve zihinsel gerilik bulunmaktadır. Klinik olarak PMD teşhis edilen hastaların yaklaşık yüzde 80'i kromozom Xq21.3-Xq22 bölgesinde bulunan, oligodentrositlerde bol miktarda anlatılan proteolipid protein 1 (PLP1) ve DM20 proteinlerini kodlayan, PLP1 geninin mutasyonlarıyla ilişkilendirilmiştir. Kromozom 1q41-42 bölgesindeki ara bağlantı proteini α12 (*GJA12*) geninin mutasyonları Pelizaeus-Merzbacher-benzeri hastalık (PMLD) diye adlandırılan ve otozomal çekinik geçiş gösteren PMD olgularının en az birkaçından sorumludur.

Bu çalışma çerçevesinde, 21 Türk PMD ailesinde hastalığın moleküler temeli araştırılmıştır. Bağlantı analizi üç ailesel olguda *PLP1* gen bölgesini dışlamıştır. Patojenik mutasyonlar ailelerin yüzde 57'sinde belirlenmiştir, bunların yüzde 19'u *PLP1* duplikasyonlarından, yüzde 9 ve 29'u da, sırasıyla, *PLP1* ve *GJA12* gen mutasyonlarından kaynaklanmaktadır. Hasta grubumuzda PMD fenotipiyle ilişkilendirilmiş mutasyonların dağılımı literatürde rapor edilmiş olanlardan farklıdır. Toplumumuzda akraba evliliğinin ve otozomal çekinik olguların sık olması nedeniyle bu farklılığın ortaya çıktığı düşünülmektedir. Analiz edilen hastaların yüzde 43'ünde *PLP1* ve *GJA12* gen mutasyonlarının bulunmaması PMD'de bilinenden daha fazla genetik heterojenliğin varolduğunu göstermektedir. Hastalarımızda belirlenen iki *PLP1* mutasyonunun etkilerini tanımlamak amacıyla *in vitro* deney ortamında immünositokimyasal analizler yapılmıştır. Mutant proteinlerin endoplazmik retikulumda biriktiği ve katlanmamış protein yanıtı (UPR) yolağını, ardından hücre ölümünü tetiklediği gözlenmiştir. Ancak, mutasyonlardan

biri için protein izoformu DM20'nin endoplazmik retikulumda birikmediği belirlenmiştir. Buna rağmen, hastaların klinik özellikleri arasında bir fark görülmemiştir. Sonuçlar, PLP1 ve DM20 proteinlerinin miyelinde farklı görevlerinin olabileceğini düşündürmüştür.

TABLE OF CONTENTS

LIST OF FIGURES

LIST OF TABLES

LIST OF SYMBOLS / ABBREVIATIONS

APS	Ammoniumpersulfate
ASK1	Apoptosis-Signaling Kinase 1
ATF 6	Activating Transcription Factor 6
ATP	Adenosine Triphosphate
CHOP	CCAAT/Enhancer-Binding-Protein Homologous Protein
CMT1A	Charcot-Marie-Tooth disease type 1A
CNS	Central Nervous System
Cx47	Connexin 47
DAPI	4,6-diamidino-2-phenylindole
DMEM	Dulbecco's Modification of Eagle's Medium
DMSO	Dimethyl Sulfoxide
DNA	Deoxyribonucleic Acid
dNTP	Deoxyribonucleosidetriphosphates
EDTA	Diaminoethanetetraacetic Acid
eIF2α	Eukaryotic Translation Initiation Factor 2 alpha
ERSEI	Endoplasmic Reticulum Stress Response Elements
EtBr	Ethidium Bromide
FISH	Fluorescence *in situ* Hybridization
FITC	Flourescein Isothiocyanate
GJA12	Gap Junction Protein alpha 12
IPTG	Isopropyl β-D-1-thiogalactopyranoside
IRE 1	Inositol-Requiring Enzyme 1
JNK	Jun NH2-Terminal Kinase
LB	Luria Broth
LCR	Low-Copy Repeats
MRI	Magnetic Resonance Imaging
NAHR	Non-Allelic Homologous Recombination
OD	Optical Density
PBS	Phosphate Buffered Saline
PCR	Polymerase Chain Reaction

PERK	Pancreatic Endoplasmic Reticulum Kinase
PFA	Paraformaldehyde
PLP1	Proteolipid Protein 1
PMD	Pelizaeus-Merzbacher Disease
PMLD	Pelizaeus-Merzbacher-Like Disease
RBC	Red Blood Cell
RFLP	Restriction Fragment Length Polymorphisms
RNA	Ribonucleic Acid
RNase	Ribonuclease
S1P	Site-1 Protease
S2P	Site-2 Protease
SDS	Sodiumdodecylsulphate
SPG2	Spastic Paraplegia Type 2
TBS	Tris Buffered Saline
TEMED	N,N,N',N'-Tetramethylethylenediamine
TRAF2	Tumor-Necrosis-Factor-Receptor-Associated Factor 2
UPR	Unfolded Protein Response
UPRE	UPR Element

1. INTRODUCTION

1.1. Pelizaeus-Merzbacher Disease

Pelizaeus-Merzbacher disease (PMD) is one of a class of inherited neurological diseases known as leukodystrophies, disorders that affect the formation of the myelin sheath on axons in the central nervous system (CNS) (Berger *et al*., 2001).

1.1.1. Historical Background

In 1885, a German physician, Friedrich Pelizaeus, described a family with five patients who manifested the development in early infancy of involuntary oscillatory eye movement, spasticity in the limbs, very limited head and trunk control, and delay in cognitive development (Pelizaeus, 1885). He observed that all patients were males and sons of healthy sisters, and cited a quotation from the family that "the disease is passed on by the mother but does not hurt her". In 1910, another German pathologist, Ludwig Merzbacher, re-examined the same family, which by then had 14 affected individuals including two girls, although he at first did not realize that these cases belonged to the previously reported family (Merzbacher, 1910). He performed a detailed brain autopsy on one of the affected males and confirmed the widespread lack of myelin staining in the central white matter, as predicted by Pelizaeus. The description of this family provides the first clinical, genetic, and pathological characterization of PMD: a rare X-linked dysmyelinating disorder of the CNS.

1.1.2. Clinical and Neuropathological Characteristics

In the following 100 years, new PMD cases have been described and resulted in the accumulation of clinical and pathological findings. The prevalence of PMD in the United States is estimated to be about 1/200,000 to 1/500,000 (Garbern *et al*., 2006). In a survey of leukodystrophies in Germany, the incidence of PMD was about 0.13 per 100,000 live births (Heim *et al*., 1997).

Clinically, PMD usually begins during infancy and signs of the disease may be present at birth or in the first few weeks of life (Boulloche and Aicardi, 1986; Hodes *et al*., 1993; Cailloux *et al*., 2000). The first recognizable sign is a form of involuntary movement of the eyes called nystagmus. The eye movements can be circular, as if the child is looking around the edge of a large circle, or horizontal to-and-fro movements. The nystagmus tends to improve with age. Some infants have stridor (labored and noisy breathing). They may show hypotonia (lack of muscle tone; floppiness) initially, but most develop spasticity (a type of increased muscle tone or stiffness of the muscles and joints) over several years. Motor and intellectual functions are delayed. Most PMD individuals learn to understand speech, but verbal output can vary from normal speech to almost complete mutism. Head and trunk control may be a problem and tremor of the upper body (titubation) when sitting is common. Trouble with coordination (ataxia) is also common. Vision is usually reduced to some degree.

The common pathological features of PMD include lack or reduction of myelin sheaths in large areas of the white matter, which is usually prominent in the lateral periventricular regions than in the subcortical regions and well-conserved structure of neurons and their axons (Seitelberger, 1970; Seitelberger, 1995). Typically, the brain is shrunken, particularly in the cerebellum and brain stem, and the white matter is atrophic and sclerotic. The diffuse hypomyelination of the CNS is associated with a reduced number of oligodendrocytes; specialized glial cells that form myelin in the CNS. Neurophysiological and magnetic resonance imaging (MRI) studies have provided evidence that the dysmyelinating process is limited to the CNS (Boulloche and Aicardi, 1986).

1.1.3. Subtypes

The clinical severity, age of onset, and rate of progression in PMD vary widely, primarily depending on the nature of the causative mutation and additionally upon other genetic and environmental influences. Based on both clinical and pathological criteria, PMD is classified into three subtypes: classic, transitional and connatal forms, in order of increasing severity (Table 1.1) (Seitelberger, 1970).

Table 1.1. Clinical spectrum of PMD symptoms.

Phenotype	Connatal PMD	Classic PMD	SPG2
Age of onset	Neonatal	Year 1	Year 1-5
Age of death	Childhood to 3rd decade	3rd-7th decade	Normal
Nystagmus	Present	Present	Often present
Hypotonia	Present	Initially present	Absent
Ataxia	Present	Titubation	Present
Spasticity	Severe	Spastic quadriparesis	Spastic gait
Other neurological signs	Stridor Pharyngeal weakness Seizures	Dystonia Athetosis	Spastic urinary bladder
Cognition	Impaired	Impaired	Normal
Ambulation	Absent	Partial	Present
Speech	Absent	Present	Present

Classic PMD is the most common form of the disease. The presentation of the disease is of infantile-onset typically within the first two to six months of life, nystagmus, hypotonia and titubation, followed by development of ataxia and spasticity. Occasionally, a child can walk, although movement is impaired by weakness and spasticity. Walking ability is usually lost by adolescence or earlier. Language ability can be mildly to moderately impaired, and some cognitive delay is usual. These patients may survive to the sixth decade of life or longer. Histochemical staining of the white matter in these patients is non-uniform and typically has areas of relatively preserved myelin staining, giving the white matter a tigroid (patchy) appearance.

Connatal PMD is the less frequent and most severe form of the disease with nystagmus present from birth or within the first few weeks of life. Patients typically have hypotonia, pharyngeal weakness, stridor and seizures. As they age, severe spasticity usually replaces the hypotonia. They have poor head control, do not sit without support, and are unable to walk. Growth is poor; developmental milestones are significantly delayed or never achieved. Verbal expression is severely limited, but comprehension may be significant. They usually die during infancy or childhood. Neuropathological examinations reveal total lack of myelin.

Transitional PMD shows clinical severity intermediate between connatal and classic forms. The onset of the phenotype is soon after the neonatal period. Death of the patients with this form of the disease is usually between five to 10 years of age.

X-linked spastic paraplegia type 2 (SPG2), which is an allelic form of PMD, shares clinical features of PMD but has a later onset and milder phenotype (Saugier-Veber *et al*., 1994). Individuals with SPG2 present childhood-onset spastic paraplegia, mild cognitive impairment, and ataxia. Survival to the sixth decade or later is characteristic. Typically, neurological signs progress gradually.

1.2. Myelin in CNS

The efficient conduction of action potentials in the vertebrate nervous system is dependent on the myelin sheath. Myelin is a spiral structure constituted of extensions of the plasma membrane of the myelinating glial cells, the oligodendrocytes in the CNS (Figure 1.1) (Bunge *et al*., 1962; Peters, 1964). These cells send out extensions of their cytoplasmic membrane, each of which forms a segment of sheathing around an axon (Baumann and Pham-Dinh, 2001; Morell *et al*., 1994; Peters *et al*., 1991; Pham-Dinh, 1998). Myelin is the essential constituent of white matter in the CNS which contains about 40-50 per cent myelin on dry weight basis. It is a poorly hydrated structure containing 40 per cent water in contrast to gray matter (80 per cent). Myelin dry weight consists of 70 per cent lipids and 30 per cent proteins. The insulating properties of the myelin sheath, which favor fast nerve conduction velocity, are largely due to its structure, its thickness, its low water content and its richness in lipids.

Several structural features characterize myelin (Figure 1.1). The major dense line forms as the cytoplasmic surfaces of the expanding myelinating processes of the oligodendrocytes are brought into close apposition. The fused two outer leaflets (extracellular apposition) form intraperiodic lines (minor dense lines). The periodicity of the lamellae is 12 nm. Each myelin sheath segment or internode appears to be 150-200 μm in length (Butt and Ransom, 1989). Internodes are separated by the nodes of Ranvier, spaces where myelin is lacking (Bunge, 1968). The nodes of Ranvier play a major role in nerve impulse conduction; they allow the saltatory conduction, by which the impulse

jumps from node to node, rather than progressing slowly along the axon. In addition to the conduction of nerve impulses, the myelin sheath has also roles in clustering of voltage-gated sodium channels at the nodes of Ranvier during axogenesis, axonal development and maintenance, but also inhibition of axonal growth and regeneration (Sanchez *et al*., 1996; Klugmann *et al*., 1997; Blight, 1998; Bandtlow and Schwab, 2000).

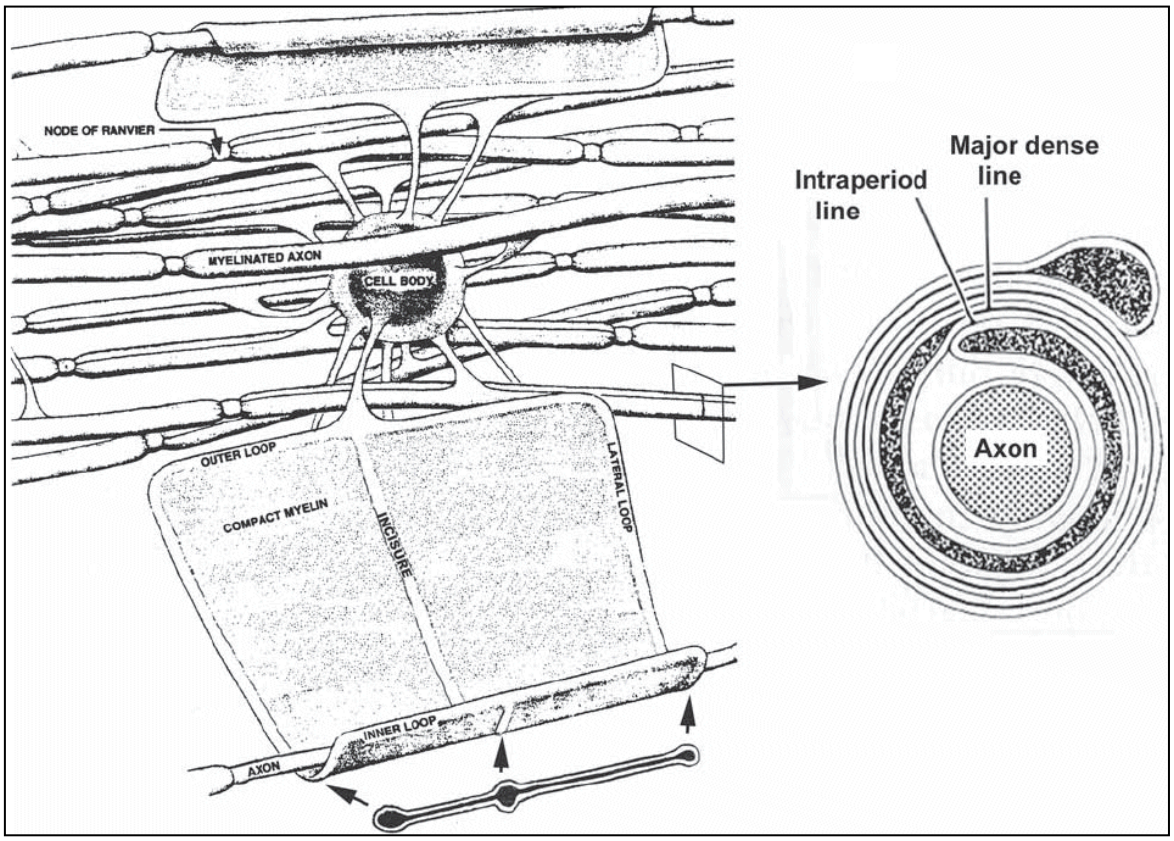

Figure 1.1. CNS myelin (Garbern, 2007).

During the development of CNS, oligodendrocyte precursors originate from neuroepithelial cells of the ventricular zones, at very early stages during embryonic life (Curtis *et al*., 1988; Hardy and Reynolds, 1991). The sequential expression of developmental markers divides the lineage into distinct phenotypic stages which are characterized by proliferative capacities, migratory abilities and changes in morphology (Figure 1.2) (Lubetzki *et al*., 1997). Myelination requires an extraordinary capacity for oligodendrocytes to synthesize membranes at a given time, specific for a species and a region of the CNS. A single oligodendrocyte can myelinate up to about 50 separate axonal segments, synthesizing about 1000-fold more membrane than its perikaryal surface area (Pfeiffer *et al*., 1993).

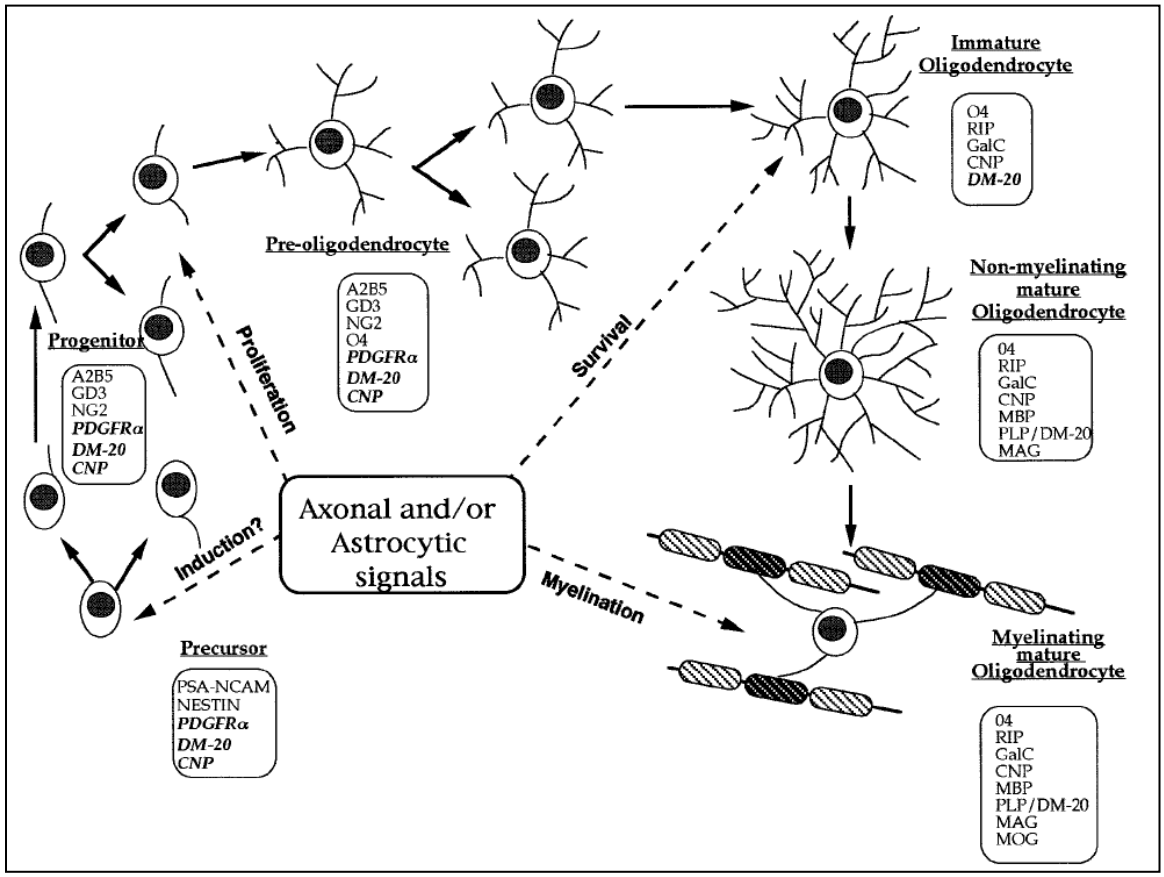

Figure 1.2. Schematic representation of the developmental stages of oligodendrocyte lineage (Lubetzki *et al*., 1997).

1.3. Genetics of PMD

Reconsideration of the original descriptions of PMD by Zeman *et al*. (1964) as well as Boulloche and Aicardi (1986) incorporated the genetic, clinical and neuropathological criteria for its diagnosis. This comprehensive approach to the diagnosis of PMD has been critical for the discovery of the gene(s) responsible for the disease.

On the basis of comparison of the gene maps of the human and mouse X chromosomes, PMD was mapped to the middle of the long arm of the human X chromosome (Xq13-Xq22) (Buckle *et al*., 1985). This was the region to which Willard and Riordan (1985) assigned the human proteolipid protein 1 (*PLP1*) gene by Southern blot analysis of somatic cell hybrids using the bovine PLP1 cDNA probe. To localize the *PLP1* gene more precisely, the position of the gene was analyzed by *in situ* hybridization and mapped to Xq22 (Mattei *et al*., 1986). Expression of *PLP1* in the oligodendrocytes,

association of its mutations with PMD phenotype, and X-linked dysmyelinating disease observed in different animal mutants led to the identification of the *PLP1* gene as the causative locus in PMD (Campagnoni and Macklin, 1988; Hudson and Nadon, 1992).

1.3.1. *PLP1* Gene

The *PLP1* gene is present as a single copy in the genome, located on the X chromosome (Milner *et al*., 1985; Gardinier *et al*., 1986). It is a member of the lipophilin gene family, whose members encode highly hydrophobic integral membrane proteins exhibiting identical topologies and similar lipid-like physical properties (Gow, 1997). The entire DNA sequence of the *PLP1* gene is known for human, rat, mouse, cow, pig and rabbit (Kronquist *et al*., 1987; Dautigny *et al*., 1985; Sorg *et al*., 1987; Naismith *et al*., 1985; Baumgartner and Brenig, 1996; Tosic *et al*., 1994). The general structure of the gene is quite similar between these species.

Diehl *et al.* (1986) determined that the human *PLP1* gene spans approximately 17 kb in genomic DNA and comprises seven exons (Figure 1.3). The 5' region contains both positive and negative regulatory sequences with multiple sites for nuclear proteins (Nave and Lemke, 1991). Possible TATA and CAAT boxes are found at positions -189 and -331, respectively (Ikenaka *et al*., 1992). It contains two transcription initiation sites and three polyadenylation sites. Regulatory sequences may also be present in the first and the largest intron (Wight and Dobretsova, 1997; Wight *et al*., 1997). The first exon encodes only the initiator methionine, which is removed from the nascent protein. The third exon contains an internal splice donor site, which is 105-bp downstream the 5' splice donor site (Nave *et al*., 1987). Use of this alternative splice site generates a transcript, which encodes a smaller protein lacking 35 amino acids of the full-length protein. PLP1 transcripts are heterogeneous in size not only because of alternative splicing, but also due to the use of multiple transcription initiation and polyadenylation sites.

As for other myelin genes, regulation of the *PLP1* gene expression is primarily at the level of transcription, RNA splicing and mRNA stability although control at subsequent stages also exists. The factors controlling transcriptional regulation are only partly known (Hudson *et al*., 1996, Hudson *et al*., 1997; Montague and Griffiths, 1997). It is very

probable that axon-derived signals are responsible for the up-regulation associated with CNS myelination (Matsuda *et al*., 1997) and axonal contact is necessary to maintain the high level transcriptional activity in the myelinated CNS (McPhilemy *et al*., 1990).

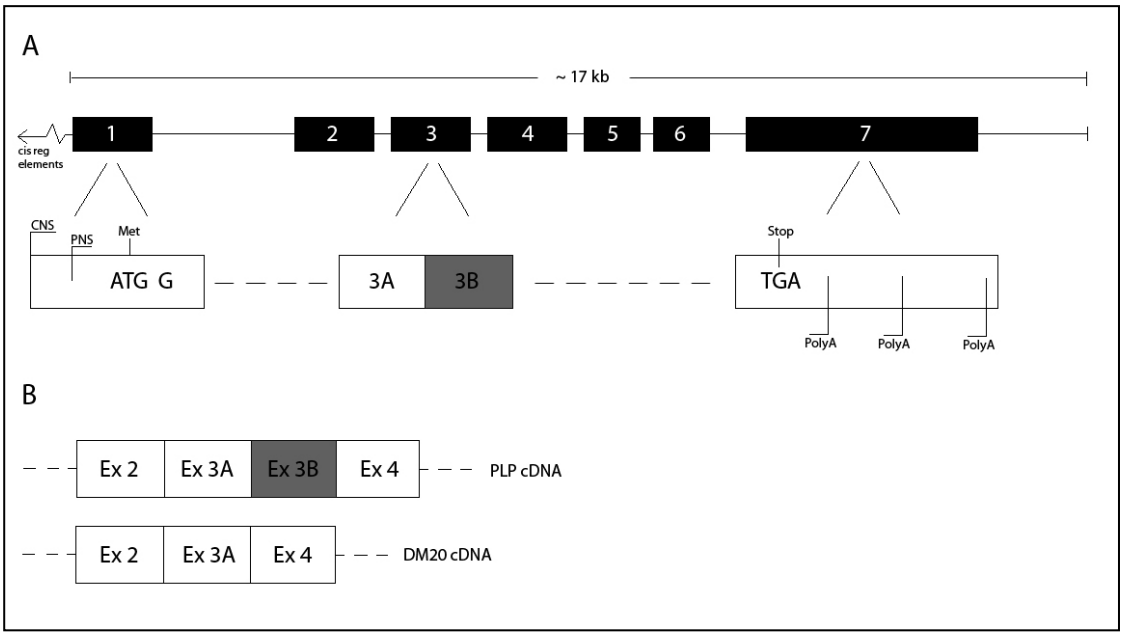

Figure 1.3. Organization of the *PLP1* gene (A) and PLP1 and DM20 transcripts (B) (Griffiths *et al*., 1995).

1.3.2. PLP1 Protein

The *PLP1* gene encodes two alternatively spliced products: PLP1, the major component of CNS myelin, making up about 50 per cent of the protein mass of myelin, and DM20, a minor component of mature myelin (Nave *et al*., 1987; Lees and Bizzozero, 1991). PLP1 (25 kDa) and DM20 (20 kDa) are extremely hydrophobic integral membrane proteins of 276 and 241 amino acids, respectively (Figure 1.4) (Griffiths *et al*., 1998a). The protein sequences of PLP1 and DM20 are remarkably conserved across mammalian species; human, rat and mouse proteins show 100 per cent sequence conservation (Yool *et al*., 2000).

PLP1 and DM20 have four transmembrane domains with the amino- and carboxyl-termini exposed to the cytoplasm (Figure 1.4) (Weimbs and Stoffel, 1992). In addition to the abundance of hydrophobic amino acids, the proteins are also covalently modified by

six fatty acids linked to the cysteine residues via an autocatalytic post-translational mechanism (Bizzozero *et al*., 1987). The fatty acids attached to the intracellular loop of the protein have been proposed to mediate the association of the protein with the adjacent lipid leaflet in compact myelin (Spörkel *et al*., 2002). PLP1 and DM20 are identical except that DM20 lacks a 35-amino acid peptide (residues 116-150) of the cytoplasmic loop that contains two acylation sites. Although DM20 shares transmembrane topology similar to that of PLP1, this difference may account for the altered conformation and physical properties observed for DM20 (Gow *et al*., 1997; Helynck *et al*., 1983; Skalidis *et al*., 1986).

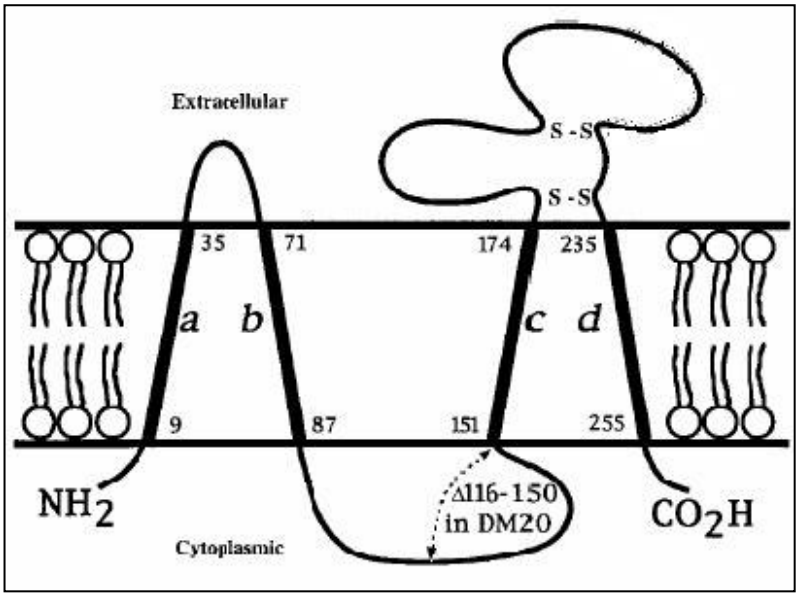

Figure 1.4. Schematic representation of PLP1/DM20 topology in the lipid bilayer (Kitagawa *et al*., 1993).

PLP1 and DM20 proteins are synthesized in the rough endoplasmic reticulum and subsequently transported through the Golgi complex, where the myelin lipid constituents associate with the PLP1 and DM20 in membrane rafts (Gow *et al*., 1997; Simons *et al*., 2000). Raft formation is one of the initial stages of myelin assembly and is followed by the vesicular transport of the protein to the myelin membrane. In addition to its membrane anchoring role, N-terminal fatty acylation also appears to serve as a signal targeting the PLP1 and DM20 proteins to newly synthesized myelin membrane (Schneider *et al*., 2005).

The expression of PLP1 and DM20 is spatially and temporally regulated during development (Campagnoni and Skoff, 2001). The major site of expression in the CNS is the oligodendrocytes for both isoforms of the protein which are located predominantly in the compact myelin sheaths. Outside of the CNS, PLP1 and DM20 are also expressed at a lower level in non-oligodendrocytic cells, including Schwann cells, brainstem neurons, heart, spleen and thymus (Griffiths *et al*., 1995; Campagnoni *et al*., 1992; Pribyl *et al*., 1996). In the CNS, DM20 is the predominant product at early stages of myelination during embryonic stages, but postnatally, PLP1 expression rapidly overtakes that of DM20 and predominates by the peak of myelination (Fujimoto *et al*., 1976; Timsit *et al*., 1995).

Despite the fact that PLP1 was identified more than 50 years ago (Folch and Lees, 1951) no clear physiological function for this protein has been identified. The abundance and location of PLP1 in compact myelin suggests a structural role in the stability and maintenance of the myelin sheath in CNS (Klugmann *et al*., 1997; Boison *et al*., 1995). It is not fully understood whether PLP1 and DM20 have distinct roles. DM20 appears to represent the evolutionary prototype, based upon the finding that three cDNAs cloned from the CNS of shark, DMα, DMβ and DMγ, have considerable homology to DM20 but lacks the cytoplasmic PLP1-specific segment. The addition of highly charged PLP1-specific sequence does not change membrane topology, but resulted in different chemical, cellular and molecular properties of PLP1 that are not present in DM20 (Gow *et al*., 1997). The finding that DM20 alone cannot fully compensate for lack of PLP1 further confirms that the two isoforms are not functionally equivalent (Spörkel *et al*., 2002; Stecca *et al*., 2000). As DM20 is the predominant isoform in oligodendrocyte progenitors, it may play a major role in oligodendrocyte differentiation and survival (Schindler *et al*., 1990; Timsit *et al*., 1992). Functions proposed for PLP1 include myelin compaction, maintenance of myelinated axons, intercellular signaling and cytoplasmic protein/lipid interactions (Shy *et al*., 2003; Boucher *et al*., 2002; Yamaguchi *et al*., 1996; Gudz *et al*., 2002).

1.4. Genetic and Molecular Mechanisms Involved in PMD

About 80 per cent of patients clinically diagnosed with PMD have been shown to carry a mutation in the *PLP1* gene (Garbern and Hobson, 2002). Three different types of mutations have been identified in PMD patients: in declining order of frequency,

duplications, point mutations, and deletions (Figure 1.6). Clinical severity is found to correlate with the nature of the mutation (Cailloux *et al*., 2000). The clinical phenotype for patients with duplications may generally be milder than that of patients with point mutations in the *PLP1* gene, whereas patients with complete deletion of *PLP1* appear to be less severely affected.

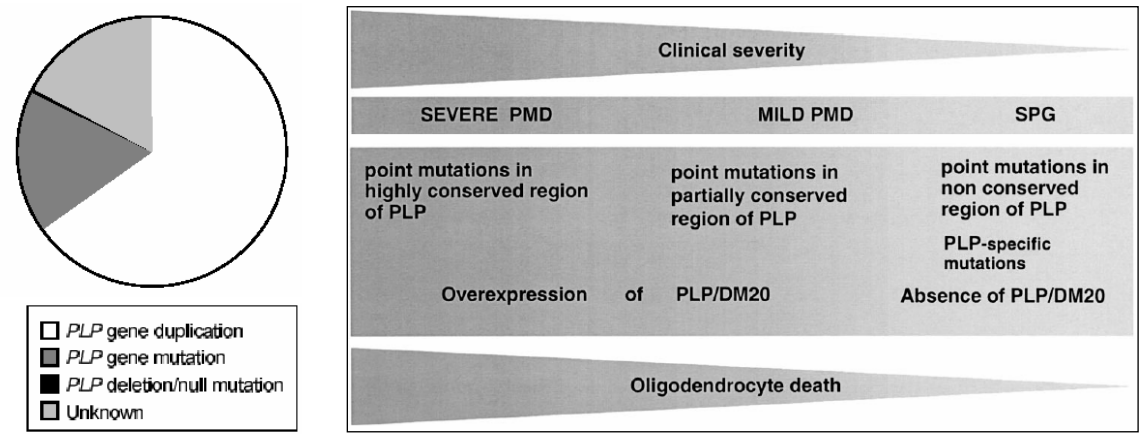

(A) (B)

Figure 1.5. Genetic mechanisms for PMD (A) and genotype-phenotype correlation in PMD (B) (Woodward and Malcolm, 2001; Cailloux *et al*., 2000).

The interactions and stability of the mutated proteins are thought to have a major effect on the severity of the disease. Clinical observations and studies of *PLP1* mutations in animals and cell cultures suggest that there may be at least three distinct molecular mechanisms that cause PMD (Figure 1.6) (Inoue, 2005). (i) Missense and other small mutations in the *PLP1* gene result in the disruption of normal folding. The altered conformation of PLP1/DM20 prevents the transport of the protein through endoplasmic reticulum to the cell membrane. The accumulation of the misfolded proteins induces the unfolded protein response (UPR) pathway, triggering oligodendrocyte cell death by apoptosis (Figure 1.6A). (ii) Overexpression of the *PLP1* gene due to the duplication leads to the accumulation of PLP1 and together with cholesterol and other lipids in the endosome and lysosome compartments, impairing the stoichiometry of myelin constituents (Figure 1.6B). (iii) Deletions of the *PLP1* gene result in the absence of PLP1/DM20. In patients with null mutations, the number of oligodendrocytes is not reduced and myelination occurs normally; however, axon swellings develop. These findings suggest that the lack of

PLP1/DM20 neither induces the UPR nor prevents myelin assembly, but impairs the maintenance of the myelin sheath (Figure 1.6C).

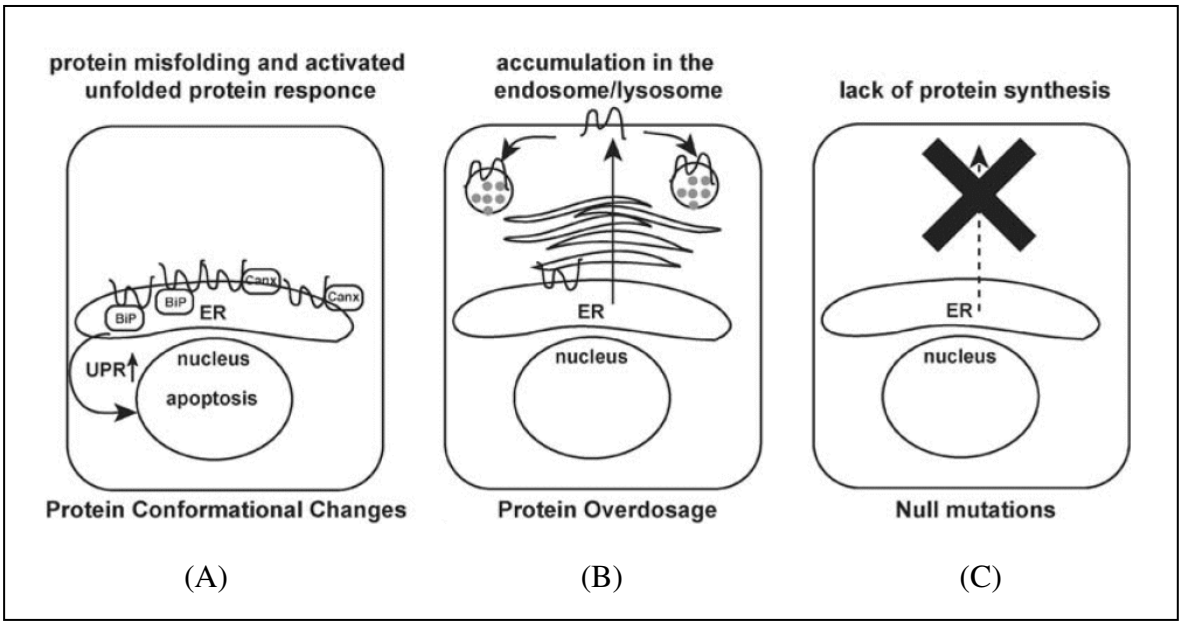

Figure 1.6. Three distinct mutational mechanisms that cause PMD: point and small mutations (A), duplications (B) and deletions (C) of the *PLP1* gene (Inoue, 2005).

1.4.1. Duplication of the *PLP1* Gene

The most common genetic mechanism that causes PMD is the duplication of the region of the X chromosome that contains the entire *PLP1* gene, with the frequency of approximately 60-70 per cent of *PLP1* mutations (Mimault *et al*., 1999). Clinical manifestations vary in severity, but in general, patients with duplication have the classic form of PMD (Inoue *et al*., 1999). A suggestion that increased dosage of *PLP1* may be the mechanism responsible for the clinical phenotype came from the examination of a patient with a large, cytogenetically visible, *de novo* duplication of Xq21-q22 (Cremers *et al*., 1987). The boy showed multiple abnormalities: muscular hypotonia, growth retardation, and a severe disorder of myelination suggestive of PMD at autopsy. Dosage studies showed *PLP1* to be within this large duplicated region (Cremers *et al*., 1988). The finding that the duplication does not interrupt either the coding sequence of the *PLP1* gene or the flanking regions supports the suggestion that increased dosage of the *PLP1* gene, rather than disruption of *PLP1* coding or regulatory regions, may cause PMD (Ellis and Malcolm,

1994). This situation is analogous to the duplication of the peripheral myelin protein 22 (*PMP22*) gene found in the majority of patients with the peripheral neuropathy, Charcot-Marie-Tooth disease type 1A (CMT1A) (Lupski, 1998). Association of increased dosage of *PLP1* with PMD provides the second example of gene duplication for an integral myelin protein leading to destruction of myelin.

The molecular mechanisms underlying the PMD duplication have not yet been elucidated, but appear to be more complex than those observed in the duplications responsible for CMT1A. In PMD patients with *PLP1* duplication, the rearrangement breakpoints are not common, yielding duplicated genomic segments of varying lengths. Molecular studies revealed that the size of the duplicated fragments in PMD varies from 0.3 Mb to >1.8 Mb, containing the entire *PLP1* locus (Woodward *et al*., 1998; Inoue *et al*., 1999). The duplications include other genes in addition to *PLP1*, but it is not known whether these other genes affect the disease phenotype. Inclusion of flanking genes in addition to the *PLP1* and/or disruption of a flanking gene may explain differences in phenotypic severities among patients with the duplication.

Unlike many genomic disorders in which the rearrangements are mediated by non-allelic homologous recombination (NAHR) between flanking low-copy repeats (LCRs), the molecular mechanism underlying *PLP1* duplication events is likely to occur through a coupled homologous and non-homologous recombination mechanism. Analysis of duplication breakpoints suggests that generation of *PLP1* duplications involves repair of a double-stranded break by one-sided homologous strand invasion of a sister chromatid, followed by DNA synthesis and non-homologous end-joining with the other end of the break (Figure 1.7). However, what makes the genomic region surrounding *PLP1* susceptible to rearrangement remains to be elucidated. Rearrangements are typically tandem head-to-tail duplications within Xq22.2, and probably arise during meiosis in the maternal grandfather. Several atypical cases of apparent transposition events have also been described in which an additional copy of the *PLP1* gene has integrated at non-contiguous sites on the X chromosome (Xp22 and Xq26) (Hodes *et al*., 2000; Woodward *et al*., 2003). The mechanism by which these atypical non-tandem duplication events in PMD arise is currently unknown (Woodward *et al*., 1998; Woodward *et al*., 2000; Inoue *et al*., 1999; Mimault *et al*., 1999).

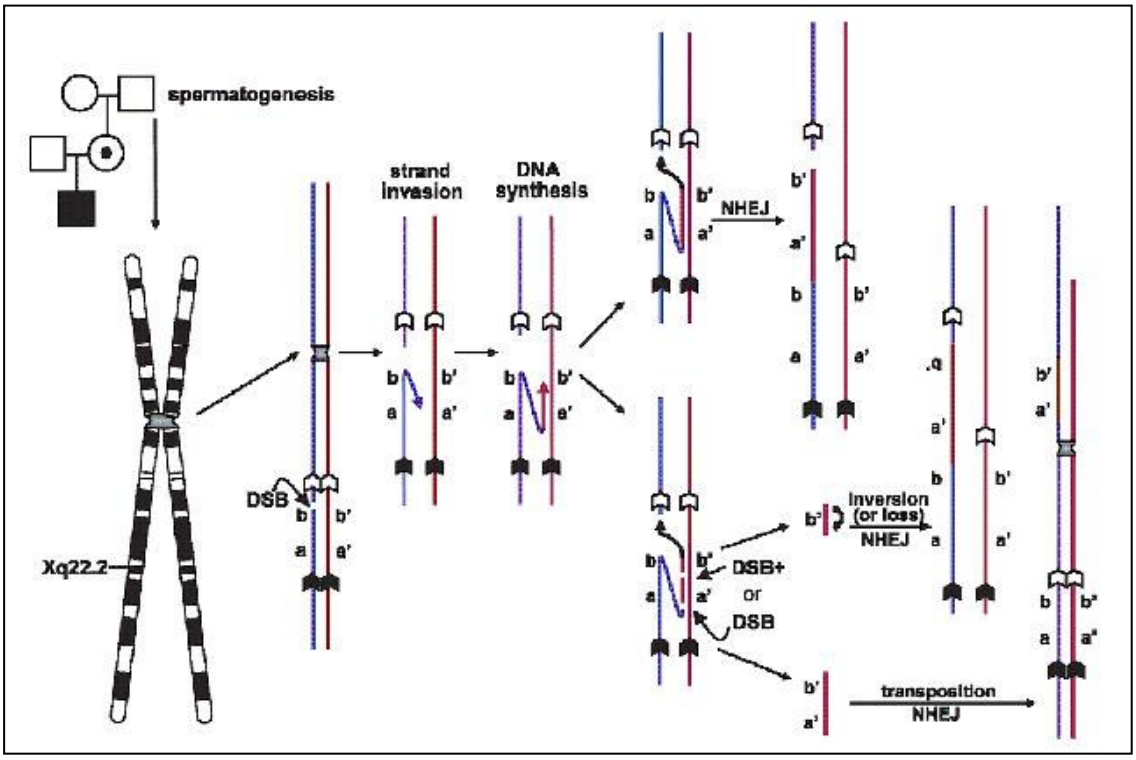

Figure 1.7. General model for *PLP1* duplication rearrangements (Lee *et al*., 2006a).

The genetic mechanism in patients with PMD due to the duplication followed by increased dosage of *PLP1* produces a toxic gain-of-function of the protein (Garbern *et al*., 1999). Excessive amounts of normal PLP1 and DM20 have been shown to accumulate in the late endosome and lysosomal compartments of cells overexpressing *PLP1* gene (Simons *et al*., 2002). Since PLP1 and DM20 typically associate with cholesterol and other lipids to form myelin rafts during trafficking through the Golgi complex, the transport of excess PLP1 and DM20 into the endosomal and lysosomal compartments depletes the myelin lipids from the Golgi complex (Simons *et al*., 2000). Consequently, the transport and assembly of myelin constituents are altered in cells overexpressing PLP1 and DM20. Thus, excessive PLP1 and DM20 create an imbalance in myelin constituents that adversely affects the subsequent stage of nascent myelin assembly in the Golgi network.

1.4.2. Mutations within the *PLP1* Gene

In addition to the duplication of the entire *PLP1* gene, other mutations in the coding and non-coding regions of the *PLP1* gene have been found to cause PMD. Many of these mutations are missense mutations but frameshifts, small insertions and deletions, nonsense,

and splice-site mutations have also been reported for PMD patients (Hodes *et al*., 1993). To date, over 100 distinct mutations (mostly, in exon 4) have been identified, but these only account for about 30 per cent of families in which the disease segregates with the *PLP1* locus (Garbern and Hobson, 2002).

PMD patients carrying mutations within *PLP1* present a wide range of clinical severity; however, the disease severity correlates well with the type of mutation (Cailloux *et al*., 2000). The severe forms of PMD are frequently associated with missense mutations in exons 2 and 4, leading to amino acid changes at highly conserved positions of the protein. The mild forms of PMD are mostly caused by mutations resulting in the production of truncated proteins or by missense mutations, which mostly affect exon 5 and lead to the substitution of amino acids partly conserved in the extracellular loop between the third and fourth transmembrane domains of the protein. Splice-site mutations affecting *PLP1* mRNA formation result in a more severe phenotype than do missense and nonsense mutations in *PLP1* (Hobson *et al*., 2000). The severity can be also correlated with the type of protein mutated, i.e. mutated PLP1 with normal DM20 causes the mildest phenotype, whereas mutated DM20 causes mild or severe forms depending on changes in the interactions of mutated proteins.

Mutated *PLP1* gene products have gain-of-function properties. At the cellular level, a trafficking defect at an early stage of secretory pathway is likely involved in the pathology (Southwood and Gow, 2001). Mutant proteins accumulate in the endoplasmic reticulum and cannot reach their normal target, cytoplasmic membrane (Gow *et al*., 1998). The accumulation of misfolded PLP1 is mediated by direct and stable binding of the endoplasmic reticulum chaperone molecule calnexin to a transmembrane domain of PLP1 (Swanton *et al*., 2003). Calnexin functions in the folding and quality control of PLP1. When misfolded, PLP1 is retained in the endoplasmic reticulum because of a stable and prolonged interaction with calnexin, possibly leading to a failure of the endoplasmic reticulum-associated protein degradation pathway to dispose the misfolded mutant proteins efficiently. In addition, accumulation of PLP1 and DM20 mutant proteins activate the UPR, a feedback signaling pathway that couples endoplasmic reticulum accumulation of misfolded proteins with nuclear transcriptional suppression and subsequent apoptotic cell death (Southwood *et al*., 2002; Gow *et al*., 1998).

The UPR signaling pathway was first described in the budding yeast *Saccharomyces cerevisiae* (Patil and Walter, 2001). Higher eukaryotes have additional sensors that generate a coordinately regulated response, promoting either stress adaptation or cell death (Figure 1.8). Three independent sensors are activated by the accumulation of unfolded proteins in the endoplasmic reticulum lumen. (i) IRE1, a transmembrane serine/threonine protein kinase that also has intrinsic endoribonuclease (RNase) activity, is one of the sensors for the UPR. Upon activation of the UPR, the RNase of IRE1 is activated by dimerization and *trans*-autophosphorylation, leading to removal of a 26-nucleotide intron from *XBP1* mRNA, which encodes a bZIP transcription factor X-box DNA binding protein (Yoshida *et al*., 2001; Calfon *et al*., 2002). This cleavage causes a translational frameshift, generating a potent transcriptional activator of UPR elements (UPRE). (ii) The activating transcription factor 6 (ATF6) is another regulatory protein that, like *XBP1*, can bind endoplasmic reticulum stress response elements (ERSEI) in the promoters of UPR-responsive genes (Yoshida *et al*., 1998). After activation of the UPR, ATF6 is cleaved by site-1 protease (S1P) and site-2 protease (S2P) (Ye *et al*., 2000). Transcription of UPR-responsive genes is induced when the cleaved form of ATF6 activates the *XBP1* promoter. Therefore, signaling through ATF6 and IRE1 merges to induce *XBP1* transcription and mRNA splicing, respectively. ATF6 increases *XBP1* transcription to produce more substrate for IRE1-mediated splicing that generates more active XBP1, providing a positive feedback for UPR activation. (iii) The UPR also alters cellular patterns of translation. UPR induction activates pancreatic endoplasmic reticulum kinase (PERK) which phosphorylates the α subunit of eukaryotic translation initiation factor 2 (eIF2α) and attenuates general protein synthesis (Harding *et al*., 2000). The PERK pathway also induces transcription of a subset of UPR-activated genes, including the transcription factor ATF4 and thereby maintaining activation of these genes under conditions of stress despite inhibition of general protein synthesis. These three endoplasmic reticulum stress-sensing pathways are regulated by the chaperone protein BiP/Grp78, which promotes proper folding of proteins in the endoplasmic reticulum in an ATP-dependent manner (Kaufman, 1999). In normal physiological conditions, BiP/Grp78 binds IRE1, ATF6 and PERK proteins but in the presence of stress, BiP/Grp78 is released from the three sensor molecules and activation of these pathways finally increases BiP/Grp78 expression, providing negative feedback to downregulate UPR signaling.

In contrast to UPR-signaling adaptation in response to endoplasmic reticulum stress, prolonged UPR activation results in a series of changes that ultimately leads to apoptotic cell death. Activation of IRE1 recruits the cytosolic adaptor tumor-necrosis-factor-receptor-associated factor 2 (TRAF2) to the endoplasmic reticulum membrane (Urano *et al*., 2000). This recruitment has two consequences. First, TRAF2 activates the apoptosis-signaling kinase 1 (ASK1), which then activates both the jun NH2-terminal kinase (JNK) and mitochondria-dependent caspase activity (Nishitoh *et al*., 2002). Second, IRE1 activation induces TRAF2 release from procaspase 12, an endoplasmic reticulum-specific effector of the caspase cascade, thereby activating a caspase-dependent apoptotic pathway (Yoneda *et al*., 2001). Furthermore, the activation of IRE1, PERK, and ATF6 all lead to the transcription of several pro-apoptotic genes such as that encoding the CCAAT/enhancer-binding-protein homologous protein (CHOP).

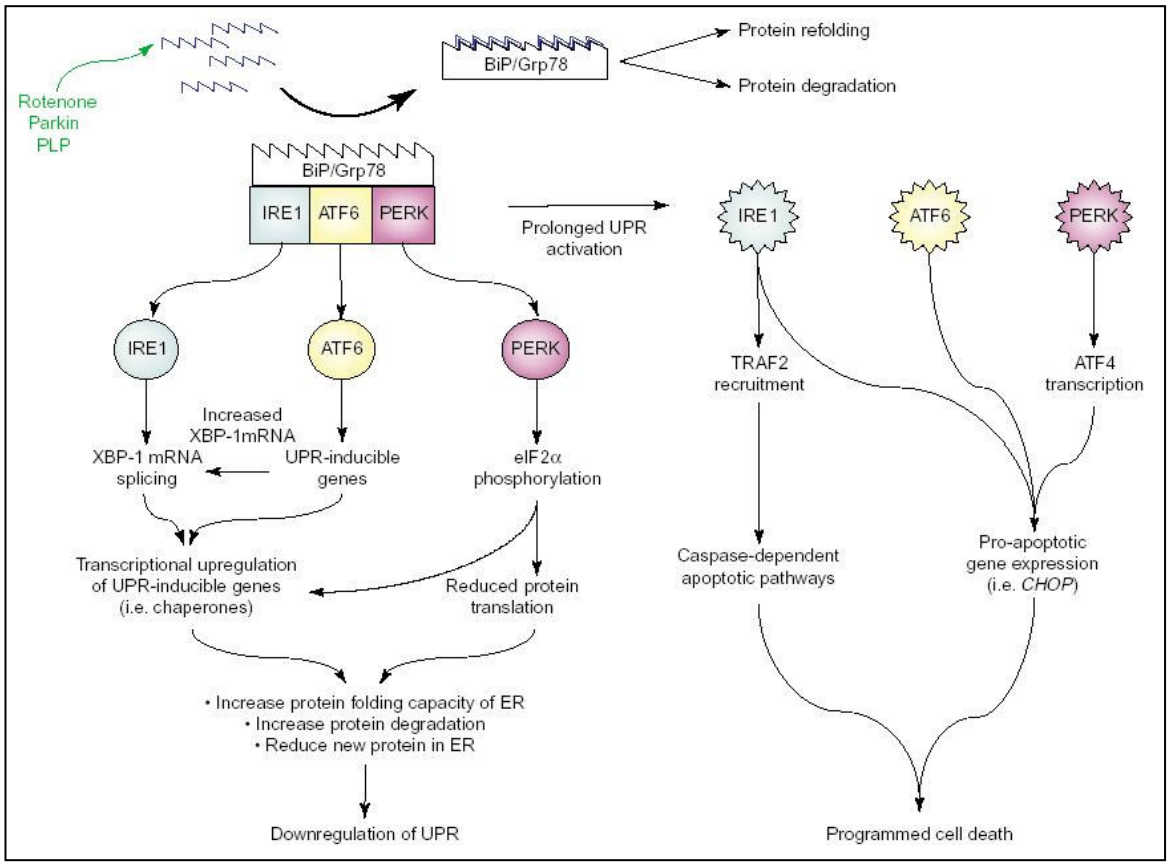

Figure 1.8. UPR signaling pathway showing the flow of information from the endoplasmic reticulum into the cytoplasm and ultimately the nucleus (Forman *et al*., 2003).

1.4.3. Deletion of the *PLP1* Gene

Deletions of the entire *PLP1* gene also cause PMD but account for less than 1 per cent of *PLP1* mutations (Inoue *et al*., 2002). Analysis of the DNA sequence flanking the *PLP1* deletion breakpoints revealed *Alu-Alu* recombination in one family. In the other two families, no homologous sequence flanking the breakpoints was found, but the distal breakpoints were embedded in low-copy repeats, which may stimulate these rearrangements. In another family, junction sequences revealed a more complex recombination event. These data suggest that *PLP1* deletions are likely generated by non-homologous end joining (Inoue *et al*., 2002; Woodward *et al*., 1998; Inoue *et al*., 1999).

Genomic mapping of the deleted segments revealed that the deletions are smaller than most of the duplications and less variable in size (Raskind *et al*., 1991; Inoue *et al*., 2002). The infrequent observation of *PLP1* deletion may be explained by the limited viable size for deletion, i.e. larger deletions might result in a reduced fertility and embryonic lethality.

Complete deletion of the *PLP1* gene, which results in loss of PLP1 and DM20 functions give rise to a mild form of PMD with patients having a greater life expectancy (Raskind *et al*., 1991; Sistermans *et al*., 1996). Pathogenesis of the disease due to *PLP1* overexpression or due to expression of a mutant form of *PLP1* is primarily caused by a defect in CNS myelination rather than maintenance of axons. In contrast, null *PLP1* mutations do not cause oligodendrocyte apoptosis, confirming that PMD is not caused by the absence of functional protein (Woodward and Malcolm, 1999). However, late-onset axon degeneration develops, suggesting that after myelination is complete, correct expression of *PLP1* is needed for oligodendrocyte function, which also involves maintaining the interaction between the oligodendrocyte and axon (Griffiths *et al*., 1998b).

1.5. Disease Expression in Females

PMD is typically found in males, and females are affected rarely (Ziereisen *et al*., 2000). A number of point mutations have been described in females manifesting PMD, but no affected female has been found to carry the *PLP* duplication (Hodes *et al.*, 1997). These

observations can be explained in terms of X-inactivation. Females carrying the duplication have skewed pattern of X-inactivation, i.e. the X chromosome having the duplication is preferentially inactivated, and thus they are asymptomatic. In female carriers with point mutations, X-inactivation is random and the fate depends on the nature of the mutation (Woodward *et al.*, 2000). However, identification of female patients with *PLP* duplications suggests that there exists an alternative disease mechanism (Inoue *et al*., 2001).

Female carriers of point mutations that result in a severe form of PMD in males are usually asymptomatic. In contrast, *PLP1* mutations that result in a mild PMD phenotype in affected males have been associated with adult-onset PMD among carrier females (Hodes *et al*., 1995; Nance *et al*., 1996; Sivakumar *et al*., 1999). This inverse relationship between the severity of manifestations in affected males and the likelihood of heterozygous females becoming symptomatic has been explained by normalization of the oligodendrocyte population (Hudson, 2001). As the result of random X-inactivation, a heterozygous female carrier has two distinct oligodendrocyte precursor populations, cells only expressing the normal *PLP1* allele and cells only expressing the mutant *PLP1* allele. Severe *PLP1* mutations may affect differentiation of oligodendrocytes and lead to subsequent apoptosis. As a result, the remaining oligodendrocytes of mature myelin represent a population of cells expressing a normal *PLP1* allele. On the other hand, oligodendrocytes expressing mild *PLP1* mutations may survive through development and form myelin, resulting in a mosaic population in mature myelin. Because the mutant myelin may be incomplete or unstable, and probably is subject to degradation, subsequent late-onset clinical manifestations may occur in carrier females. Experimental evidence is required to understand the exact nature of this paradigm.

1.6. Animal Models

Analogous animal models with spontaneous mutations in the *PLP1* gene, transgenics carrying additional copies of the wild-type gene and *PLP1*-knockout models have been available. *PLP1* mutants include the jimpy ($PLP1^{jp}$) mouse and its alleles, myelin synthesis-deficient ($PLP1^{jp\text{-}msd}$) and rumpshaker ($PLP1^{jp\text{-}rsh}$) mice, the myelin-deficient ($PLP1^{md}$) rat, the shaking ($PLP1^{sh}$) pup, and the rabbit with paralytic tremor ($PLP1^{pt}$) (Table 1.2) (Gencic and Hudson, 1990; Schneider *et al*., 1992; Boison and Stoffel, 1989;

Nadon *et al*., 1990; Tosic *et al*., 1994). In addition, three lines of transgenic mice having extra copies of the *PLP1* gene and two lines of mice that lack functional PLP1 protein have been generated as models of PMD caused by *PLP1* gene duplications or deletions (Readhead *et al*., 1994; Boison and Stoffel, 1994). These animal mutants with X-linked *PLP1* deficiency are valuable tools for studying pathogenesis in PMD since the amino acid sequence of PLP1 is completely conserved between mice, rats, and humans.

Table 1.2. Summary of mutations affecting *PLP1* gene in different species.

Species	Allele	Mutation
Mouse	jp	Frameshift, truncated C-terminal
	jp^{msd}	Missense, exon 6
	jp^{rsh}	Missense, exon 4
Rat	md	Missense, exon 2
Dog	sh	Missense, exon 3A
Rabbit	pt	Not determined

The spectrum of disease phenotypes in animals is very broad as it is in man. Studies of mutations and dosage effects of the *PLP1* gene have shown similar results in human and mouse (Woodward and Malcolm, 1999). In mice with the same genetic background, disease phenotypes among the *PLP1* mutants can be divided into severe and mild forms. *PLP1* overexpression or expression of a mutant form of the *PLP1* gene is associated with severe disease. Transgenic mice with extra copies of the wild-type PLP1 gene exhibit a phenotype of abnormal CNS myelination and premature death, supporting *PLP1* duplications as a molecular basis for the disease (Kagawa *et al*., 1994; Readhead *et al*., 1994; Inoue *et al*., 1996). Neurological symptoms and severity of the disease in transgenic mice correlates with *PLP1* gene copy number and with the level of overexpression. The point mutations result in inhibition of oligodendrocyte development and dysmyelination. These findings suggest that pathogenesis of the disease is primarily caused by a defect in CNS myelination rather than maintenance of axons. In contrast, the *PLP1* knockout mice exhibit a milder phenotype with normal oligodendrocyte development, indicating that it is the presence of the mutant protein that inhibits oligodendrocyte development and not the absence of the normal protein (Boison and Stoffel, 1994).

1.7. Pelizaeus-Merzbacher-Like Disease

Patients with PMD phenotype but without mutations of the *PLP1* gene are considered to have Pelizaeus-Merzbacher-like disease (PMLD) (Uhlenberg *et al*., 2004). Like PMD, PMLD is an inherited dysmyelinating disorder of the CNS in which myelin is not formed properly. It is characterized by nystagmus, progressive ataxia, spasticity and developmental delay, with onset in early infancy. Lack of myelin deposition is observed in the brain.

PMLD is an autosomal recessive disease caused by mutations in gap junction protein α12 (*GJA12*) gene on chromosome 1q41-42 (Uhlenberg *et al*., 2004; Bugiani *et al*., 2006). *GJA12* gene encodes for a 439-amino acid gap junction protein of approximately 47 kDa, connexin 47 (Cx47), which is highly expressed in oligodendrocytes (Figure 1.9) (Menichella *et al*., 2003).

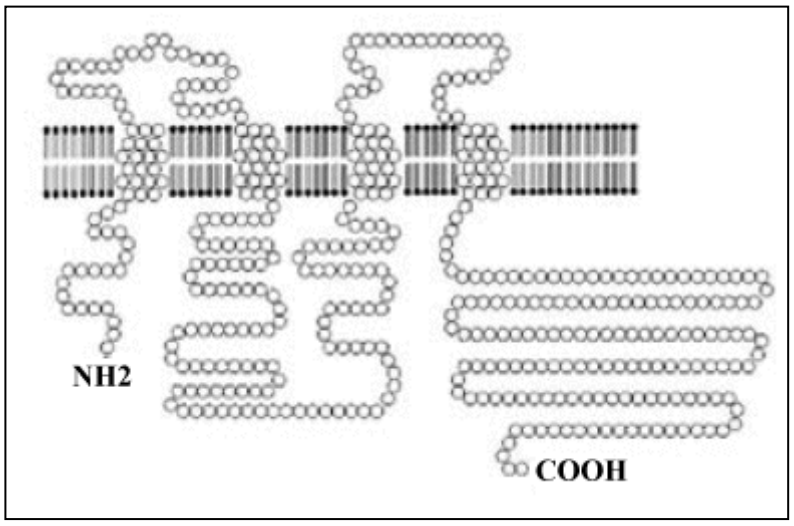

Figure 1.9. Schematic representation of the Cx47 protein (Salviati *et al*., 2007).

GJA12-related PMLD is the second human myelin disorder due to mutations in connexin genes. Mutations in gap junction protein β1 (*GJB1*) gene, encoding connexin 32 (Cx32), which is expressed in both Schwann cells and oligodendrocytes, cause the X-linked form of CMT disease (Bergoffen *et al*., 1993; Takashima *et al*., 2003). Gap junction proteins are members of a large homologous connexins and have four transmembrane, two extracellular and three cytoplasmic domains (Willecke *et al*., 2002; Nagy and Rash, 2003;

Nagy *et al*., 2003). They have been identified in a broad range of mammalian tissues and most tissues express more than one type of connexin protein. The formation of homo- and heteromeric hemichannels (connexons) by six connexins results in a high level of diversity in channel composition. Two connexons span the plasma membrane of adjacent cells and form the intercellular channels, thus allowing the exchange of a variety of small molecules, including ions and second messengers. More than half of the approximately 20 known mammalian connexins are expressed in the nervous system. In neurons, they form electrical synapses, whereas in non-excitable cells, they are involved in signal transduction, organ development and tissue homeostasis (Söhl *et al*., 2005; Levin, 2002).

The identification of homozygous mutations resulting in the synthesis of aberrant and truncated polypeptides demonstrates that the loss of Cx47 function is the cause of the disease. In mice, the GJA12 ortholog is mainly expressed in oligodendrocytes and partially co-localizes with GJB1. Both *GJA12*- and *GJB1*-knockout mice show no obvious morphological and behavioral abnormalities, suggesting functional redundancy. Double knockout animals with no *GJA12* and *GJB1* display severe defects of CNS myelin and early death, indicating that the expression of both connexins is critical for normal central myelination in mice (Menichella *et al*., 2003; Odermatt *et al*., 2003).

The clinical symptoms of PMD patients with PLP1 mutations and that of PMLD cases with *GJA12* mutations and other genetically undefined defects are almost identical. This phenotypic similarity in spite of genetic heterogeneity suggests that a common pathogenic process may lead to arrest in myelination. Cx47 together with other connexins and PLP1 are all part of a well-orchestrated myelinogenic program that provides the correct expression and targeting of PLP1 protein to the myelin sheath (Menichella *et al*., 2003). Any defect leading to the perturbation of this program could prevent myelin formation by disrupting the PLP1 synthesis, posttranslational modification, localization or stability.

2. AIM OF THE STUDY

PMD is a rare dysmyelinating disorder of the CNS. It is primarily caused by mutations of the *PLP1* gene on chromosome Xq22 although further genetic heterogeneity is suggested. The gene encodes two proteins expressed abundantly in oligodendrocytes, the PLP1 and its alternatively spliced isoform DM20. In the framework of this study, we aimed to investigate the genetic mechanism(s) responsible for the PMD phenotype in order to better understand the molecular pathogenesis of PMD and ultimately the mechanisms in CNS myelination. The specific aims of the project were:

- to investigate the X-linked recessive inheritance in familial PMD cases,
- to analyze the pattern of X-inactivation in female PMD patients in order to test its role for the disease phenotype,
- to establish various techniques to detect the duplication and deletion of *PLP1* gene in PMD patients,
- to identify the mutations within the *PLP1* gene in PMD patients without duplication or deletion,
- to re-examine the PMD patients with no mutation of *PLP1* gene by analyzing for the mutations in the *GJA12* gene, which is responsible for the PMLD phenotype,
- to examine the subcellular localization of PLP1 mutants and the UPR activation in these mutants,
- to perform genotype/phenotype correlation for PMD patients with *PLP1* and *GJA12* mutations.

3. MATERIALS

3.1. Patients

A total of 25 patients manifesting PMD phenotype (20 males and five females) from 21 unrelated Turkish families were analyzed in this study. Peripheral blood samples of the patients and their family members were provided by the neuropediatricians in Istanbul University Medical School, Department of Neurology. Informed consent to participate in the study was obtained from the patients and their family members. Ethical committee rules were strictly followed.

3.2. Chemicals

All chemicals used in this study were purchased from Merck (Germany), Sigma (USA), Riedel de-Häen (Germany), Carlo Erba (Italy) or Biochrom (Germany) unless stated otherwise in the text.

3.3. Buffers and Solutions

3.3.1. DNA Extraction from Peripheral Blood

Cell Lysis Buffer	:	155 mM NH_4Cl 10 mM $KHCO_3$ 1 mM Na_2Diaminoethanetetraacetic acid (Na_2EDTA) (pH 7.4)
Nucleus Lysis Buffer	:	10 mM Tris-HCl (pH 8.0) 400 mM NaCl 2 mM Na_2EDTA (pH 7.4)
Sodiumdodecylsulphate (SDS)	:	10 per cent (w/v) SDS in dH_2O (pH 7.2)

Proteinase K	:	20 mg/ml Proteinase K in dH_2O
NaCl	:	2.5 M NaCl
Ethanol	:	Absolute Ethanol
TE Buffer	:	20 mM Tris-HCl (pH 8.0) 0.1 mM Na_2EDTA (pH 8.0)

3.3.2. Agarose Gel Electrophoresis

10 X TBE Buffer	:	0.89 M Tris-Base 0.89 M Boric Acid 20 mM Na_2EDTA (pH 8.3)
20 X TAE Buffer	:	0.8 M Tris-Base 0.8 M Acetic Acid 20 mM Na_2EDTA (pH 8.3)
1 or 2 per cent Agarose Gel	:	1 or 2 per cent (w/v) Agarose in 0.5 X TBE or 1 X TAE Buffer
Ethidium Bromide (EtBr)	:	10 mg/ml EtBr in dH_2O
10 X Loading Buffer	:	2.5 mg/ml Bromophenol Blue 1 per cent SDS in glycerol

3.3.3. Polyacrylamide Gel Electrophoresis

10 X TBE Buffer	:	0.89 M Tris-Base 0.89 M Boric Acid 20 mM Na_2EDTA (pH 8.3)

40 per cent Acrylamide Stock (19:1)	:	38 per cent Acrylamide 2 per cent N, N'-methylenebisacrylamide
30 per cent Acrylamide Stock (29:1)	:	29 per cent Acrylamide 1 per cent N, N'-methylenebisacrylamide
8 per cent Denaturing Gel	:	8 per cent Acrylamide Stock (19:1) 8.3 M Urea 1X TBE Buffer (pH 8.3)
8 per cent Non-denaturing Gel	:	8 per cent Acrylamide Stock (29:1) 0.6 X TBE Buffer
Ammoniumpersulfate (APS)	:	10 per cent APS (w/v) in dH_2O
TEMED	:	N,N,N',N'-tetramethylethylenediamine
Glycerol	:	4 per cent Glycerol in Non-denaturing Gel
10 X Loading Buffer (denaturing)	:	95 per cent Formamide 20 mM EDTA 0.05 per cent Xylene Cyanol 0.05 per cent Bromophenol Blue

3.3.4. Silver Staining

Buffer A	:	10 per cent Ethanol 0.5 per cent Glacial Acetic Acid
Buffer B	:	0.1 per cent $AgNO_3$ in dH_2O

Buffer C	:	1.5 per cent NaOH 0.01 per cent $NaBH_4$ 0.015 per cent Formaldehyde
Buffer D	:	0.75 per cent Na_2CO_3

3.3.5. Fluorescence *in situ* Hybridization (FISH)

Lymphocyte Culture Medium	:	Roswell Park Memorial Institute (RPMI)-1640 Medium supplemented with 10 per cent Fetal Calf Serum 0.1 per cent Penicillin 2 mM L-Glutamin
KCl	:	0.56 per cent KCl
Fixative Solution	:	Methanol:Acetic Acid (3:1)
5 X Fluorophore Mix	:	2.5 mM dATP 2.5 mM dCTP 2.5 mM dGTP 2.5 mM dTTP 1 mM Biotin-16-dUTP or Digoxigenin (DIG)-11-dUTP
Sephadex G50	:	8 per cent Sephadex G50 in TE (10:1)
TE (10:1) Buffer	:	10 mM Tris-HCl (pH 8.0) 1 mM Na_2EDTA (pH 8.0)
EDTA	:	0.5 M Na_2EDTA adjusted to pH 8.0

Ethanol	:	100 per cent, 90 per cent, 70 per cent Ethanol
Sodium Acetate	:	3 M Sodium Acetate
Slide Cleaning Solution 1	:	10 per cent Tween 20
Slide Cleaning Solution 2	:	35 per cent Methanol 0.37 per cent HCl
20 X SSC	:	3 M NaCl 0.3 M Sodium Citrate adjusted to pH 7.0
Ribonuclease (RNase)	:	0.05 mg/ml in 2 X SSC
1 X PBS	:	137 mM NaCl 2.7 mM KCl 10 mM Na_2HPO_4 1.8 mM KH_2PO_4
HCl / Pepsin	:	0.01 M HCl 0.005 per cent Pepsin
PBS / $MgCl_2$	:	1 X PBS 50 mM $MgCl_2$
PBS / $MgCl_2$ / Formaldehyde	:	1 X PBS 50 mM $MgCl_2$ 3 per cent Formaldehyde
Denaturation Solution	:	50 per cent Deionized Formamide 50 mM NaH_2PO_4 / Na_2HPO_4 2 X SSC

SSC / Tween 20	:	4 X SSC 0.2 per cent Tween 20
SSC / Formamide	:	2 X SSC 50 per cent Formamide
SSC / Tween 20 / Dry Fat Milk:		4 X SSC 0.2 per cent Tween 20 5 per cent Dry Fat Milk
Detection Solution I	:	1 µg/ml Anti-DIG-Rhodamine SSC / Tween 20 / Dry Fat Milk
Detection Solution II	:	10 µg/ml Avidin-Fluorescein 20 µg/ml Anti-Sheep Immunoglobulin (IgG)-Texas Red SSC / Tween 20 / Dry Fat Milk
SSC / Tween 20 / 4,6-diamidino-2-phenylindole (DAPI)	:	4 X SSC 0.2 per cent Tween 20 0.1 µg/ml DAPI

3.3.6. Site-directed Mutagenesis

Luria Broth (LB) Medium	:	10 g/l Tryptone 5 g/l Yeast Extract 10 g/l NaCl
LB-Agar	:	10 g/l Tryptone 5 g/l Yeast Extract 10 g/l NaCl 15 g/l Agar

Ampicillin	:	50 mg/ml Ampicillin in dH_2O
X-Gal	:	100 mg/ml X-Gal in Dimethylformamide
Isopropyl β-D-1-thiogalactopyranoside (IPTG)	:	0.1 M in dH_2O
Glycerol	:	50 per cent Glycerol
Solution I	:	50 mM Glucose 25 mM Tris-HCl (pH 8.0) 10 mM Na_2EDTA (pH 8.0)
Solution II	:	0.2 M NaOH 1 per cent SDS
Solution III	:	5 M Potassium Acetate (pH 4.8)
2-Propanol	:	Absolute 2-Propanol
TE (10:1) Buffer	:	10 mM Tris-HCl (pH 8.0) 1 mM Na_2EDTA (pH 8.0)
Ethidium Bromide (EtBr)	:	10 mg/ml EtBr in dH_2O
TE / CsCl	:	6 M CsCl in TE (10:1)
Water-saturated 1-Butanol	:	1-Butanol: Water (70:30)
Ethanol	:	95 per cent, 70 per cent Ethanol

3.3.7. Cell Culture

Culture Medium 1	:	Dulbecco's Modification of Eagle's Medium (DMEM) with glucose
Culture Medium 2	:	DMEM with glucose, supplemented with 10 per cent Fetal Calf Serum 2 mM Glutamine 0.1 per cent Penicillin/Streptomycin
PBS	:	Dulbecco's Phosphate-Buffered Saline
Trypsin-EDTA	:	25 per cent Trypsin-EDTA
0.5 M Phosphate Buffer	:	0.5 M NaH_2PO_4 0.5 M Na_2HPO_4 adjusted to pH 7.2
Paraformaldehyde (PFA)	:	4 per cent (w/v) PFA 0.1 M Phosphate Buffer
2 per cent PFA	:	PFA:DMEM (1:1)
10 X TBS	:	0.1 M Tris-base 0.4 M Tris-acid 1.5 M NaCl adjusted to pH 7.5
Saponin	:	10 per cent (w/v) Saponin
TBS / Saponin	:	1 X TBS 0.1 per cent Saponin

TBSGBA	:	1 X TBS (pH 7.5) 0.1 per cent Gelatin 1 per cent BSA 0.05 per cent Sodium Azide
Blocking Solution	:	TBSGBA 2 per cent goat serum 0.1 per cent Saponin
DAPI	:	50 µg/ml DAPI in dH_2O

3.4. Fine Chemicals

3.4.1. Enzymes

Taq DNA Polymerase (supplied with 10 X Mg^{2+}-free *Taq* buffer and 25 mM $MgCl_2$) was purchased from Fermentas (Lithuania). The restriction enzymes and their appropriate buffers were from Fermentas (Lithuania) or New England Biolabs (USA). RNase and pepsin were purchased from Sigma (Germany) and Roche (Germany), respectively.

3.4.2. Oligonucleotide Primers

The oligonucleotide primers used in the framework of this thesis were synthesized by Iontek (Istanbul), Integrated DNA Technologies (USA) or Invitrogen (USA). The sequences and PCR conditions for the primers are given in Table 3.1 through Table 3.8.

3.4.3. Probes

The cosmid clone, cU125A1, containing the *PLP1* gene and the control cosmid, cU144A10, mapping ~850 kb distal to the *PLP1* gene were kindly provided by Dr. Karen Woodward, Institute of Child Health, London, UK.

Table 3.1. Microsatellite markers used in the analysis of linkage to *PLP1* locus.

Marker	Primer Sequence (5'→3')	Product Size (bp)	Repeat Type	Annealing Temperature (°C)
DXS7129	F: TTCTGCACATGTATCCCAGA	181	Tetra	56.2
	R: TTCCCCAAACATAGATGGTG			
DXS6803	F: GAAATGTGCTTTGACAGGAA	113	Tetra	57.5
	R: CAAAAAGGGACATATGCTACTT			
DXS6801	F: AGTCATTTCCTCTAACAAGTCTCC	134	Tetra	56.2
	R: TCCAGAGAGTCAGAATCAGTAGG			
DXS6809	F: TGAACCTTCCTAGCTCAGGA	255	Tetra	55.0
	R: TCTGGAGAATCCAATTTTGC			
DXS6789	F: TTGGTACTTAATAAACCCTCTTTT	149	Tetra	56.2
	R: CTAGAGGGACAGAACCAATAGG			
DXS6799	F: ATGAATTCAGAATTATCCTCATACC	252	Tetra	60.9
	R: GAACCAACCTGCTTTTCTGA			
DXS8063	F: AAAATCGGTGATTAGGAAAATACA	253	Di	52.1
	R: CCTCCAGCAGCCAAAG			
PLP-102	F: TGCCACAGATTCAGTCACTTG	200	Tetra	54.6
	R: TGGGGAAGCCTAAAACTTCA			
CA-PLP	F: CAACAGCATCTGGACTATCTTG	150	Di	56.2
	R: CCCAATGCTTGCACATAAATTG			
DXS1191	F: AACAGCTATTGTGCCTGGCAGAGAA	237	Di	58.4
	R: GCCCCGTTTGATGCTTCTAAATTG			
PLP-103	F: TCAGGAGGATTGTTTTAGCTCC	195	Tetra	53.5
	R: CCATCCCTCACTTAAATGCAA			

Table 3.2. Primers used in the X chromosome inactivation analysis.

Marker	Primer Sequence (5'→3')	Product Size (bp)	Repeat Type	Annealing Temperature (°C)
AR	F: GCTGTGAAGGTTGCTGTTCCTCAT	288	Tri	65.0
	R: TCCAGAATCTGTTCCAGAGCGTGC			
ZNF261	F: ATGCTAAGGACCATCCAGGA	271	Tri	58.5
	R: GGAGTTTTCCTCCCTCACCA			

Table 3.3. Primers used in the RFLP analysis.

Marker	Primer Sequence (5'→3')	Product Size (bp)	Annealing Temperature (°C)
PLP4	F: TCTCGAATTCCCATGTCAATCATTTT	227	55.0
	R: TCTCGAATTCGCACCCGTACCCTAACTC		
DXS17	F: GCAATTATCTGTATTACTTGAAT	620	57.0
	R: GGTACATGACAATCTCCCAATAT		

Table 3.4. Primers used in the quantitative fluorescent multiplex PCR (*: labeled with 6-FAM).

Marker	Primer Sequence (5'→3')	Product Size (bp)	Annealing Temperature (°C)
CA-PLP	F*: CCCAATGCTTGCACATAAATTG	137	53.0
	R: CAACAGCATCTGGACTATCTTG		
PM-7	F*: ATCGGACTTCCAGTCAAGTG	305	53.0
	R: TGTGGTTAGAGCCTCGCTAT		
PRNP	F*: ACTGCGTCAATATCACAATC	227	53.0
	R: TCCCACTATCAGGAAGATGA		

Table 3.5. Primers used in quantitative real-time PCR.

Marker	Primer Sequence (5'→3')	Product Size (bp)	Annealing Temperature (°C)
PLP-3	F: AGATTCCCTGGTCTCGTTTG	435	59.0
	R: TCTTCCTGACCTTCTCGTTC		
PLP-6	F: AAAGATATCAACACATTCAG	277	59.0
	R: TCAAGGATGGAAGCAGTCTA		
PRX-6	F: CGTGCAAGTGGGCAGAACTA	383	59.0
	R: TGACAAGACAGAGGGCAAGG		

Table 3.6. Primers used in the exon amplification of *PLP1*gene.

Gene	Region	Marker	Primer Sequence (5'→3')	Product Size (bp)	Annealing Temperature (°C)
PLP1	Promoter	PLP-P	F: GCTGCATATCCCACACCAATT	438	53.7
			R: GGCTGGCTAGTCTGCTTTGTG		
	Exon 1	PLP-1	F: CAGTGAAAGGCAGAAAGAGA	351	58.1
			R: CTGTGTCCTCTTGAATCTTC		
	Exon 2	PLP-2	F: TACCTACTGGATGTGCCTGA	296	56.2
			R: TCTCTATCTCCAGGATGGAG		
	Exon 3	PLP-3	F: AGATTCCCTGGTCTCGTTTG	435	58.1
			R: TCTTCCTGACCTTCTCGTTC		
	Exon 4	PLP-4	F: CATCTGCAGGCTGATGCTGA	258	52.0
			R: AGTGGGTAGGAGAGCCAAAG		
	Exon 5	PLP-5	F: TAGAGATGGAAGAAGGGCTC	315	58.1
			R: AGGCACACTTAGCCAACATG		
	Exon 6	PLP-6	F: AAAGATATCAACACATTCAG	277	52.0
			R: TCAAGGATGGAAGCAGTCTA		
	Exon 7	PLP-7	F: ATCGGACTTCCAGTCAAGTG	305	58.1
			R: TGTGGTTAGAGCCTCGCTAT		

Table 3.7. Primers used in the exon amplification of *GJA12* gene.

Gene	Region	Marker	Primer Sequence (5'→3')	Product Size (bp)	Annealing Temperature (°C)
GJA12	Promoter	GJA-P	F: CGTTTAAGGCGGTAAGCTCC	300	68.0 / 56.0
			R: GAGTAGATGGCCTCGCCG		
	Exon 1	GJA-1	F: GATCCACAACCACTCCACCT	284	68.0 / 56.0
			R: GCTCCTGCTCAGACGCAC		
	Exon 1	GJA-2	F: TTCCAGATTGTGGTCATCTCC	298	62.0 / 51.0
			R: CCTTAGTGCACGCCTCCT		
	Exon 1	GJA-3	F: GAGGAGGAGCCCATGCTG	286	66.0 / 54.0
			R: CGAAGCCGTACAGCAGGTA		
	Exon 1	GJA-4	F: GAGGAGGCGTGCACTAAGG	330	66.0 / 54.0
			R: ACAGAGGTTGAGCAGCAGG		
	Exon 1	GJA-5	F: GACGGTCTTCCTGCTGGTTA	265	66.0 / 54.0
			R: GTTTGCCAGGTTCTGGTCAT		
	Exon 1	GJA-6	F: CGACTACAGCCTGGTGGTG	290	63.0 / 51.0
			R: CACTGCCCTTCTCGGAGC		
	Exon 1	GJA-7	F: TACCTCTGCGGGCACTGT	275	70.0 / 58.0
			R: CTTCCCTGAGCAGCCTGG		

3.8. Primers used in the site-directed mutagenesis.

Marker	Primer Sequence (5'→3')	Product Size (bp)	Annealing Temperature (°C)
P215S	F: CTCCCATGGAACGCGTTCTCTGGCAAGGTTTGTGG	6047, 5942	55.0
	R: CCACAAACCTTGCCAGAGAACGCGTTCCATGGGAG		
F232S	F: CCATCTGCAAAACCGCGGAGTCCCAAATGACCTTC	6047, 5942	55.0
	R: GAAGGTCATTTGGGACTCCGCGGTTTTGCAGATGG		
Control	F: CCATGATTACGCCAAGCGCGCAATTAACCCTCAC	4500	55.0
	R: GTGAGGGTTAATTGCGCGCTTGGCGTAATCATGG		

3.4.4. Vectors

The pCMV5 vector was kindly provided by Dr. David W. Russell, Southwestern Medical Center, University of Texas, USA. The vector had been previously digested with *Eco*RI enzyme and ligated with hPLP1 (1.4 kb) and hDM20 (1.3 kb) cDNAs to generate pCMV5-hPLP1^{wt} (6047 bp) and pCMV5-hDM20^{wt} (5942 bp) constructs, respectively (Figure 3.1).

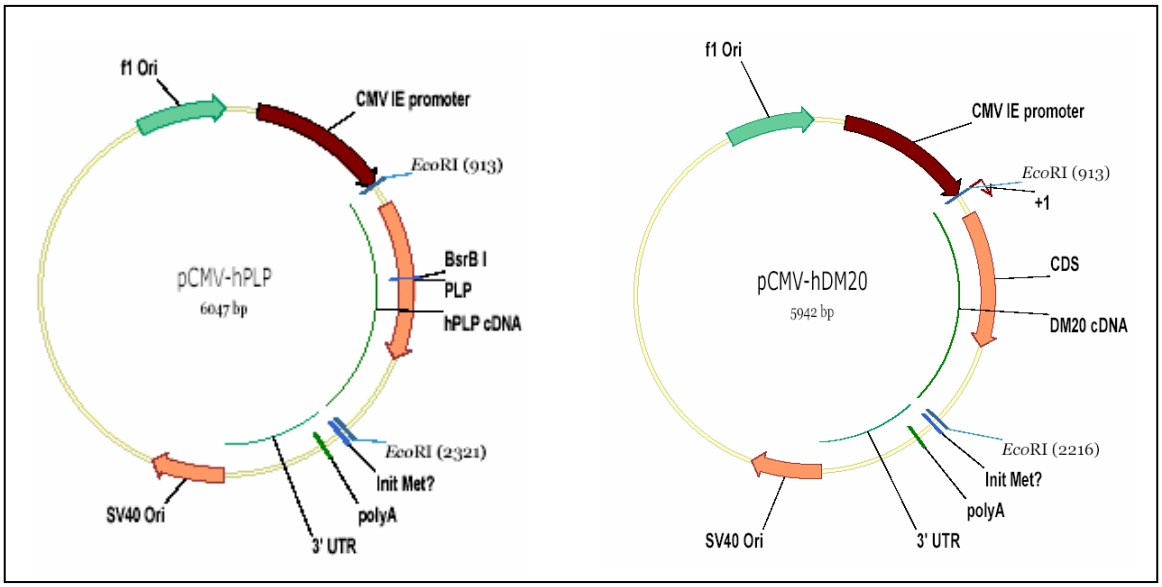

Figure 3.1. pCMV5-hPLP1^{wt} and pCMV5-hDM20^{wt} vectors.

3.4.5. Cell Line

The COS-7 cell line, which is an African green monkey kidney fibroblast-like cell line, was purchased from American Type Culture Collection (USA), and stored as frozen at a concentration of 1x10^6 to 1x10^7 cells/ml.

3.4.6. Antibodies

The primary antibodies and their corresponding secondary and tertiary antibodies used in this study were listed in Table 3.9.

3.4.7. DNA Molecular Weight Markers

Lambda DNA/*BstE*II marker, PhiX174 DNA/*Hinf*I marker and 100 bp DNA ladder were purchased from New England Biolabs (USA), Promega (USA) or Fermentas (Lithuania).

Table 3.9. Antibodies used in this study.

Primary Antibody	Origin	Secondary Antibody	Tertiary Antibody
Anti-PLP1 (AGMED) (1:100)	Rat-M	Rabbit Anti-Rat IgG (H+L) / FITC (Vector Laboratories) (1:100)	-
Anti-BiP (Stressgen) (1:100)	Rabbit-P	Goat Anti-Rabbit IgG (H+L) / Biotin (Southern Biotech) (1:200)	Streptavidin / Texas Red (AmershamPharmaciaBiotech) (1:300)
Anti-Golgin97 (Molecular Probes) (1:100)	Mouse-M	Goat Anti-Mouse IgG_1 / Biotin (Southern Biotech) (1:100)	Streptavidin / Texas Red (AmershamPharmaciaBiotech) (1:300)
Anti-LAMP2 (eBioscience) (1:1000)	Mouse-M	Goat Anti-Mouse IgG_1 / Biotin (Southern Biotech) (1:100)	Streptavidin / Texas Red (AmershamPharmaciaBiotech) (1:300)
Anti-ATF3 (Santa Cruz) (1:200)	Rabbit-P	Goat Anti-Rabbit IgG (H+L) / Biotin (Southern Biotech) (1:100)	Streptavidin / Texas Red (AmershamPharmaciaBiotech) (1:300)
Anti-CHOP3 (Santa Cruz) (1:100)	Rabbit-P	Goat Anti-Rabbit IgG (H+L) / Biotin (Southern Biotech) (1:100)	Streptavidin / Texas Red (AmershamPharmaciaBiotech) (1:300)
Anti-Caspase3 (Neuromics) (1:200)	Rabbit-P	Goat Anti-Rabbit IgG (H+L) / Biotin (Southern Biotech) (1:100)	Streptavidin / Texas Red (AmershamPharmaciaBiotech) (1:300)

3.4.8. Other Fine Chemicals

Deoxyribonucleosidetriphosphates (dNTPs) were purchased from Fermentas (Lithuania). DMSO was from Sigma (Germany).

The nick translation mix, biotin-16-dUTP, digoxigenin-11-dUTP, avidin-fluorescein, anti-digoxigenin-rhodamine and FuGENE 6 transfection reagent were purchased from Roche (Germany). Anti-sheep IgG-texas red and Vectashield mounting medium were from Vector Laboratories (USA). Phytohaemagglutinin M (PHA-M) and human Cot-1 DNA were purchased from Kibbutz Beit Haemek (Israel) and Biochrom (Germany), respectively.

3.5. Kits

QIAquick PCR purification kit and QIAprep spin miniprep kit were purchased from Qiagen (Germany). ABI PRISM Taq DyeDeoxy Terminator cycle sequencing kit was from Applied Biosystems (USA). SYBR *Premix Ex Taq* was purchased from TaKaRa (Japan). QuikChange site-directed mutagenesis kit was purchased from Stratagene (USA).

3.6. Electronic Databases

The databases used for obtaining the physical maps of markers and genes in the relevant loci were the Genome Database (http://www.gdb.org) and the GenBank (http://ww.ncbi.nlm.nih.gov).

The databases used for designing primer pairs and obtaining information about the restriction enzyme sites were the Biology WorkBench (http://workbench.sdsc. edu), the USCS Genome Bioinformatics (http://www.genome.ucsc.edu), the Tandem Repeats Finder (http://tandem.bu.edu) and the NEBcutter V2.0 (http://tools.neb.com/NEBcutter2).

3.7. Softwares

Two-point linkage analyses were performed using the MLINK program of the LINKAGE computer package, version 5.1 which was obtained from the Laboratory of Statistical Genetics at Rockefeller University (http://linkage.rockefeller.edu).

The quantitative fluorescent multiplex PCR products were analyzed using the ABI PRISM GeneScan and Genotyper softwares (Applied Biosystems) were used.

The real-time PCR products were quantitatively analyzed using the Light Cycler software 4.0 (Roche).

The primers used in the site-directed mutagenesis were designed using the Vector NTI7 (Invitrogen) and MacVector 8.0.2 (Accelrys) softwares.

The images observed by the fluorescent and confocal miscroscopes were captured using the Isis digital FISH imaging system (Metasystems, Germany) and the OpenLab software module (Improvision, USA), respectively.

Statistical significance of differences between values was assessed by ANOVA program of the SPSS 15.0 (Statistical Package for Social Sciences), followed by Bonferonni's post hoc comparison test or by Student's *t* test, as appropriate.

3.8. Equipment

The experiments in this study were performed using the facilities of the Department of Molecular Biology and Genetics at Boğaziçi University (Istanbul, Turkey) and the Center for Molecular Medicine and Genetics at Wayne State University (Detroit, USA).

The quantitative fluorescent multiplex PCR and automated sequencing analyses were performed using ABI PRISM 377 DNA Sequencer at Iontek (Istanbul, Turkey).

Autoclave	:	Model MAC-601 (Eyela, Japan)
Balances	:	Electronic Balance Model VA124 (Gec Avery, UK) Electronic Balance Model CC081 (Gec Avery, UK)
CCD Camera	:	CCD Camera (JAI Corporation, Japan)
Centrifuges	:	Centrifuge 5415C (Eppendorf, Germany) Universal 16R (Hettich, Germany) Genofuge 16M (Techne, UK) Mini Centrifuge 17307 (Cole Parmer,USA) Centrifuge B5 (B. Braun Biotech International, Germany) Sorvall RT6000B (USA)

		Sorvall RC5C (USA) Beckman L8-70M (USA)
Deep Freezers	:	-20°C (Bosch, Germany) -70°C (GFL, Germany)
Documentation System	:	BioDoc Video Documentation System (Biometra, Germany) GelDoc Documentation System with Quantity One 1-D Analysis Software (BioRad, USA)
Electrophoretic Systems	:	Horizon 58, Model 200 (BRL, USA) Sequi-Gen Sequencing Cell (Bio-Rad,USA) DGGE System Model # DGGE-200 (C.B.S. Scientific Co., USA) PROTEAN xi Vertical Electrophoresis System (Bio-Rad,USA)
Filters	:	DAPI Chroma 11000 (Germany) FITC Chroma 41001 (Germany) Texas Red Chroma 41004 (Germany)
Heat Blocks	:	DRI-Block DB-2A (Techne, UK) Hotplate SH1D (Cytocell, UK)
Hydrophobic Marker	:	Pap Pen (Daido Sangyo Co., Japan)
Incubators	:	Shake'n'Stack (Hybaid, UK) Oven EN400 (Nuve, Turkey) DH AutoFlow CO_2 Automatic Air-Jacketed Incubator (NuAire, USA)

Laminal Flow Cabinets	:	Labcaire BH18 (UK) Forma Scientific (USA)
Magnetic Stirrer	:	Chiltern Hotplate Magnetic Stirrer, HS31 (UK)
Micropipettes	:	Gilson (France) Rainin (USA)
Microscopes	:	B3000 (Prior, UK) Nikon Eclipse TS100 (USA) Zeiss Axioscope (Germany) Leica DMRA2 (USA)
Nitrogen Tank	:	Locator 4 Plus Cryobiological Storage Systems (Thermolyne, USA)
pH Meter	:	WTW (Germany)
Pump	:	Pump 79112 (Neuberger, Germany)
Ovens	:	Microwave Oven (Vestel, Turkey) 65dC EN400 (Nuve, Turkey) 56 dC (LEEC, UK)
Power Supplies	:	Power Pac Model 3000 (Bio-Rad, USA) PSU 400/200 (Scie-Plus, UK)
Refrigerator	:	4°C (Arçelik, Turkey)
Sealer	:	Vacuplus FS400A (Electric Petra, Germany)
Shaker	:	Lab-Line Universal Oscillating Shaker (USA)

Spectrophotometers	:	CE 5502 Scanning Double Beam 5000 Series (CECIL Elegant Technology, UK) NanoDrop ND-1000 (USA)
Thermal Cyclers	:	iCycler (Bio-Rad, USA) LightCycler 1.5 (Roche, Germany) Thermal Reactor TR1 (Hybaid, UK) PTC-200 (MJ Research, USA) Techne (Progene, UK) T3 (Biometra, USA)
UV Transilluminator	:	Chromato-Vue Transilluminator, Model 1TM-20UVP (USA)
Vortex	:	Nuvemix (Nuve, Turkey)
Water Bath	:	TE-10A (Techne, UK)
Water Purification System	:	WA-TECH Ultra Pure Water Purification System (Germany)

4. METHODS

4.1. DNA Extraction from Peripheral Blood Samples

Genomic DNA of each patient and his/her family members was isolated from peripheral blood sample that had been collected into a sterile vacutainer tube containing K_3EDTA as anticoagulant. Thirty milliliter (ml) of ice-cold cell lysis buffer was added to 10 ml of blood sample in a 50-ml Falcon tube and mixed thoroughly. The mixture was kept at 4°C for 15 minutes (min) to lyse the cell membranes and then centrifuged at 5000 revolution per minute (rpm) at 4°C for 10 min. The supernatant containing the red blood cell (RBC) debris was discarded, and the pellet containing the leukocyte nuclei was suspended in 10 ml of cell lysis buffer by vortexing. Centrifugation of the nuclei was repeated at 5000 rpm at 4°C for 10 min. After discarding the supernatant, the nuclear pellet was re-suspended in 5 ml of nucleus lysis buffer and vortexed until all clumps were dissolved. Forty µl of proteinase K (20 mg/ml) and 50 µl of 10 per cent SDS were added and the lysate was gently mixed. The mixture was then incubated either at 37°C overnight or at 56°C for three hrs to digest the nuclear proteins. When incubation was complete, 10 ml of 2.5 M NaCl solution was added to remove the proteins, and the tube was shaken vigorously. The sample was centrifuged at 5000 rpm at 20°C for 20 min and the supernatant was transferred into a clean 50-ml Falcon tube. Two volumes of ethanol were added to precipitate the DNA, and the mixture was shaken gently by inverting the tube several times until the DNA threads became visible. DNA was then fished out using a micropipette tip and transferred into a 1.5-ml Eppendorf tube. Finally the DNA sample was air-dried, dissolved in 300-400 µl of TE buffer, and stored at -20°C.

4.2. Spectrophotometric Analysis

The concentration of the isolated DNA was determined by spectrophotometry. The DNA sample was diluted with distilled water (dH_2O) in a ratio of 1:100, and the optical densities at 260 (OD_{260}) and 280 nm (OD_{280}) were measured. Knowing that 50 µg of

double-stranded DNA has an absorbance of 1.0 at 260 nm, the concentration of DNA was calculated using the following formula:

$$\text{Concentration } (\mu g/ml) = 50\ \mu g/ml \times OD_{260} \times \text{dilution factor}$$

The ratio between the OD_{260} and OD_{280} provides an estimate of the purity of the DNA sample. Pure samples have a value of 1.8 for OD_{260} / OD_{280}. Values greater than 1.8 indicate RNA contamination whereas those less than 1.8 indicate protein contamination.

4.3. Linkage Analysis

X-linked recessive inheritance was investigated in three familial PMD cases. Linkage to PLP1 locus on chromosome Xq22 was tested using flanking and internal microsatellite markers, which were selected from the Genome Database and the GenBank (Table 3.1).

4.3.1. PCR Amplifications of Polymorphic Markers

Eleven polymorphic markers were used to perform haplotype analysis. Before starting to amplify all samples, amplification conditions for each marker were optimized (Table 3.1).

The PCR reaction for each marker was performed in a total volume of 25 µl containing 200 ng of genomic DNA, 1 X Mg^{2+}-free PCR buffer, 1.5 mM of $MgCl_2$, 0.4 µM of each primer, 0.25 mM of each dNTP, 0.5 U of Taq DNA polymerase and sufficient dH_2O to adjust the volume. The cycling conditions were 94ºC for 5 min, followed by 32 cycles of 94ºC for 45 sec, appropriate annealing temperature for 45 sec, 72ºC for 1 min, with a final extension of 72ºC for 10 min.

4.3.2. Agarose Gel Electrophoresis of PCR Products

To check the amplification products, a 5 µl aliquot of the PCR product was mixed with 5 µl of 1 X loading buffer, loaded on a 1 per cent agarose gel containing ethidium bromide. Electrophoresis was performed in 0.5 X TBE at 150 Volts (V) for 10-20 min,

depending on the size of the product. The bands were then visualized on a UV light transilluminator.

4.3.3. Preparation of Denaturing Polyacrylamide Gels

The samples were electrophoresed on an eight per cent denaturing acrylamide gel. The gel was cast in a 40 cm long sequencing apparatus that was assembled using 0.4 mm spacers. Forty ml of 8 per cent denaturing acrylamide solution was mixed with 300 µl of 10 per cent APS and 30 µl of TEMED, and poured between the glass plates of the apparatus. A shark's tooth comb was inserted in an inverted position, and the gel was allowed to polymerize for at least one hr before use.

4.3.4. Electrophoresis of PCR Products on Denaturing Polyacrylamide Gels

The denaturing polyacrylamide gel was initially pre-run in hot 1 X TBE buffer at a constant power of 45 Watts (W) for 15 min in order to allow the gel temperature to rise to 40-45ºC. In the meantime, the PCR products were mixed with the 10 X denaturing loading buffer in a 1:1 ratio. Before loading the samples, they were denatured at 94ºC for 5 min immediately chilled on ice for 5 min. After the comb was re-oriented in the correct position, 3 µl of each sample was loaded in each slot. The gel was run at a constant power of 30 W for 2 to 3 hrs to resolve the fragments.

4.3.5. Silver Staining

After electrophoresis was complete, the apparatus was disassembled and the glass plates were separated gently by allowing the gel to remain intact on one of them. The gel was removed from the glass plate with the help of a Whatmann paper that was placed on the gel. The gel together with the Whatmann paper was soaked in buffer A and shaken for 3 min. Buffer A was replaced with buffer B, in which the gel was left for 10 min. After a short wash with dH_2O, the gel was shaken in freshly prepared buffer C until the bands appeared. Lastly, the gel was incubated in buffer D for 5 min and then transferred to a transparent folder, which was sealed on all four sides to store the gel. Paper towels were used to prevent tearing and folding of the gel while discarding the buffers after each step.

As the next step, the genotypes of members of each family were determined and the haplotypes were constructed. Two-point lod scores were calculated under the assumption of equal marker-allele frequencies using the MLINK program of the LINKAGE computer package, version 5.1. The disease was analyzed as a recessive mode of inheritance with 50 per cent penetrance in carrier females and with disease-allele frequency of 0.00001.

4.4. X Chromosome Inactivation Analysis

The most commonly used assay for determining X chromosome inactivation patterns rely on a highly polymorphic repeat in the androgen receptor (*AR*) gene that is adjacent to several CpG methylation-sensitive restriction enzyme sites (*Hha*I and *Hpa*II) that are differentially methylated on the active and inactive X chromosomes.

Initially, genomic DNA of each patient was digested with the *Hha*I. The restriction enzyme digestion was performed in a total volume of 20 µl, containing of 2 µl of genomic DNA, 1 X restriction buffer, 10 U *Hha*I enzyme and sufficient dH_2O to adjust the volume. The samples were then incubated at 37ºC for overnight.

Both the *Hha*I-digested and undigested genomic DNA samples for each patient were then amplified with a pair of primers flanking the repeat region in the *AR* gene or zinc finger protein 261 (*ZNF261*) gene (Table 3.2). The PCR reaction was performed in a total volume of 25 µl containing 200 ng of DNA, 1 X Mg^{2+}-free PCR buffer, 1.0 mM of $MgCl_2$, 10 per cent dimethyl sulfoxide (DMSO), 0.4 µM of each primer, 0.25 mM of each dNTP, 0.5 U of Taq DNA polymerase and sufficient dH_2O to adjust the volume. The cycling conditions were 94ºC for 5 min, followed by 35 cycles of 94ºC for 30 sec, 65ºC for 30 sec, 72ºC for 45 sec, with a final extension of 72ºC for 10 min. After the PCR products were checked using 1 per cent agarose gel, they were run on eight per cent denaturing polyacrylamide gel and silver stained as described in Sections 4.3.2, 4.3.3, 4.3.4 and 4.3.5.

4.5. Restriction Fragment Length Polymorphism (RFLP) Analysis

Two RFLP markers located within the *PLP1* gene, PLP4 (exonic) and DXS17 (intronic), were used (Table 3.3). In male patients detection of heterozygosity and in

female patients observation of three alleles or dosage differences between the alleles would indicate the presence of the *PLP1* duplication.

The PCR reaction for each marker was performed in a total volume of 25 µl containing 200 ng of genomic DNA, 1 X Mg^{2+}-free PCR buffer, 1.5 mM of $MgCl_2$, 0.4 µM of each primer, 0.25 mM of each dNTP, 0.5 U of Taq DNA polymerase and sufficient dH_2O to adjust the volume. The cycling conditions were 94ºC for 5 min, followed by 32 cycles of 94ºC for 45 sec, appropriate annealing temperature for 45 sec, 72ºC for 1 min, with a final extension of 72ºC for 10 min.

The PCR products for markers PLP4 and DXS17 were subsequently digested with the *Aha*II and *Taq*I restriction enzymes, respectively. The enzyme digestion was performed in a total volume of 20 µl, consisting of 8 µl of the amplified product, 1 X restriction buffer, 5 U *Aha*II or *Taq*I enzyme and sufficient dH_2O to adjust the volume. The samples digested with *Aha*II enzyme were incubated at 37ºC while those with *Taq*I at 65ºC, both for overnight. The digested samples were then run on two per cent agarose gel and visualized under UV light.

4.6. Fluorescence *in situ* Hybridization (FISH)

4.6.1. Lymphocyte Cell Culture

Lymphocyte cells were cultured from peripheral blood sample collected into a sterile vacutainer tube containing 100 U of lithium heparin. Each sample was studied in duplicate. Twenty five drops of blood sample was added into a canted neck culture flask containing 10 ml of lymphocyte cell culture medium, followed by incubation at 37ºC for overnight. Cultured cells were then transferred to a sterile 15 ml Falcon tube and precipitated by centrifugation at 1000 rpm at room temperature for 6 min. After discarding the supernatant, the cells were re-suspended in 10 ml of pre-warmed 0.56 per cent KCl and incubated at 37ºC for 20 min. Then 0.6 ml of freshly prepared and cooled methanol:acetic acid fixative (3:1) was added and centrifuged at 1000 rpm at room temperature for 6 min. The supernatant was discarded, 8 ml of methanol:acetic acid fixative (3:1) was added and re-suspended by vortexing. After incubation of the cells at 4ºC for 1 hr, the mixture was

centrifuged at 1000 rpm at room temperature for 6 min and the supernatant was discarded. The steps of adding of methanol:acetic acid fixative (3:1), incubation at 4ºC for 1 hr and centrifugation at 1000 rpm at room temperature for 6 min were repeated for two more times. Finally, cells were suspended in a volume of 500 to 750 µl of fixative solution depending on the amount of the cells. In order to check the morphology of the cells, a few drops of the cell suspension was dropped onto a slide from about 1 m above and observed under 10 X objective of a light microscope. Cells were stored in the fixative solution at -20ºC.

4.6.2. Labeling of the Probes

A cosmid clone, cU125A1, containing the *PLP1* gene and a control cosmid, cU144A10, mapping ~850 kb distal to the *PLP1* gene were used as probes. cU125A1 and cU144A10 were labeled with biotin-16-dUTP and DIG-11-dUTP, respectively, by nick translation kit (Roche). The labeling reaction for each probe was performed by combining 1µg of template DNA in 12 µl of sterile dH_2O, 4 µl of 5 X fluorophore-labeling mix and 4 µl of nick translation mix, followed by incubation at 15ºC for 90 min.

In the meantime, a Sephadex G50 column was prepared for each probe to remove non-incorporated dNTPs in the labeling reaction. The stamp of a 1 ml syringe was removed and a plug of silanized glass wool was put up to 0.1 ml level of the syringe. The syringe was then filled with Sephadex G50 up to 1 ml level and placed in a 15 ml Falcon tube, followed by centrifugation at 3000 rpm at 20ºC for 3 min. Since Sephadex G50 moved down, more Sephadex G50 was added and centrifuged again at 3000 rpm at 20ºC for 3 min. The column was then washed by adding 100 µl of TE and centrifugation at 3000 rpm at 20ºC for 3 min, and kept at 4ºC until use.

The labeling reaction was stopped by adding 1 µl of 0.5 M EDTA. The labeled probe mixture was then transferred to the Sephadex G50 column and centrifuged at 3000 rpm at 20ºC for 3 min. For hybridization of each slide, 60 ng of each purified probe were mixed, and 2 µg of Cot-1 DNA and 10 µg of Herring Testis DNA were added. In order to precipitate the probe DNA, 500 µl of absolute ethanol and 0.1 volumes of 3 M sodium acetate solution were added and incubated at -20ºC for overnight.

4.6.3. Preparation and Pre-treatment of Slides

Before use, the slides were washed in dH_2O containing approximately 10 per cent Tween 20 for overnight, followed by washing in dH_2O for three to four times, and stored in methanol:HCl mixture. Depending on the density of cells, 20 to 50 µl from each cell culture was dropped onto a slide from a distance of approximately 1 m, and allowed to air-dry. Cells were visualized with 10 X objective of light microscope. The slide was washed in 2 X SSC solution at room temperature for 5 min. Hundred µl of RNase was added onto each slide, covered with a 24 mm x 60 mm coverslip, and incubated at 37ºC for 15 min in a moist chamber. The coverslip was then removed, and the slide was washed in 2 X SSC solution at room temperature for 2 min for three times and 1 X PBS solution for 5 min for once. Subsequently, the slide was left in pre-heated 0.01 M HCl solution containing 0.005 per cent pepsin at 37ºC for 10 min. Subsequently, they were washed in 1 X PBS containing 50 mM $MgCl_2$ for 5 min and in 1 X PBS containing 50 mM $MgCl_2$ and 3 per cent formaldehyde for 10 min. A further 1 X PBS wash was performed for 5 min, followed by washing in dH_2O momentarily for twice. Serially, they were rinsed in cold 70 per cent, 90 per cent and 100 per cent ethanol for 3 min, and left to air-dry.

4.6.4. Denaturation of Probe and Chromosomal DNAs

Probe DNA were centrifuged at 13000 rpm at 4ºC for 30 sec. After the supernatant was discarded, 500 µl of 70 per cent ethanol was added and centrifuged at 13000 rpm at 4ºC for 5 min. The supernatant was poured off, and the pellet was air-dried and dissolved by adding 10 µl of denaturation solution for each slide. The probes were then denatured at 75ºC for 6 min, followed by incubation at 37ºC for 25 min for pre-hybridization.

In the meantime, chromosomes on the slide were also denatured. One hundred µl of freshly prepared denaturation solution was added onto each slide, which was covered with a 24 mm x 60 mm coverslip and incubated on a 75ºC hot plate for 130 sec. After the coverslip was removed, the slide was washed serially in cold 70 per cent, 90 per cent and 100 per cent ethanol for 3 min each.

4.6.5. Hybridization and Post-Hybridization Washing

After the slide was air-dried, 10 µl of denatured probe mix was added onto each slide, which was covered with a 24 mm x 60 mm coverslip and sealed with fixogum. The slide was then placed in a moist chamber and left for hybridization at 37ºC for three overnights.

After hybridization, the coverslip was removed and the slide was washed momentarily in 4 X SSC solution containing 0.2 per cent Tween 20. Next washes were in 2 X SSC solution containing 50 per cent formamide pre-heated to 45ºC and in 2 X SSC solution, pre-heated to 37ºC; these washes were for 5 min for three times in each solution. Then the slide was rinsed in 4 X SSC solution containing 0.2 per cent Tween 20. One hundred µl of 4 X SSC solution containing 0.2 per cent Tween 20 and 5 per cent dry fat milk was added onto each slide, covered with a coverslip and incubated at 37ºC in a moist chamber for 10 min.

4.6.6. Visualization of the Probes

After the coverslip was removed, the slide was washed in 4 X SSC solution containing 0.2 per cent Tween 20 momentarily. Fifty µl of detection solution I containing anti-DIG-rhodamine (Roche) was added onto each slide, covered with a coverslip and incubated at 37ºC in a moist chamber for 30 min. The coverslip was then removed and the slide was washed in 4 X SSC solution containing 0.2 per cent Tween 20 momentarily for once and for 3 min for three times.

Subsequently, 50 µl of detection solution II containing avidin-fluorescein (Roche) and anti-sheep IgG-texas red (Vector Laboratories) was added onto each slide, covered with a coverslip and incubated at 37ºC in a moist chamber for 75 min. The coverslip was then removed and the slide was washed in 4 X SSC solution containing 0.2 per cent Tween 20 momentarily for once and for 3 min for three times.

Cells were then incubated in 4 X SSC solution containing 0.2 per cent Tween 20 and DAPI (in a final concentration of 0.1 µg/ml) for 10 min, followed by washing in dH_2O for

two to three times and air-drying. Finally, a drop of Vectashield mounting medium was added onto the slide, covered with a coverslip, and kept at -20ºC for overnight. The nuclei were then analyzed using Zeiss Axioscope fluorescent microscope and the pictures were captured with Meta-Isis digital imaging system using a CCD camera.

4.7. Quantitative Fluorescent Multiplex PCR

Three pairs of primers, the forwards being labeled with the fluorescent phoshoramidite 6-FAM at the 5' end, were used for the multiplex PCR (Table 3.4). Three PCR products were obtained, two from the PLP1 gene (one from an intragenic CA-dinucleotide repeat polymorphism and the other from exon 7) and one from an autosomal reference gene, exon 2 of the prion protein (PRNP) gene on chromosome 20.

Multiplex PCR was performed in a total volume of 25 µl containing 200 ng of genomic DNA, 10 pmol (for CA-PLP and PM-7) or 5 pmol (for PRNP) of each primers and 2X QuantiTect Probe PCR Master Mix (QIAGEN). The cycle number was optimized by multiple control analysis. Cycling conditions were initial denaturation of 13.5 min at 95ºC, followed by 25 cycles of 30 sec at 95ºC, 1 min at 53ºC, 1 min at 72ºC and a final extension of 2 min at 72ºC.

Multiplex PCR products were analyzed on an ABI 377 DNA sequencer using the GENESCAN and GENOTYPER softwares (Applied Biosystems). For each individual, the analysis was performed three times. Fluorescence profiles were produced for each reaction, with three peaks representing the three PCR products. The area under each peak correlates to the quantity of each PCR product. The PLP1 gene copy number in each individual was determined as the quantitative ratio of the averaged areas of two PLP1 peaks to that of the internal control PRNP peak, within each individual fluorescence profile. To obtain a reference range for normal males and females, who carry one and two PLP1 allele(s), respectively, 16 normal controls (eight males and eight females) were examined. The PLP1:PRNP ratios of the patients were then compared with those for normal controls.

4.8. Quantitative Real-Time PCR

Each DNA sample was amplified using the primer pairs for PLP-3, PLP-6 and PRX-6 (as the reference region) (Table 3.5) with Light Cycler (Roche). In each PCR turn, a normal male and a normal female for the PLP1 region were included as controls. DNA samples of various concentrations (5 ng, 10 ng and 20 ng) from a normal female were also included to construct a standard curve. Melting point analysis was performed on all PCR products to check for any nonspecific amplicons. The ratios between the target regions and the reference region were determined by the relative quantitative analysis program of the Light Cycler software 4.0.

The real-time PCR reaction was performed in a total volume of 20 µl, containing 20 ng of the genomic DNA, 10 µl 2X SYBR Green I PCR Master Mix (TaKaRa), 5 pmol of each primer and sufficient dH_2O. Aliquots of 20 µl were transferred into the LC glass capillaries (Roche Diagnostics). The real-time PCR protocol includes an initial denaturation step of 95°C for 2 min, followed by amplification and quantification steps repeated for 35 cycles of 95°C for 5 sec, 59°C for 10 sec, 72°C for 20 sec. This step was followed by a melting curve program (from 65°C to 98°C, with an increasing rate of 0.2°C/sec and a continuous fluorescence measurement) and terminated by cooling to 40°C.

4.9. Mutation Analysis

All patients were further screened for the presence of point mutations in *PLP1* and *GJA12* genes by Single Strand Conformational Polymorphism (SSCP). This technique is based on the fact that single stranded DNA under non-denaturing conditions assumes a secondary conformation based on its primary sequence. A base variation within the primary sequence results in a different conformation, which in turn is detected by a mobility shift in SSCP gels.

4.9.1. PCR Amplifications for the Analysis of *PLP1* and *GJA12* Genes

The promoter, coding exons and the flanking intronic sequences of each of the *PLP1* and *GJA12* genes were amplified using eight primer sets (Table 3.6; Table 3.7). Before

starting to amplify all samples, amplification conditions for each fragment were optimized. PCR reactions were carried out in a total volume of 25 µl containing 200 ng of genomic DNA, 1 X Mg^{2+}-free PCR buffer, 1.5 mM of $MgCl_2$, 10 per cent DMSO (only in the amplification of GJA12 fragments), 0.4 µM of each primer, 0.25 mM of each dNTP, 0.5 U of Taq DNA polymerase and sufficient dH_2O to adjust the volume. The cycling conditions for PLP1 fragments were 94ºC for 5 min, followed by 32 cycles of 94ºC for 1 min, appropriate annealing temperature for 1 min, 72ºC for 1 min, with a final extension of 72ºC for 10 min. The amplification of *GJA12* fragments were performed using a touch-down cycling program as follows: one cycle of 95ºC for 4 min, 20 cycles of 95ºC for 45 sec, appropriate annealing temperature with a decrease of 0.5ºC/cycle for 45 sec, 72ºC for 30 sec, followed by 25 cycles of 95ºC for 45 sec, appropriate annealing temperature for 45 sec, 72ºC for 30 sec, with a final extension of 72ºC for 10 min.

Before loading the PCR products into the SSCP gels, they were checked on 1 per cent agarose gel as described in Section 4.3.2.

4.9.2. Preparation of SSCP (Non-denaturing Polyacrylamide) Gels

Amplification products were run on eight per cent acrylamide gels with or without 4 per cent glycerol. The gel plates were 20 cm × 20 cm in size and were assembled using 0.75-mm spacers. Nine point three ml of 30 per cent (29:1 acrylamide-bisacrylamide, in dH_2O) stock acrylamide solution was mixed with 2.1 ml of 10 X TBE buffer, and the volume was adjusted to 35 ml with dH_2O. Three hundred and fifty µl of 10 per cent ammonium persulfate (APS) and 35 µl of TEMED were added, and the solution was poured between the glass plates. A 20-well comb was inserted, and the gel was left to polymerize for at least one hr before use.

4.9.3. SSCP Electrophoresis

Ten µl of the PCR product was mixed with 10 µl of denaturing loading dye. Just before loading, they were denatured at 94°C for 5 min, and chilled on ice for 5 min. Eight µl of the denatured sample was loaded. Electrophoresis of the samples was carried out in 0.6 X TBE buffer at 150-250 V for 18 hrs.

After electrophoresis was complete, the gels were silver stained as explained in Section 4.3.5.

4.9.4. DNA Sequence Analysis

For samples that exhibited variant patterns in SSCP, DNA sequencing analysis of both sense and anti-sense strands was performed on QIAquick-spin column purified PCR products using the same primers as for the SSCP analysis. The sequencing reactions were prepared with the ABI PRISM Taq DyeDeoxy Terminator cycle sequencing kit and analyzed using the ABI PRISM 377 automated DNA sequencer (Applied Biosystems).

4.9.5. Restriction Enzyme Analysis

The sequencing chromatograms of the patients were compared with that of a normal DNA. If there was a mutation, it was confirmed either by sequencing with reverse primer or by restriction analysis, if the mutation created or abolished a restriction enzyme site . For restriction analysis, 8 µl of the amplified product was digested with 5 U of the corresponding restriction enzyme in a final volume of 20 µl. Digestions were incubated at 37°C for overnight, and run on 3 per cent agarose gel or 8 per cent non-denaturing polyacrylamide gel, and visualized under UV light or by silver staining, respectively.

4.10. Site-directed Mutagenesis

The PLP1 mutations, P215S and F232S, identified in this study were generated *in vitro* using the QuikChange site-directed mutagenesis kit (Stratagene) in order to examine the behavior of the mutant proteins in COS-7 cell line.

4.10.1. Primer Design

The mutagenic oligonucleotide primers were designed individually according to the desired mutation using Vector NTI7 and MacVector 8.0.2 programs (Table 3.8). While designing the primers, the following considerations were made:

- Both of the mutagenic primers contained the desired mutation and annealed to the same sequence on opposite strands of the plasmid.
- The desired mutation was in the middle of the primer with approximately 10-15 bases of perfect complementarity to the template sequence on both sides.
- Both primers included silent base changes to create a restriction site, which was used to track the generated mutation.

4.10.2. Mutant Strand Synthesis Reaction

Each mutation was generated on both wild-type hPLP1 and hDM20 cDNA templates that had been previously cloned into pCMV5 plasmid (Figure 3.5). The sample reaction was prepared using 1 X reaction buffer, 10 ng of dsDNA template, 100 ng of each mutagenic primer, 1 µl of dNTP mix and dH_2O to a final volume of 50 µl. Then 2.5 U of *Pfu Turbo* DNA polymerase was added. The reaction was cycled using the following cycling parameters: one cycle of 95ºC for 30 sec, followed by 16 cycles of 95ºC for 30 sec, 55ºC for 1 min, 68ºC for 6.5 min.

The pWhitescript 4.5 kb plasmid was included as a control to test the efficiency of mutant plasmid generation using the QuikChange site-directed mutagenesis kit. The pWhitescript control plasmid contains a stop codon (TAA) at amino acid 9 of the protein where a glutamine codon (CAA) would normally appear in the β-galactosidase gene of the pBluescript II SK(-) phagemid. XL1-Blue supercompetent cells transformed with this control plasmid appear white on LB-ampicillin agar plates containing IPTG and X-gal since β-galactosidase activity has been destroyed. The oligonucleotide control primers create a point mutation on the pWhitescript control plasmid that reverts the T residue of the stop codon (TAA) at amino acid 9 of the β-galactosidase gene to a C residue, to produce the glutamine (CAA) found in the wild-type sequence. Following transformation, colonies can be screened for the β-galactosidase$^+$, blue phenotype. The control reaction was prepared similar to sample reaction, using 1 X reaction buffer, 10 ng of pWhitescript control plasmid, 125 ng of each control primer, 1 µl of dNTP mix and dH_2O to a final volume of 50 µl. Then 2.5 U of *Pfu Turbo* DNA polymerase was added and the reaction was cycled using the same cycling parameters above.

4.10.3. *Dpn*I Digestion of the Amplification Products

In order to digest the parental supercoiled dsDNA, 10 U of the *Dpn*I restriction enzyme was added and incubated at 37ºC for 1 hr.

4.10.4. Transformation of *E.coli* XL1-Blue Supercompetent Cells

The XL1-Blue supercompetent cells were thawed on ice. For each control and sample reaction to be transformed, 50 µl of the supercompetent cells was aliquoted to a pre-chilled 14 ml BD Falcon round-bottom tube. One µl of the *Dpn*I-treated DNA from each control and sample reaction was transferred to separate aliquots of the supercompetent cells. The transformation efficiency of the XL1-Blue supercompetent cells was verified by adding 0.1 ng of the pUC18 control plasmid to a 50 µl aliquot of the supercompetent cells. The transformation reactions were swirled gently and incubated on ice for 30 min, followed by heat pulse at 42ºC for 45 sec. The reactions were then placed on ice for 2 min. Five hundred µl of LB medium was added onto each transformation reaction and incubated at 37ºC for 1 hr with shaking at 225 rpm. One hundred µl of each transformation reaction was plated on LB-ampicillin agar plates. For the mutagenesis and transformation controls, the cells were spread on LB-ampicillin agar plates containing 80µg/ml X-gal and 20 mM IPTG. The transformation plates were incubated at 37ºC for overnight.

The mutagenesis efficiency (ME) for the pWhitescript control plasmid was calculated by the following formula:

$$ME = \frac{\text{Number of blue colony forming units (cfu)}}{\text{Total number of colony forming units (cfu)}} \text{ x 100 per cent}$$

Greater than 80 per cent of the colonies should contain the mutation and appear as blue colonies on LB-ampicillin agar plates containing X-gal and IPTG. The transformation efficiency for the pUC18 control plasmid should be observed greater than 10^8 cfu/µg.

4.10.5. Small Scale Isolation of Mutant Plasmid DNAs

A single colony from a freshly streaked LB-ampicillin agar plate was picked and inoculated in 4 ml of LB medium containing ampicillin. For each plasmid, this step was repeated for 12 different colonies. They were incubated at 37ºC with vigorous shaking for overnight. The bacterial cells were then harvested by centrifugation at 13 K for 1 min at room temperature and the plasmid DNA was isolated using the QIAprep Spin Miniprep Kit (QIAGEN).

In order to check whether the desired mutation was generated, restriction enzyme analysis was performed. One µg of each mutant plasmid DNA was digested with the corresponding enzyme at 37ºC for 1 hr in the presence of 1 X reaction buffer, 1 X BSA and dH_2O to a final volume of 10 µl.

The digestion reactions were then electrophoresed on 1 per cent agarose gel. Two of the samples with the expected digestion pattern were selected and sequenced for both the sense and anti-sense strands for further confirmation. Glycerol stocks were also prepared for the plasmids sequenced by adding 500 µl of 50 per cent glycerol onto 500 µl of the corresponding transformed cells and kept at -80ºC.

4.10.6. Large Scale Isolation of Mutant Plasmid DNAs by Double CsCl

An LB-ampicillin agar plate was streaked with bacteria from a glycerol stock containing the correct plasmid sequence and let the plate grow at 37ºC for 1.5 days to ensure good colony size. Next morning, a single colony picked from this plate was inoculated into 1 ml of LB medium containing ampicillin for growth during the day. In the afternoon, if the culture medium was turbid enough, 1 ml of it was inoculated into 500 ml of 37ºC pre-warmed LB medium containing ampicillin and let it grow at 37ºC with vigorous shaking for overnight. The bacterial culture was then placed into the cold room and 250 ml of it was transferred into the centrifuge bottle, balanced and centrifuged in the Sorvall SLA 1500 rotor at 5 K at 4ºC for 15 min. The supernatant was discarded. The remaining 250 ml of bacterial culture was added onto the pellet and the centrifugation step was repeated, the supernatant was poured off and the pellet was inverted on a paper towel

to drain for a few minutes. The bacterial pellet was then re-suspended in 20 ml of Solution I by swirling. Forty ml of freshly prepared Solution II was added, swirled and incubated on ice for 5 min. 20 ml of cold Solution III was added, mixed by inverting five to six times and incubated on ice for 15 min. Then the suspension was centrifuged in the Sorvall SLA 1500 rotor at 5 K at 4ºC for 15 min. Subsequently, the supernatant was strained through two layers of Kimwipe tissue placed into a funnel over a 250 ml centrifuge bottle to filter out the white precipitate. 0.6 volumes of 2-propanol to the net weight of supernatant in each bottle was added and mixed well, followed by balancing and centrifugation in the Sorvall SLA 1500 rotor at 6 K at 4ºC for 60 min. The supernatant was discarded and the bottle was drained inverted on a paper towel for a few minutes. 6.5 ml of TE (pH 8.0) was added to the DNA/RNA pellet, which was then dissolved by heating the tubes at 55ºC for 10 min. Then, 7.35 g of CsCl was added into an empty 50 ml Falcon tube, into which the DNA/RNA/TE mix prepared in the previous step was transferred and mixed well to dissolve. The suspension was centrifuged in the Sorvall GSA rotor at 5 K at 20ºC for 10 min to pellet the clumps of protein and lipid. To an 8.9 ml optiseal tube, 75 µl of 10 mg/ml ethidium bromide was added and the supernatant in the 50 ml Falcon tube was transferred with a pasteur pipette. The volume was adjusted to be just below the neck of the tube, followed by balancing. The tubes were sealed using the black rubber insert and brown caps and centrifuged in the Beckman ultracentrifuge with Ti80 rotor at 58 K at 20ºC for 20 hrs. Once the centrifuge was complete, the plasmid DNA band that is in the middle of the tube was removed with a 10 ml syringe and an 18 G needle. The syringed band was then added into an 8.9 ml optiseal tube containing 20 µl of 10 mg/ml ethidium bromide and the remainder of the tube was filled with TE/CsCl mix. The tube was balanced and sealed as before and centrifuged again in the Beckman ultracentrifuge with Ti80 rotor at 58 K at 22ºC for 20 to 24 hr. The bottom band was syringed as before and placed into a 15 ml Falcon tube, followed by extraction for five times with an equal volume of the top phase of the water-saturated 1-butanol. Each time after extraction, the bottom aqueous phase containing the plasmid DNA was kept. Sterile dH_2O was added to the aqueous DNA solution to make up the total volume to 15 ml, which was then transferred into a 50 ml Falcon tube. Thirty ml of 95 per cent ethanol was added to this tube and mixed well to precipitate the DNA at 4ºC for overnight. The tube was then centrifuged in Sorvall GSA rotor at 5 K at 4ºC for 20 min. The supernatant was discarded and 24 ml of 70 per cent ethanol was added onto the pellet, mixed well and re-centrifuged as before. The

supernatant was again poured off and the tube was inverted on a paper towel for a few minutes. The DNA was dried using Speed Vac and re-suspended in 500 µl of TE (pH 8.0). The concentration of each plasmid DNA was determined by spectrophotometry and the sequence of it was again checked by restriction enzyme analysis as performed in Section 4.10.5.

4.11. Cell Culture

The COS-7 cell line is an African green monkey kidney fibroblast-like cell line growing as monolayers. The line was derived from the CV-1 cell line, a simian cell line (cercopithecus aethiops), by transformation with an origin-defective mutant of SV40. The COS-7 cell line was obtained from American Type Culture Collection and stored as frozen at a concentration of $1x10^6$ to $1x10^7$ cells/ml.

4.11.1. Defrosting the COS-7 Cells

One ml of the frozen cells were rapidly defrosted in a 37ºC water bath and added into a 15 ml sterile tube containing 10 ml of DMEM with glucose, 10 per cent fetal calf serum (FCS), 1 X glutamine and 1 X penicillin/streptomycin. To get rid of the freezing solution containing $DMSO_4$, the cells were centrifuged at 2500 rpm at room temperature for 5 min. The supernatant was discarded, the pellet was re-suspended in fresh medium and the cells were plated into a vented T75 flask with 30 per cent confluency. The cells were then incubated at 37ºC with 5 per cent CO_2.

4.11.2. Passaging the COS-7 Cells

When the T75 plate reached 100 per cent confluency, the medium was sucked off using a cut off sterile 1 ml pipette connected to the vacuum line. The cells in the flask were washed by adding 10 ml of sterile PBS and swirling the PBS around the sides of the flask before sucking off the wash. This step was repeated once. Then 1 ml of 1 X trypsin-EDTA solution was added and discarded after swirling so that it covered all the cells. Subsequently, the cells were incubated at 37ºC for 1 min before hitting the sides of the flask to come off the cells from the flask. Eleven ml of fresh medium was added into the

flask, pipetted up and down five times over the flask area to detach all the cells and make a homogeneous solution ready for aliquoting into other T75 flasks or dishes. The cells were then incubated at 37ºC with 5 per cent CO_2.

4.11.3. Transfection of the COS-7 Cells Using the FuGENE 6 Reagent

The COS-7 cells were transfected with $PLP1^{wt}$, $DM20^{wt}$, $PLP1^{P215S}$, $DM20^{P215S}$, $PLP1^{F232S}$ and $DM20^{F232S}$ constructs in three independent experiments.

Cells in one T75 flask at about 100 per cent confluency were passaged and splitted into six 60 mm dishes at 50 per cent confluency. As the next step, transfection was performed on these freshly trypsinized cells on the same day. For this purpose, six µl of vortexed FuGENE 6 solution was directly added to the 94 µl of DMEM solution in an autoclaved microfuge tube and incubated at room temperature for 5 min. In the meantime, 4 µg of plasmid DNA was added into another sterile microfuge tube. After the 5 min incubation, the DMEM/FuGENE 6 solution was added dropwise to the DNA tube, mixed gently and incubated at room temperature for 15 min. Then the DNA/DMEM/FuGENE 6 solution was gently pipetted around the 60 mm dish containing the COS-7 cells which was rocked from side to side to evenly distribute the DNA/DMEM/FuGENE 6 solution. The cells were then incubated at 37ºC with 5 per cent CO_2 for overnight.

Next morning, after noting the level of confluency of the cells in the 60 mm dish, the cells were passaged as described in Section 4.11.2 and splitted into the 35 mm dish in duplicate. The cells were then incubated at 37ºC with 5 per cent CO_2 for overnight.

4.11.4. Immunocytochemistry

The COS-7 cells were transfected with $PLP1^{wt}$, $DM20^{wt}$, $PLP1^{P215S}$, $DM20^{P215S}$, $PLP1^{F232S}$ and $DM20^{F232S}$ constructs were double-stained using antibody against PLP1 together with antibodies against BiP, LAMP2, Golgin, CHOP, ATF3 or Caspase3 proteins (Table 3.9).

The transfected cells in the 35 mm dishes were washed with 1 ml of pre-warmed DMEM solution. Cells were then fixed in freshly prepared and pre-warmed 2 per cent paraformaldehyde solution for 30 min, followed by washing twice with 1 ml of 1 X TBS containing 0.1 per cent saponin. After the washing solution was discarded, a grease pen was applied around the edge of the 35 mm dish. One hundred µl of blocking solution per dish was added and incubated for 30 min. Any solution with blocking reagents was microfuged at 13 K at room temperature for 2 min before applying on cells. Then, primary antibody diluted in the blocking solution (100 µl/dish) was added. The 35 mm dishes were placed in 150 mm dish with wet paper and incubated for overnight. Next morning, the cells were washed twice with 1 ml of 1 X TBS containing 0.1 per cent saponin for 10 min. Secondary antibody diluted in the blocking solution (100 µl/dish) was added and incubated for 2 hr, followed by washing twice with 1 ml of 1 X TBS containing 0.1 per cent saponin for 10 min. If necessary, tertiary antibody diluted in the blocking solution (100 µl/dish) was added, incubated again for 2 hr and washed for the last time twice with 1 ml of 1 X TBS containing 0.1 per cent saponin for 10 min. DAPI was added in a final concentration of 0.1 µg/ml into the blocking solution together with the secondary or tertiary antibody. Finally, a drop of Vectashield mounting medium was added to the dish and covered with a clean coverslip. Excess antifade was gently sucked off and the coverslip was sealed onto the dish using fingernail polish. After the side of the dish was taken off using a solder iron, cells were examined and pictured using Leica DMRA2 confocal microscope.

5. RESULTS

In order to investigate the molecular basis of PMD, linkage to *PLP1* locus was tested in three families and mutation analysis of *PLP1* and *GJA12* genes was performed for all cases. The two *PLP1* point mutations identified in the study were further investigated to understand their effects on subcellular localization, unfolded protein response pathway, and apoptosis.

5.1. Patients

A total of 25 patients with PMD phenotype from 21 families were analyzed in this study. All cases had been diagnosed as PMD according to the clinical and neuropathological criteria as summarized in Table 5.1. In five of these families, the cases were classified as familial since at least two affected individuals were present. The cases in the remaining 16 families appeared to be non-familial. Parents of these 12 cases were asymptomatic and family history was not available for the other four families. The parents were consanguineous in three of the five familial and five of the 12 sporadic cases.

5.2. Linkage and X Chromosome Inactivation (XCI) Analyses

Analysis of linkage to *PLP1* locus was performed in three PMD families. Members of families were genotyped for 11 different microsatellite DNA markers that have been localized in the Xq21.3-Xq24 region. The haplotypes of the individuals in each family were then determined.

5.2.1. Family F1

A common haplotype was present in all affected individuals in family F1; however, this haplotype was also observed in two asymptomatic sisters in the family (Figure 5.1). Upon this observation, the effect of X chromosome inactivation pattern was analyzed in affected and unaffacted females. The analysis showed that the X chromosome, inherited

from the unaffected father, was active in both affected and asymptomatic siblings (Figure 5.2). This finding led to exclusion of Xq22 locus at least in this family.

Table 5.1. Clinical features of the patients analyzed in this study.

Patient No	Consanguinity	Sex	Current Age (years)	Onset Age of Nystagmus	Course of Nystagmus	Onset Age of Stridor	Dysphagia
F1.3	+	M	11	Congenital	Same	Absent	Absent
F2.3	+	F	16	1,5 years	Same	Absent	Absent
F3.3	+	M	11	2 months	Same	Absent	Absent
F4.3	-	M	14	Congenital	Same	Absent	Absent
F5.3	-	M	?	?	?	?	?
F6.3	+	M	14	3 months	Same	Absent	Absent
F7.3	-	M	16	1 month	Decreasing	Absent	Absent
F8.3	+	M	?	?	?	?	?
F9.3	-	M	26	Absent	Absent	Absent	Absent
F10.3	+	M	16	Congenital	Decreasing	Absent	Absent
F10.4	+	M	14	Congenital	Same	Absent	Absent
F11.3	-	M	11	1,5 years	Decreasing	Absent	Absent
F12.3	-	F	12	3 months	Same	Absent	Present
F13.3	+	M	25	?	Decreasing	Absent	Absent
F14.3	?	M	15	Congenital	Decreasing	Absent	Present
F15.3	-	M	4	Congenital	Decreasing	2 years	Present
F16.3	?	M	5	2 months	Decreasing	Congenital	Present
F17.3	+	F	16	1 year	Decreasing	Absent	Absent
F17.4	+	F	died at 14	1 year	Decreasing	Absent	Absent
F18.3	+	M	14	Congenital	Decreasing	Absent	Absent
F19.3	-	M	4	2,5 months	Same	Absent	Absent
F20.3	-	M	5	Congenital	Same	Absent	Absent
F21.3	-	F	6	Congenital	Same	Absent	Absent
F22.3	?	M	27	Absent	Absent	Absent	Absent
F23.3	+	M	4	Congenital	Decreasing	Absent	Absent

5.2.2. Family F10

The two affected brothers in the second family (F10), born to unaffected consanguineous parents, were found to inherit different maternal haplotypes for the Xq22

locus (Figure 5.3). Thus, linkage to Xq22 was excluded in the family. X chromosome inactivation analysis was not performed since both patients were hemizygous for the locus.

5.2.3. Family F17

The two affected sisters in the third family (F17), born to unaffected parents, were also found to inherit different maternal haplotypes for the Xq22 locus (Figure 5.4). X inactivation analysis revealed that the active chromosome in the affected sisters was the maternal one which was also active in the asymptomatic mother (Figure 5.5).

5.2.4. Lod Score Analysis

Statistical evaluation of the genotype data was performed by lod score analysis. Two-point lod-score values between the PMD locus and each of the marker loci are given in Table 5.2. Lod score values at $\theta = 0.00$ for most of the markers tested were less than -2 in the families studied. Thus, lod score analysis excluded linkage to the Xq22 locus in these families and confirmed the results of haplotype analysis. The results also confirmed X chromosome inactivation data in families F1 and F17.

5.3. Screening of *PLP1* for Duplications and Deletions

Duplications of the *PLP1* locus are the most common cause of PMD phenotype. For this reason, identification of the duplications in our cohort of patients was the first step to unravel the basis of the disease. Deletions constitute less than one per cent of the *PLP1* mutations, but can be detected by the same methods as for duplications. Four different approaches were used for the identification of duplications/deletions in the patients; RFLP analysis, quantitative fluorescent multiplex PCR, FISH, and quantitative real-time PCR.

5.3.1. RFLP Analysis

Heterozygosity for the appropriate RFLP markers in male patients would prove the presence of the *PLP1* duplication. However, restriction analysis revealed that none of the male patients in our cohort was heterozygote for the PLP4/*Aha*II and DXS17/*Taq*I

polymorphisms (Figure 5.6; Table 5.3). Presence of *Aha*II restriction site in 227 bp region produces 183 and 44 bp restriction fragments. Only F17.3 was heterozygous for the locus among the female patients, F3.3, F12.3, F17.3, and F17.4. *Taq*I digestion of the 620 bp PCR product revealed 400 and 220 bp restriction fragments. None of the female patients were informative for *Taq*I restriction site.

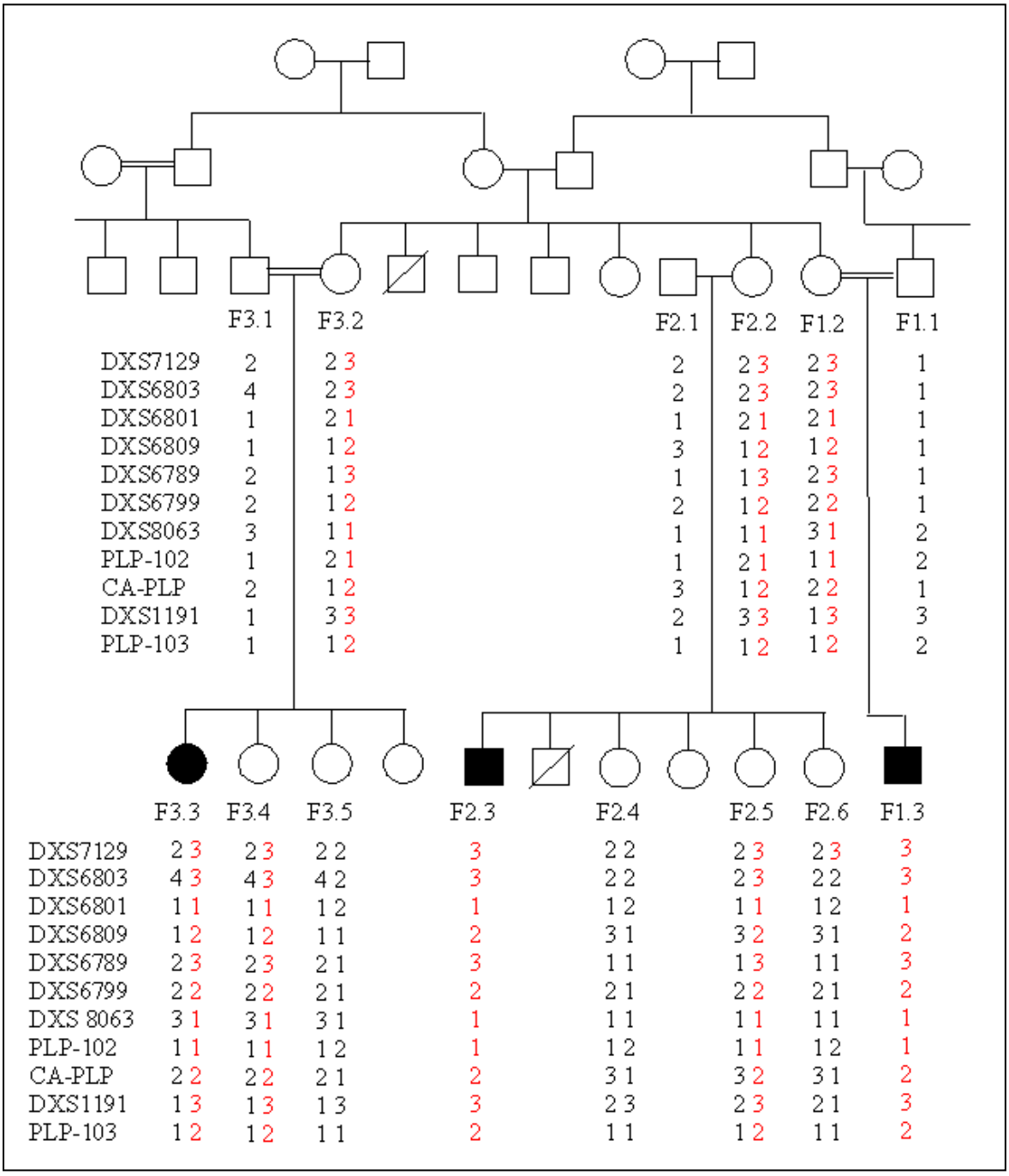

Figure 5.1. Haplotypes of the members of family F1 for the *PLP1* markers.

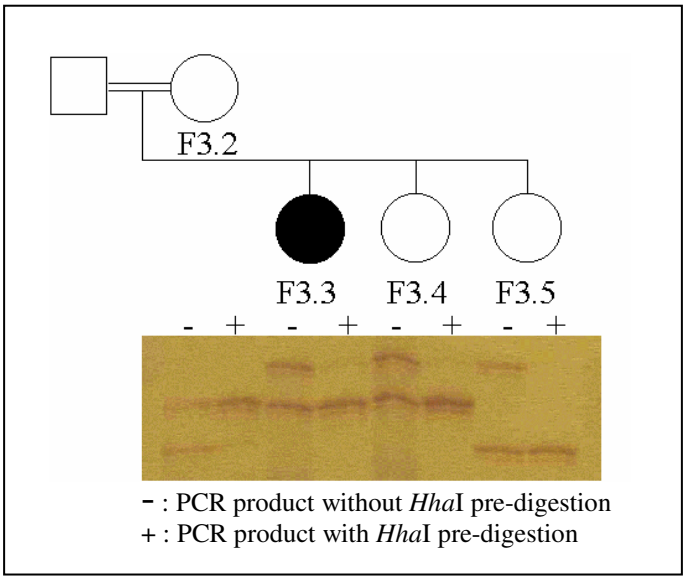

Figure 5.2. X inactivation analysis for family F1.

5.3.2. Interphase FISH Analysis

FISH analysis was performed using the biotin-labeled centromeric probe (cU144A10) and digoxigenin-labeled PLP1 cosmid (cU125A1). The control probe cU144A10 was visualized with the green fluochrome avidin-fluorescein and PLP1 probe cU125A1 was observed in red with rhodamine amplified with texas red. In male patients, 2:1 red:green signal ratio revealed the presence of the duplication. At least 100 nuclei were evaluated for each patient and the duplication was accepted to be present if 2:1 red:green signal ratio was identified in 70 per cent of the interphase nuclei analyzed (Table 5.4).

Duplication of the *PLP1* locus was identified in seven male patients among the cohort of 21 families. In Figure 5.7, duplications detected in four of these patients are represented. All male patients tested negative for *PLP1* deletions. Neither duplications nor deletions were detected in any of the five female patients.

5.3.3. Quantitative Fluorescent Multiplex PCR Analysis

Two PLP1:PRNP ratio values (PM7:PRNP and CA-PLP:PRNP) were generated for each control sample (Appendix A). The values were plotted against each other and are shown in Figure 5.8. For male controls the values were expected to cluster at the

coordinates of 0.5:0.5 and for females at 1.0:1.0. Although clustering of values for male controls was more distinct than that of females, the coordinate for the PM7/PRNP ratio shifted to a value of 1 to 2 in males. The distribution was even much wider for the female controls. Thus, a significant clustering of the ratios could not be observed and further analysis for patient screening was not performed with this method.

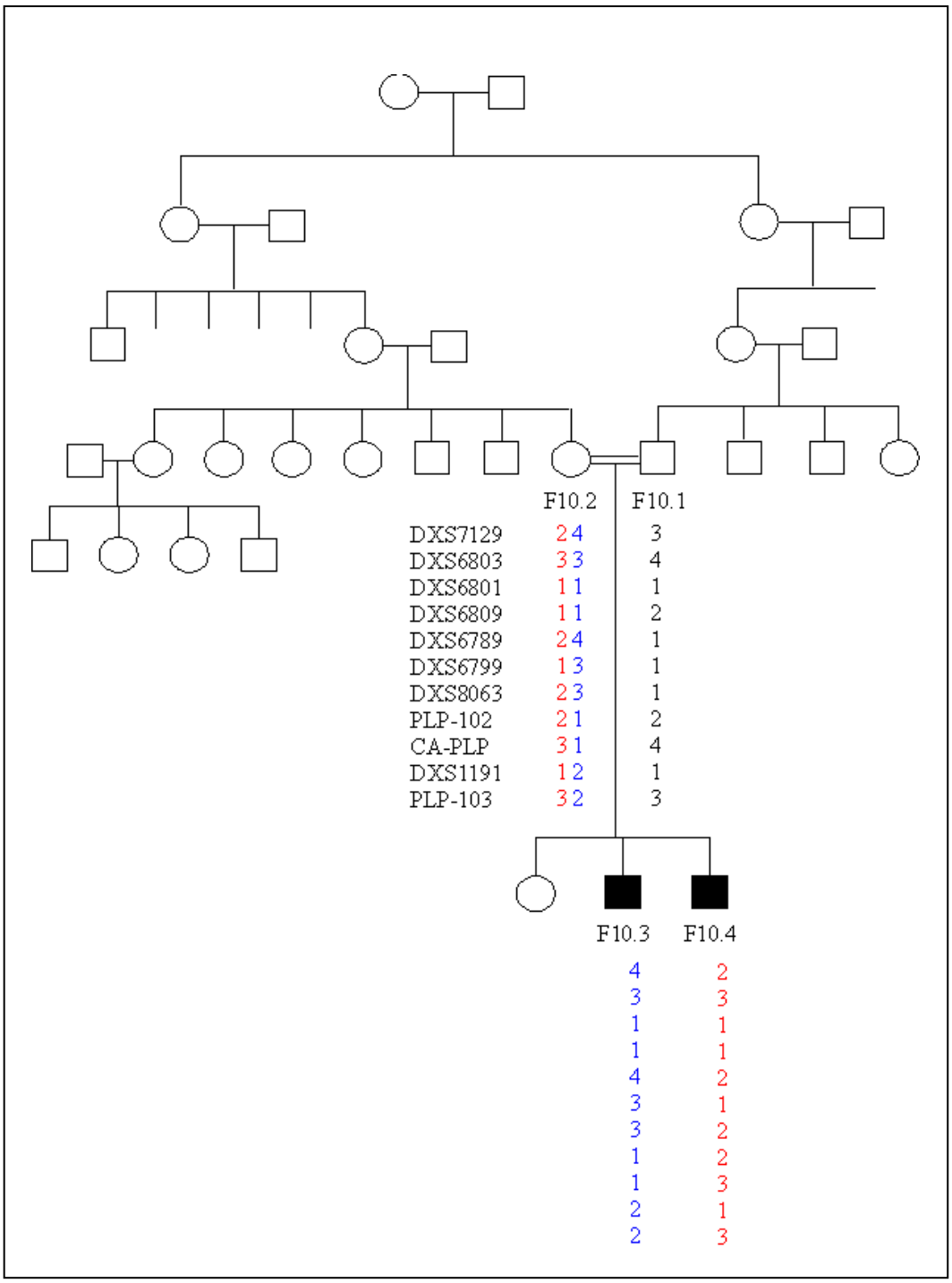

Figure 5.3. Haplotypes of the members of family F10 for the *PLP1* markers.

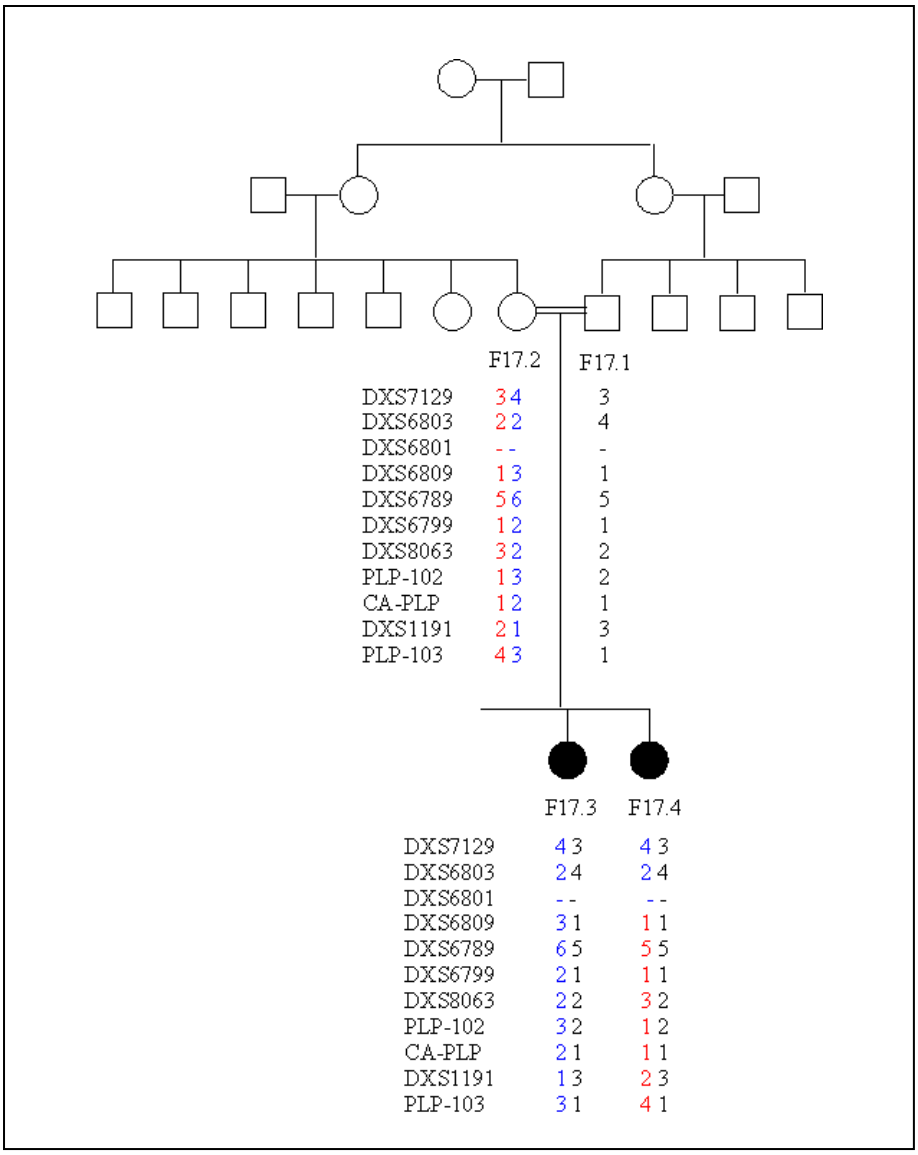

Figure 5.4. Haplotypes of the members of family F17 for the *PLP1* markers.

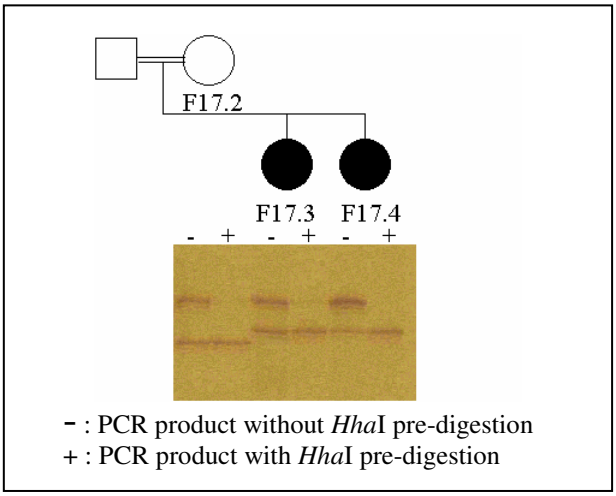

Figure 5.5. X inactivation analysis for family F17.

Table 5.2. Two-point lod scores for *PLP1* markers in families F1, F10 and F17.

Family	Locus	Lod score at θ=								
		0.00	0.01	0.05	0.10	0.20	0.30	0.40	Z_{max}	θ_{max}
F1	DXS7129	-∞	-0.57	0.03	0.20	0.23	0.15	0.04	0.23	0.20
	DXS6803	-∞	-0.57	0.03	0.20	0.23	0.15	0.04	0.23	0.20
	DXS6801	-∞	-0.57	0.03	0.20	0.23	0.15	0.04	0.23	0.20
	DXS6809	-∞	-0.57	0.03	0.20	0.23	0.15	0.04	0.23	0.20
	DXS6789	-∞	-0.72	-0.09	0.12	0.21	0.17	0.08	0.21	0.20
	DXS6799	-∞	-1.02	-0.37	-0.14	0.02	0.05	0.03	0.05	0.30
	DXS8063	0.09	0.09	0.07	0.06	0.04	0.03	0.02	0.09	0.00
	PLP-102	-∞	-1.02	-0.37	-0.14	0.02	0.05	0.03	0.05	0.30
	CA-PLP	-∞	-1.02	0.37	-0.14	0.02	0.05	0.03	0.05	0.30
	DXS1191	-∞	-∞	-∞	-∞	-∞	-∞	-∞	0.00	0.50
	PLP-103	-∞	-∞	-∞	-∞	-∞	-∞	-∞	0.00	0.50
F10	DXS7129	-∞	-1.47	-0.78	-0.50	-0.23	-0.09	-0.03	0.00	0.50
	DXS6803	-0.07	-0.07	-0.06	-0.05	-0.03	-0.02	-0.01	0.00	0.50
	DXS6801	0.22	0.22	0.20	0.18	0.12	0.07	0.03	0.22	0.00
	DXS6809	-0.07	-0.07	-0.06	-0.05	-0.03	-0.02	-0.01	0.00	0.50
	DXS6789	-∞	-1.47	-0.78	-0.50	-0.23	-0.09	-0.03	0.00	0.50
	DXS6799	-∞	-1.26	-0.59	-0.33	-0.12	-0.03	0.00	0.00	0.40
	DXS8063	-∞	-1.47	-0.78	-0.50	-0.23	-0.09	-0.03	0.00	0.50
	PLP-102	-∞	-1.26	-0.59	-0.33	-0.12	-0.03	0.00	0.00	0.40
	CA-PLP	-∞	-1.47	-0.78	-0.50	-0.23	-0.09	-0.03	0.00	0.50
	DXS1191	-∞	-1.26	-0.59	-0.33	-0.12	-0.03	0.00	0.00	0.40
	PLP-103	-∞	-1.26	-0.59	-0.33	-0.12	-0.03	0.00	0.00	0.40
F17	DXS7129	-5.27	-1.59	-0.90	-0.62	-0.37	-0.24	-0.13	0.00	0.50
	DXS6803	-4.97	-1.29	-0.62	-0.36	-0.14	-0.04	-0.00	0.00	0.50
	DXS6801	0.00	0.00	0.00	0.00	0.00	0.00	0.00	0.00	0.00
	DXS6809	-∞	-1.11	-0.48	-0.25	-0.09	-0.04	-0.01	0.00	0.50
	DXS6789	-∞	-1.11	-0.48	-0.25	-0.09	-0.04	-0.01	0.00	0.50
	DXS6799	-∞	-1.11	-0.48	-0.25	-0.09	-0.04	-0.01	0.00	0.50
	DXS8063	-∞	-1.11	-0.48	-0.25	-0.09	-0.04	-0.01	0.00	0.50
	PLP-102	-∞	-2.69	-1.34	-0.80	-0.33	-0.12	-0.02	0.00	0.50
	CA-PLP	-∞	-1.11	-0.48	-0.25	-0.09	-0.04	-0.01	0.00	0.50
	DXS1191	-∞	-2.69	-1.34	-0.80	-0.33	-0.12	-0.02	0.00	0.50
	PLP-103	-∞	-2.69	-1.34	-0.80	-0.33	-0.12	-0.02	0.00	0.50

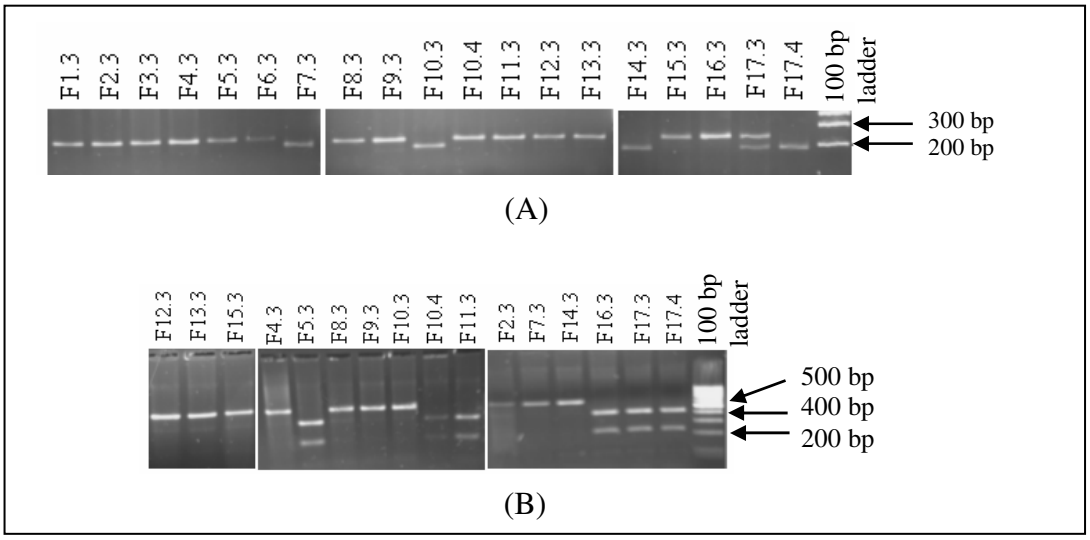

Figure 5.6. Restriction analyses for the *Aha*II (A) and *Taq*I (B) polymorphisms.

Table 5.3. Alleles obtained in the RFLP study (* female).

Patient No	Alleles for PLP4/*Aha*II Marker		Alleles for DXS17/*Taq*I Marker	
	227 bp	183 bp, 44 bp	620 bp	400 bp, 220 bp
F1.3	+		+	
F2.3	+		+	
F3.3*	+		+	
F4.3	+		+	
F5.3	+			+
F6.3	+		+	
F7.3		+	+	
F8.3	+		+	
F9.3	+		+	
F10.3		+	+	
F10.4	+			+
F11.3	+			+
F12.3*	+		+	
F13.3	+		+	
F14.3		+	+	
F15.3	+		+	
F16.3	+			+
F17.3*	+	+		+
F17.4*		+		+
F18.3	+		+	
F19.3		+	+	
F20.3	+		+	
F21.3*	+	+	+	
F22.3	+		+	
F23.3		+	+	

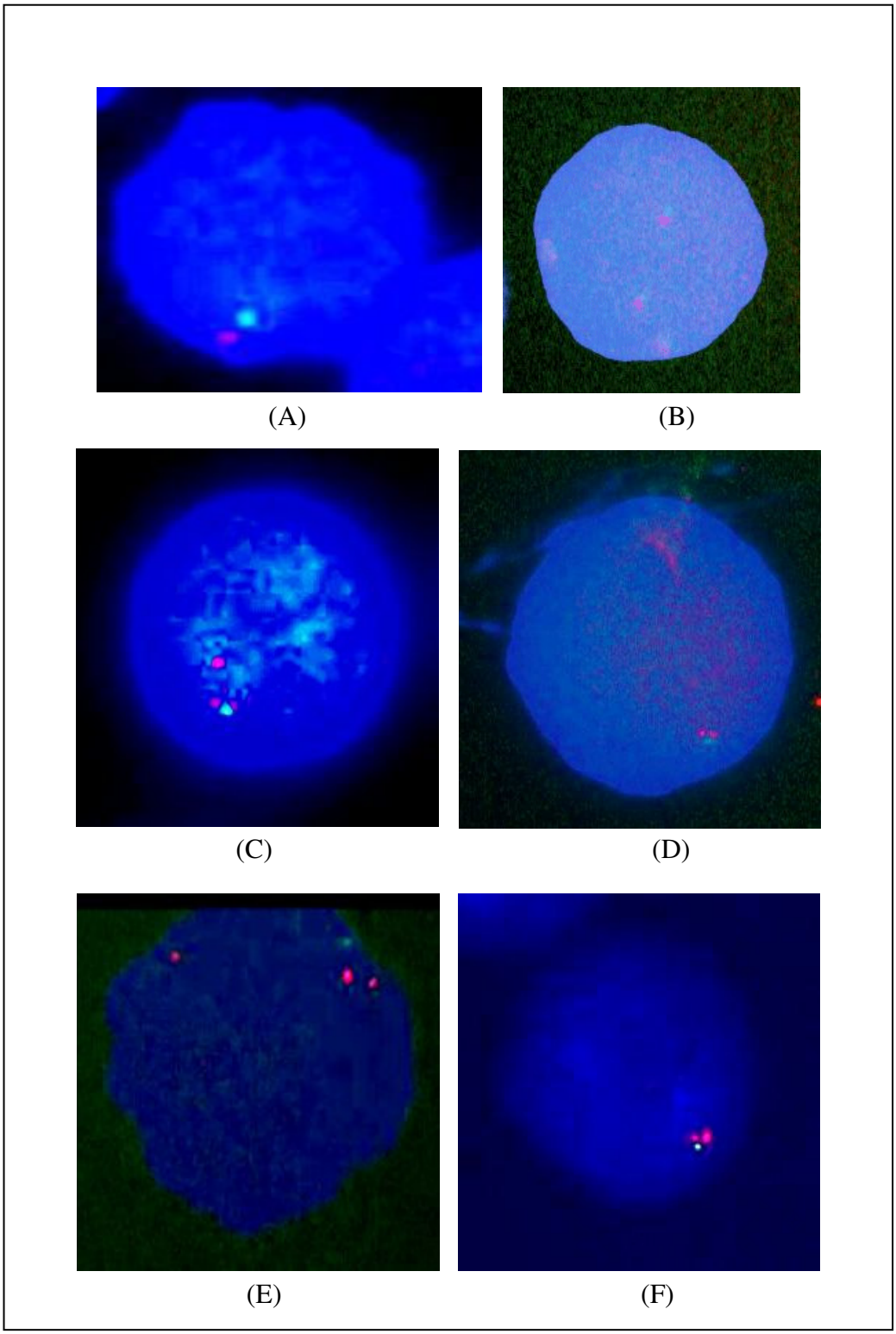

Figure 5.7. Interphase FISH images of a male control (A), a female control (B), and the male PMD patients F4.3 (C), F13.3 (D), F14.3 (E) and F19.3 (F) carrying the *PLP1* duplication (X 1000). The 2:1 red:green (PLP1 probe:control probe) signal ratio indicates the presence of the duplication in males.

Table 5.4. Red:green signal ratios obtained in the FISH analysis (* female).

Patient No	Number of Nuclei Analyzed	1:1 Red:Green Ratio (per cent)	2:1 Red:Green Ratio (per cent)	2:2 Red:Green Ratio (per cent)	3:2 Red:Green Ratio (per cent)	Presence of *PLP1* Duplication
F1.3	103	73	1	19	7	(-)
F2.3	125	72	13	6	9	(-)
F3.3*	112	12	5	69	14	(-)
F4.3	107	14	77	6	3	(+)
F5.3	101	70	12	11	7	(-)
F6.3	110	75	9	13	3	(-)
F7.3	105	72	0	24	4	(-)
F8.3	129	71	13	16	0	(-)
F9.3	116	8	76	5	11	(+)
F10.3	111	78	10	12	0	(-)
F10.4	112	70	17	6	7	(-)
F11.3	105	1	68	14	17	(+)
F12.3*	104	19	7	74	0	(-)
F13.3	109	8	73	7	12	(+)
F14.3	106	23	74	0	3	(+)
F15.3	102	91	0	8	1	(-)
F16.3	107	80	7	6	7	(-)
F17.3*	110	20	0	72	8	(-)
F17.4*	104	10	8	77	5	(-)
F18.3	126	71	12	3	14	(-)
F19.3	101	10	72	15	3	(+)
F20.3	100	6	75	5	14	(+)
F21.3*	108	11	0	84	5	(-)
F22.3	115	71	5	22	2	(-)
F23.3	119	72	10	16	2	(-)

5.3.4. Quantitative Real -Time PCR Analysis

Quantitative PCR was performed in our laboratory using Light Cycler (Roche). The ratios between the target regions, PLP-3 or PLP-6, and the reference region (PRX-6) were determined by the relative quantitative analysis program of the Light Cycler software. The results obtained are presented in Figure 5.9. The analysis confirmed the presence of the

PLP1 duplications in patients F4.3, F9.3, F19.3, and F20.3 that were previously identified by FISH analysis. Patients F11.3, F13.3, and F14.3 tested negative for the duplication in this analysis although they were found to have duplications with FISH method.

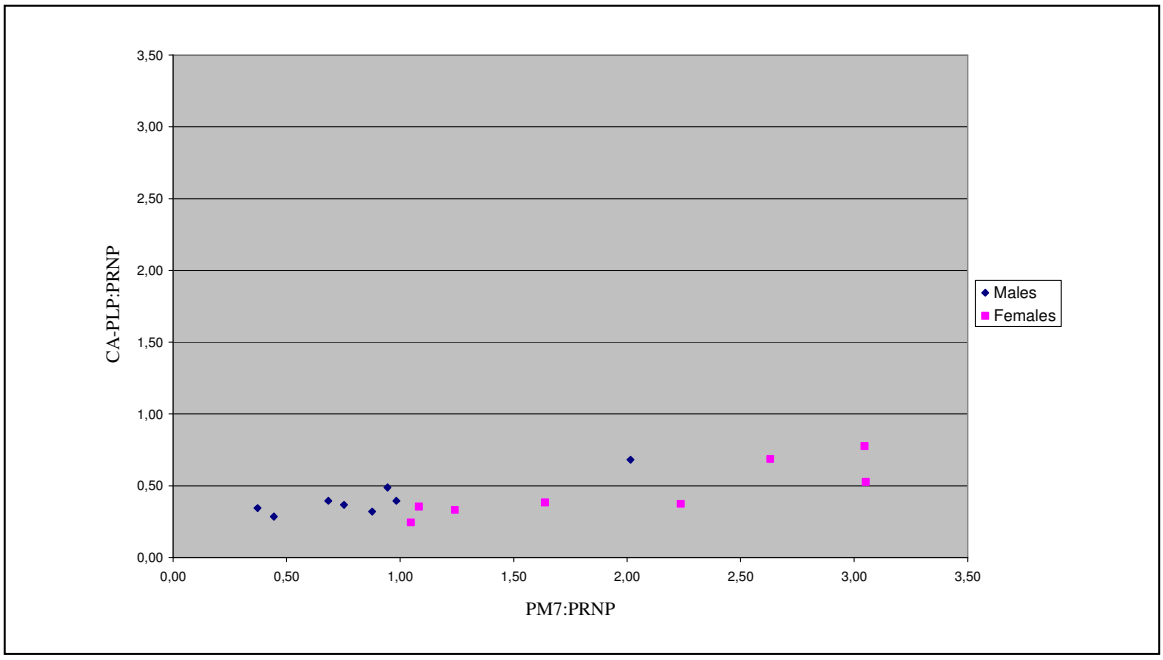

Figure 5.8. Plot of PM7:PRNP ratio against CA-PLP:PRNP ratio obtained by quantitative PCR for male and female controls.

5.4. Mutation Analysis

The PMD patients in our cohort were also investigated for the presence of point mutations within the *PLP1* and *GJA12* genes. Mutation screening was performed by SSCP analysis of the exons, exon-intron boundaries, and promoter region of the genes. Four altered migration patterns in the *PLP1* and six in the *GJA12* genes were identified. Sequence variations identified in our cohort of patients are summarized in Table 5.5.

5.4.1. Analysis of the *PLP1* Gene

The altered migration patterns observed in patients F7.3, F10.3, F14.3, F17.3, and F17.4 in the SSCP analysis of exon 4 of the *PLP1* gene were consistent with the results of RFLP analysis, showing that these altered patterns were due to the *Aha*II polymorphism (Figure 5.10).

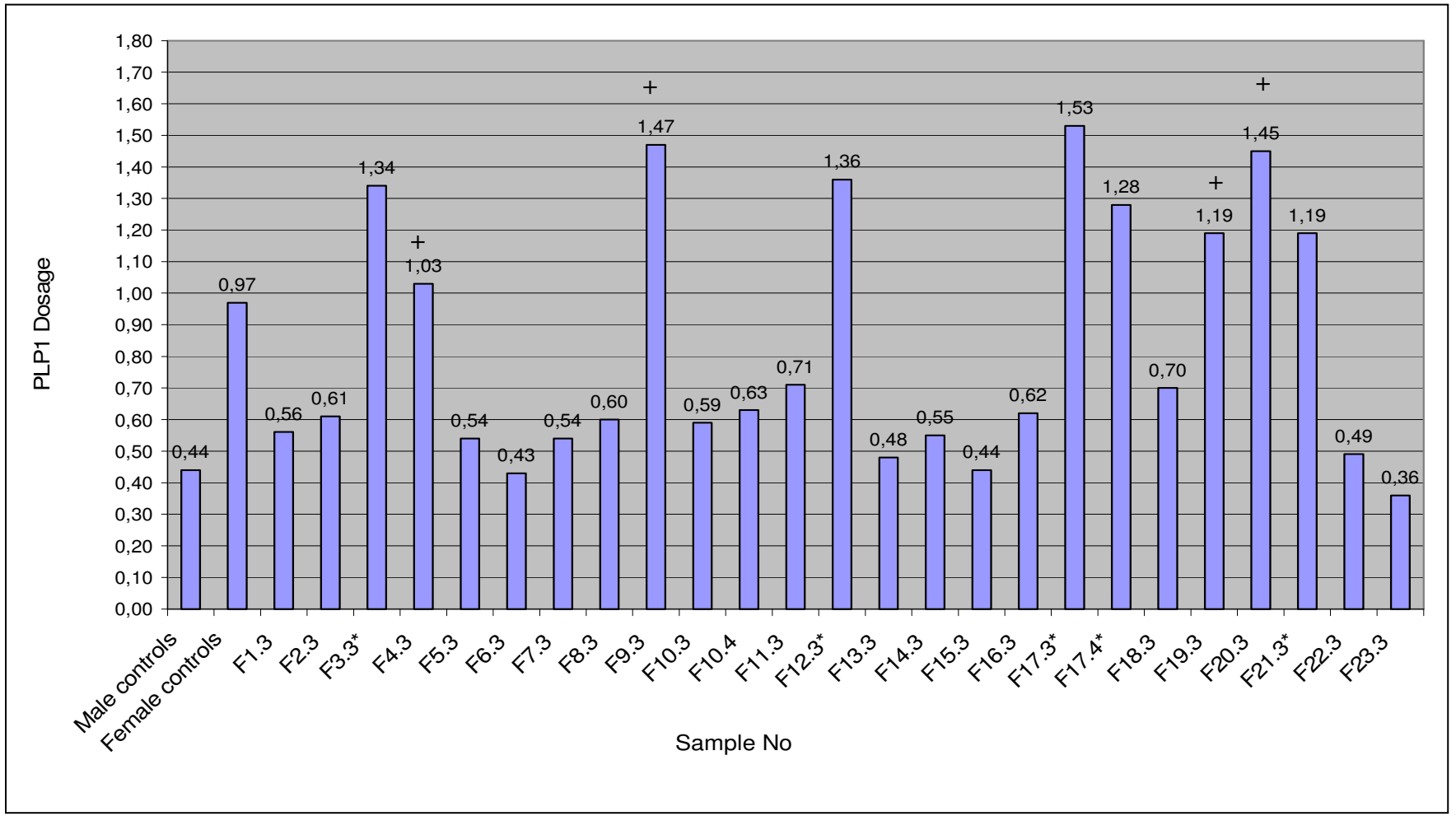

Figure 5.9. Representative results of the quantitative real-time PCR. The mean ratio was 0.44 ± 0.34 for the male control group and 0.97 ± 0.23 for the female one. + denotes the cases with *PLP1* duplication, with $p < 0.001$ by Student's *t* test as compared with the mean value for male controls. * stands for the female patients.

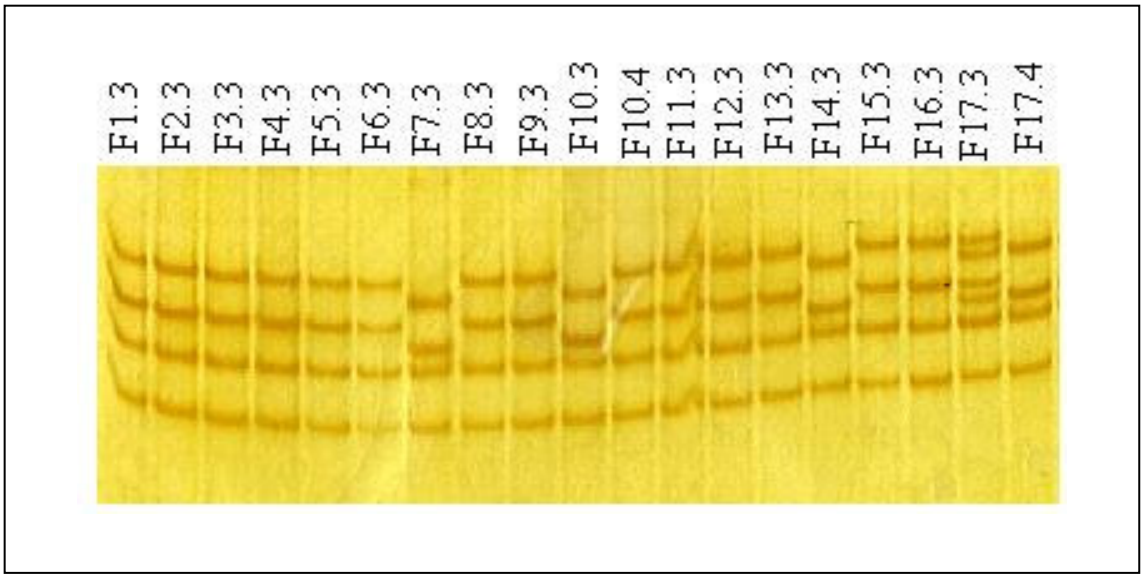

Figure 5.10. SSCP gel for screening of exon 4 of the *PLP1* gene.

5.4.1.1. Family F15. Sequencing analysis of exon 5 in patient F15.3 revealed a previously reported C→T transition at nucleotide position 643 in hemizygous condition (Figure 5.11; Figure 5.12). Restriction enzyme analysis confirmed the presence of the mutation in the patient. In the same analysis, his mother was found to be heterozygous for the mutation (Figure 5.13). The mutation abolishes the restriction site for the enzyme *Mva*I resulting in a 316-bp fragment instead of 200- and 116-bp fragments. The 643 C→T change results in the substitution of proline to serine residue at position 215 that is located in the second extracellular domain.

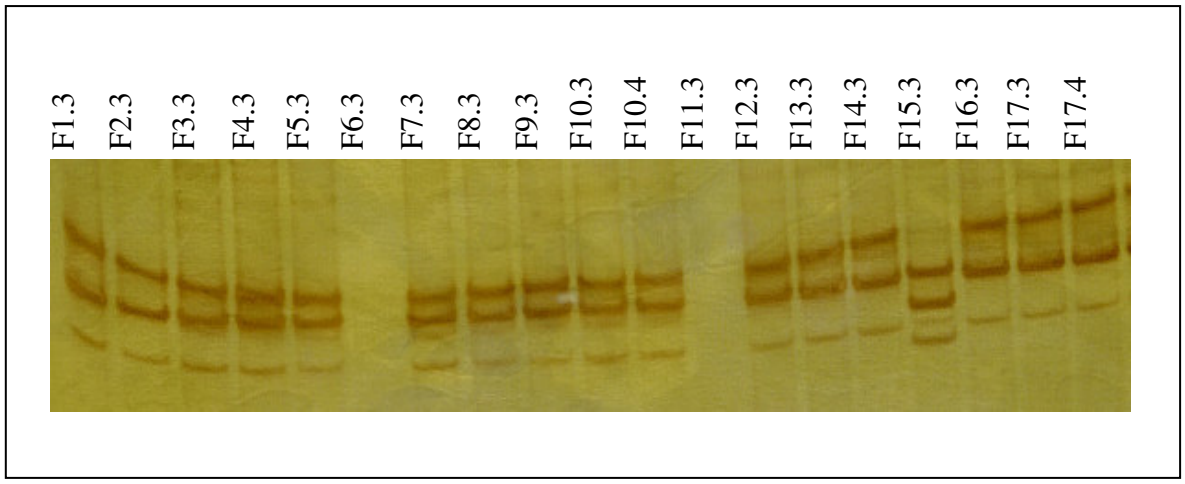

Figure 5.11. SSCP gel for screening of exon 5 of the *PLP1* gene.

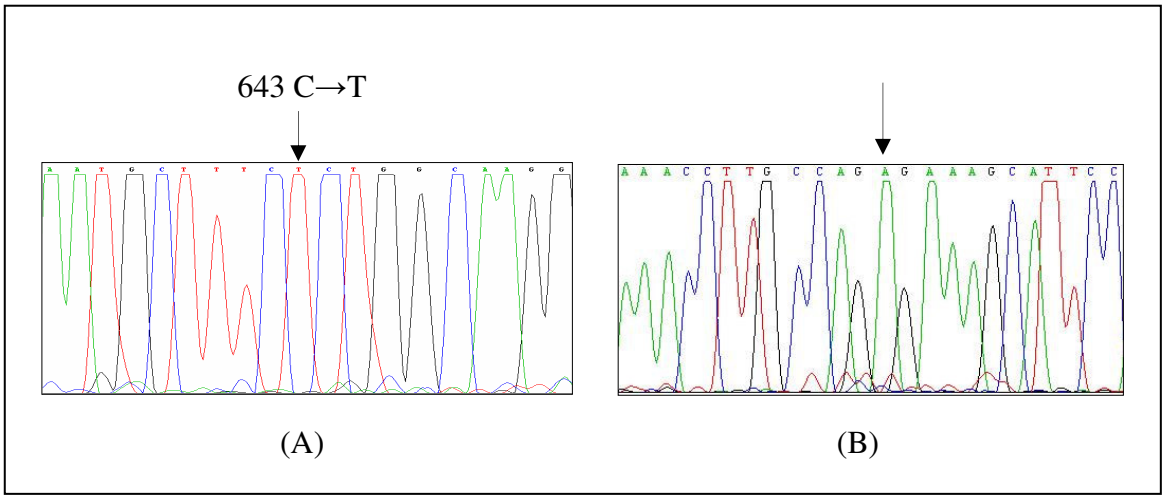

Figure 5.12. Chromatograms showing sequencing profile of the *PLP1* gene in hemizygous patient F15.3 for the sense (A) and anti-sense (B) strands.

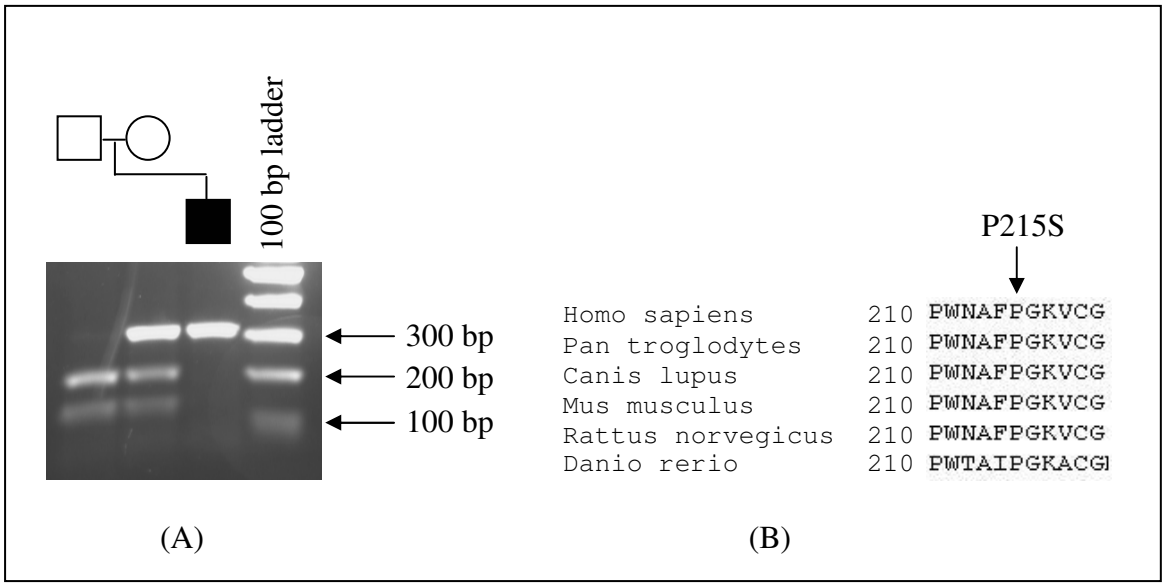

Figure 5.13. *Mva*I restriction analysis in family F15 (A) and alignment of the selected region of human *PLP1* region with orthologs of other species (B).

5.4.1.2. Family F16. A novel transition (T→C) at nucleotide position 695 in exon 6 of the *PLP1* gene was identified in patient F16.3 by sequencing both strands (Figure 5.14; Figure 5.15). This mutation leads to the change of the phenylalanine to serine at codon 232 which resides in the second extracellular loop. The mutation creates an *Bsm*FI site in 264 bp PCR product of exon 6, resulting in 180 and 84 bp fragments in the mutant. Restriction analysis with the enzyme revealed that the parents were negative for the mutation (Figure 5.16).

Absence of the restriction site in 25 normal female and 25 normal male individuals proved that the variation is pathogenic.

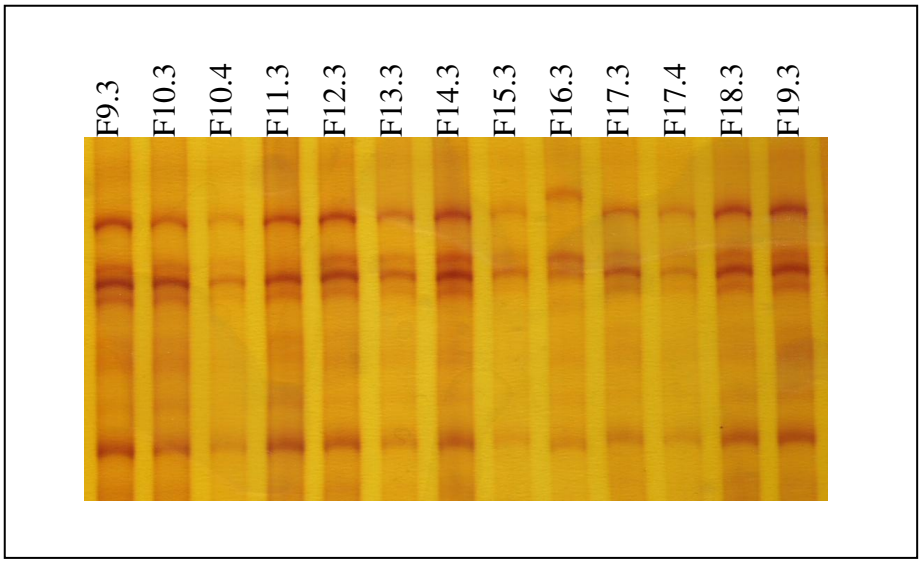

Figure 5.14. SSCP gel for screening of exon 6 of the *PLP1* gene.

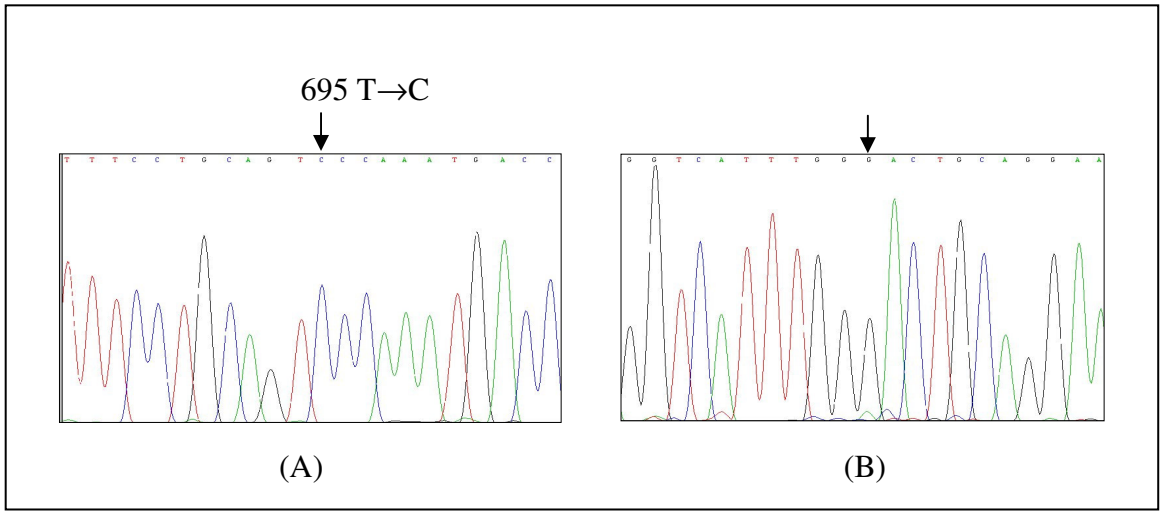

Figure 5.15. Chromatograms showing sequencing profile of the *PLP1* gene in hemizygous patient F16.3 for the sense (A) and anti-sense (B) strands.

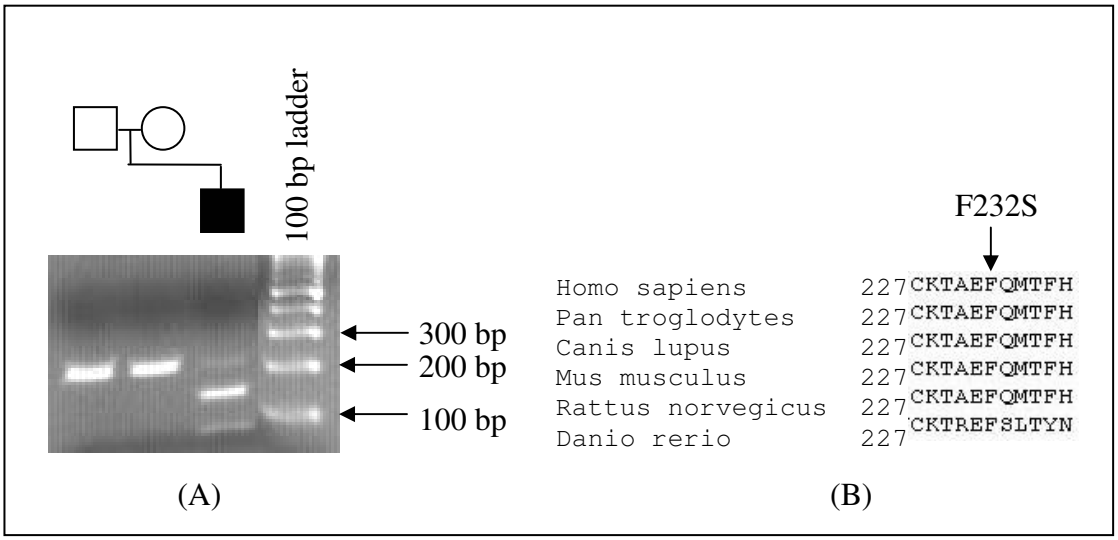

Figure 5.16. *Bsm*FI restriction analysis in family F16 (A) and alignment of the selected region of human *PLP1* region with orthologs of other species (B).

5.4.2. Analysis of the *GJA12* Gene

In six of the PMD families, alterations in the *GJA12* gene were identified.

5.4.2.1. Family F1. In family F1 for which linkage to the *PLP1* gene was excluded, a deletion of 17 bp (546-542del) was identified in the third fragment of the only *GJA12* exon (Figure 5.17; Figure 5.18). The mutation, V182fs257X, hypothetically, causes production of a 256 amino acid long truncated protein with loss of fourth transmembrane and intracellular carboxy terminal domains.

The mutation abolishes the *Hha*I restriction site in the 330 bp PCR product and results in production of a 69 bp fragment in the 313 bp mutant product. *Hha*I restriction analysis in family F1 revealed that the parents and the healthy siblings, with the exception of F2.6, were heterozygous whereas all three affected individuals were homozygous for the mutation (Figure 5.19). Screening of 100 normal chromosomes using the same technique revealed absence of the variation in the population. These findings confirm that the mutation was responsible for the disease phenotype in the family.

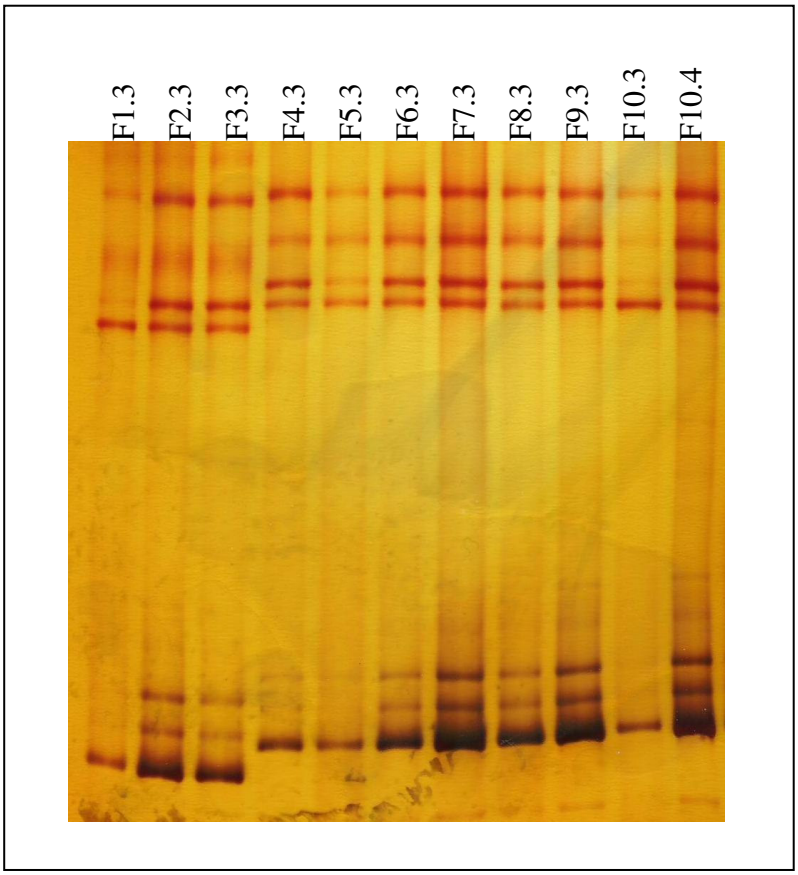

Figure 5.17. SSCP gel for screening of fragment 3 of the *GJA12* gene.

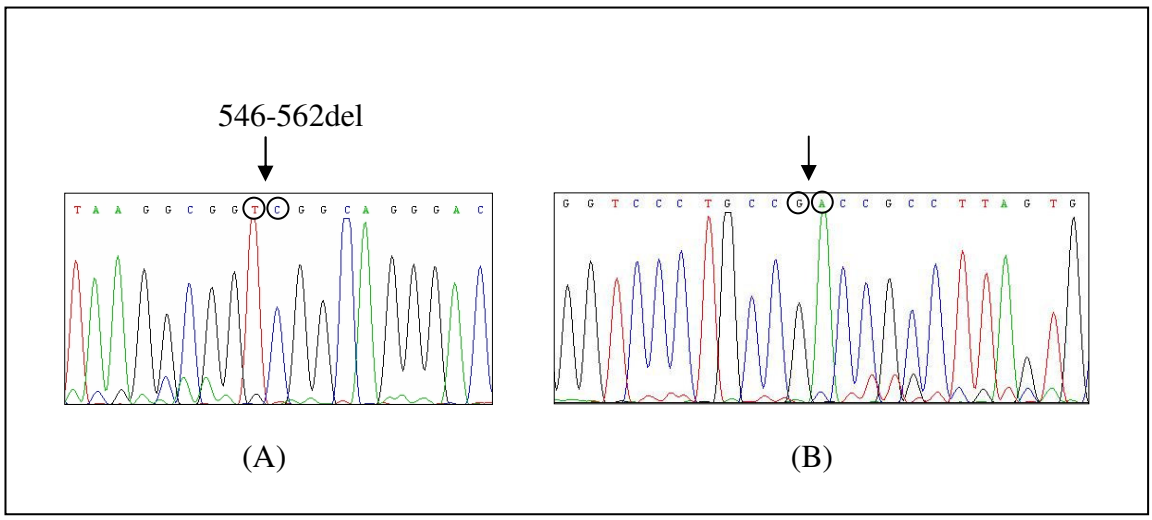

Figure 5.18. Chromatograms showing sequencing profile of the *GJA12* gene in patient F1.3 for the sense (A) and anti-sense (B) strands.

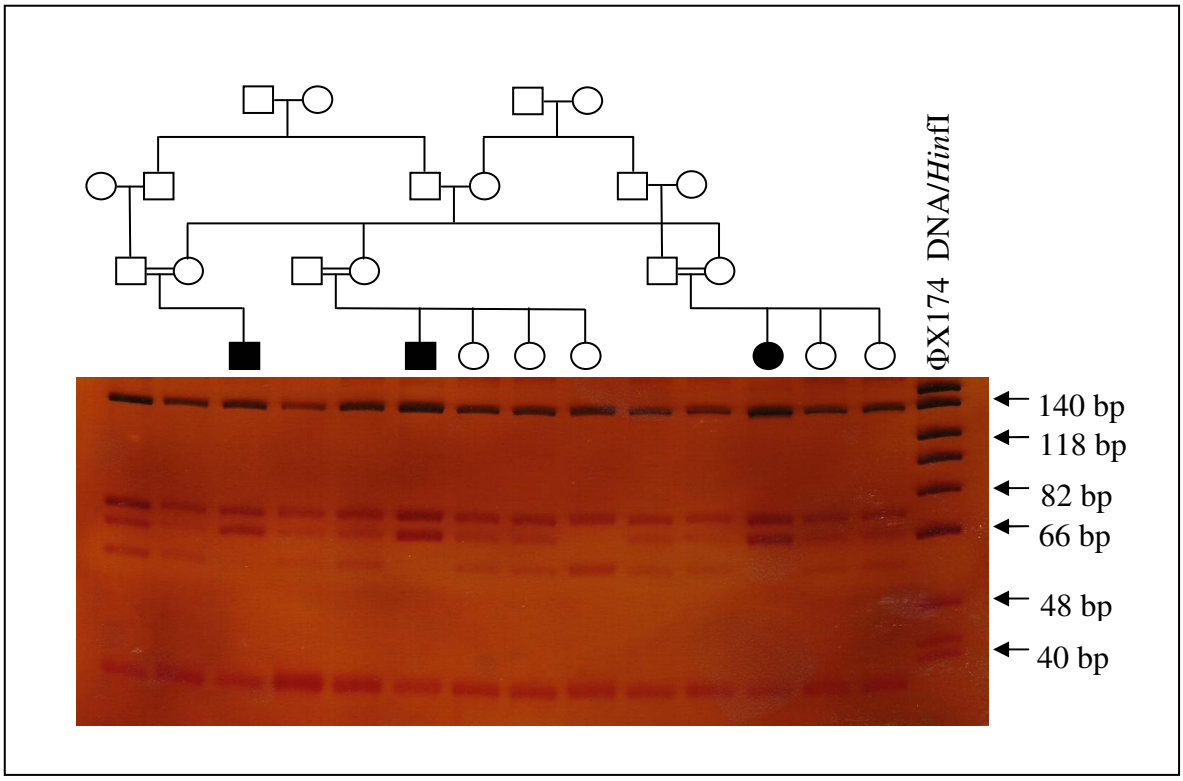

Figure 5.19. *Hha*I restriction analysis in family F1.

5.4.2.2. Family F7. The SSC polymorphism detected in patient F7.3 (Figure 5.20) revealed presence of a heterozygous 706G→C variation upon sequencing of fragment 4 (Figure 5.21). The nucleotide change leads to substitution of glycine at position 236 with arginine (G236R) in the second extracellular domain of the protein. The residue affected by this mutation is highly conserved among different species (Figure 5.22).

The nucleotide change creates an *Aci*I restriction site resulting in 90 and 33 bp fragments instead of 123 bp. The restriction analysis revealed that patient F7.3 and his father were heterozygous for the mutation whereas his mother did not carry the mutation (Figure 5.23A). The segregation of the mutant allele in the family was further confirmed by SSCP analysis (Figure 5.23B). Screening of 50 normal individuals for this variation showed that none of them had the mutant allele.

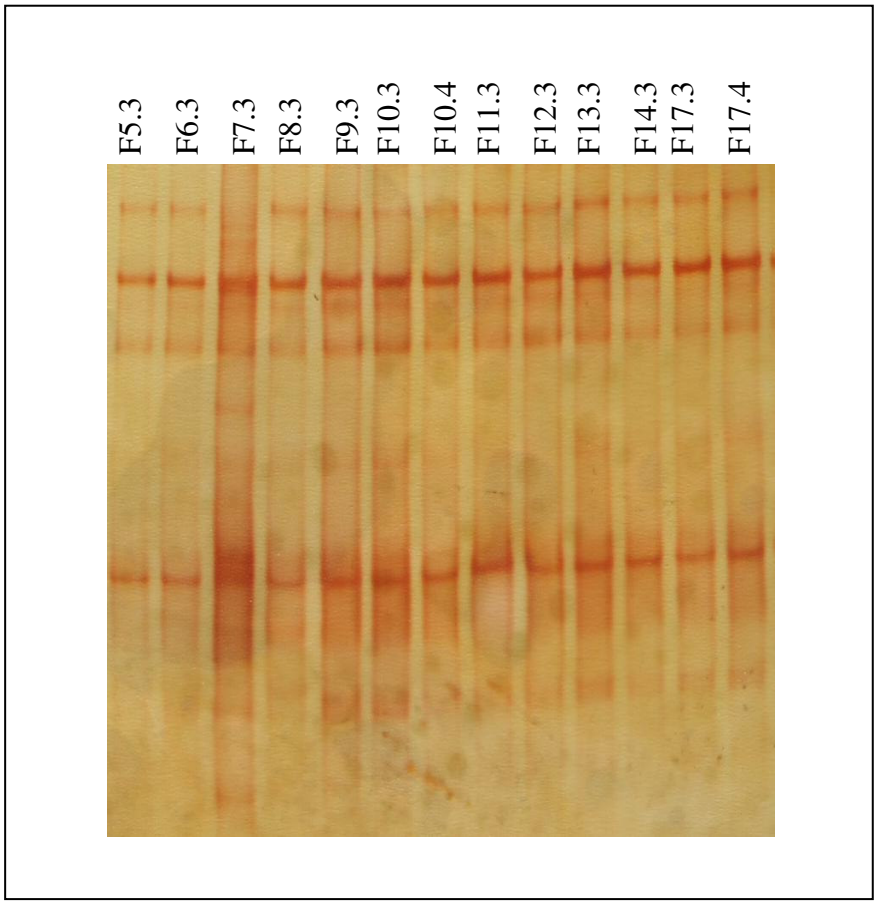

Figure 5.20. SSCP gel for screening of fragment 4 of the *GJA12* gene.

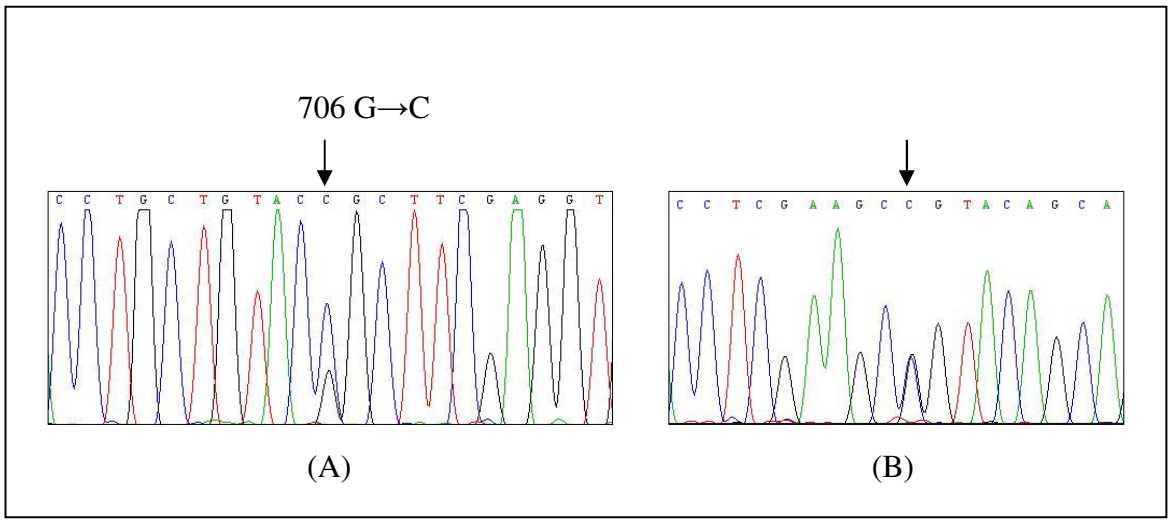

Figure 5.21. Chromatograms showing sequencing profile of the *GJA12* gene in patient F7.3 for the sense (A) and anti-sense (B) strands.

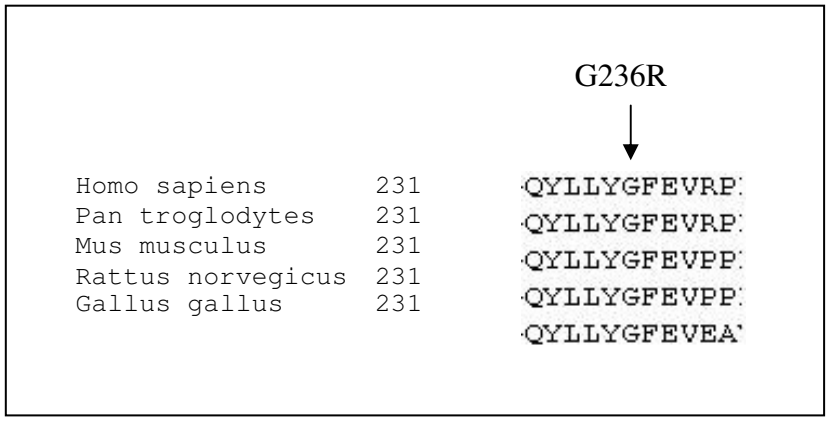

Figure 5.22. Alignment of the selected region of human *GJA*12 region with orthologs of other species.

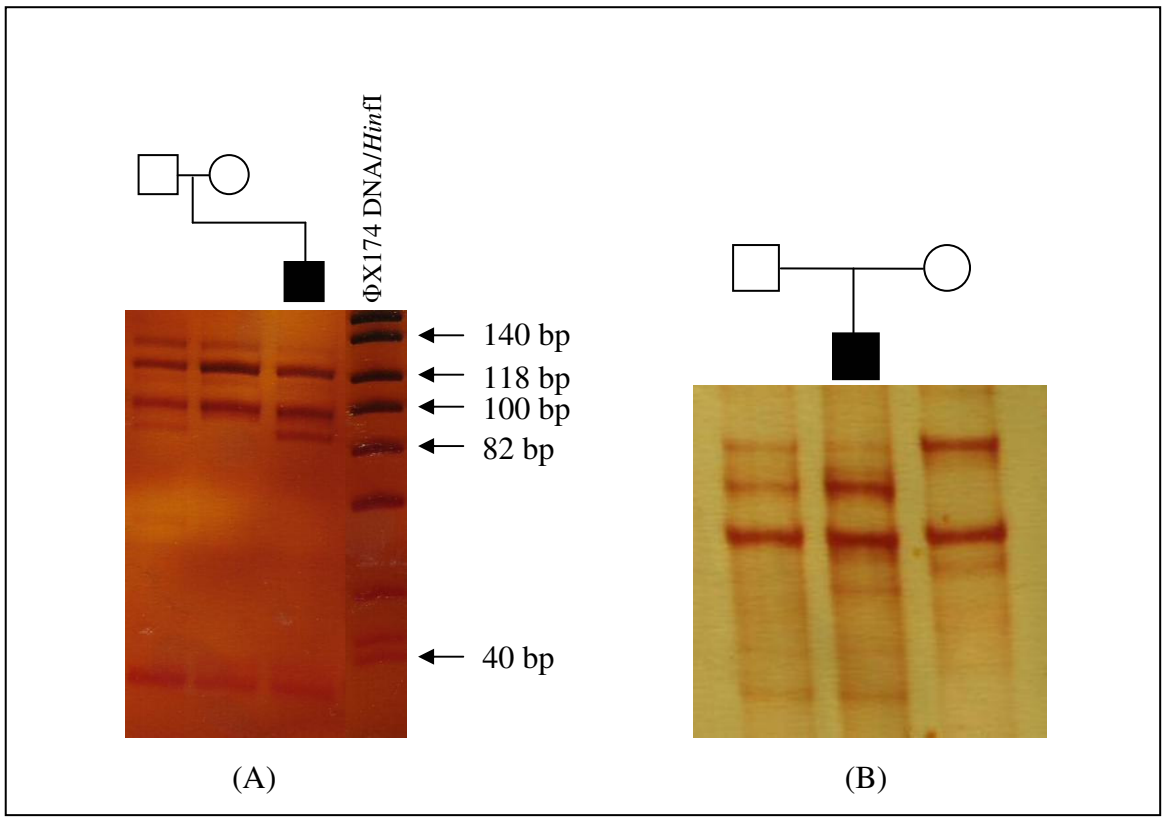

Figure 5.23. *Aci*I restriction analysis (A) and SSC polymorphisms in fragment 4 of the *GJA12* gene (B) in family F7.

5.4.2.3. Family F12. A T→G variation at nucleotide 284 was identified in fragment 1 of the patient F12.3 (Figure 5.24; Figure 5.25A). This transversion results in the change of leucine to arginine at position 95 (L95R) in the second transmembrane domain which is highly conserved (Figure 5.25B).

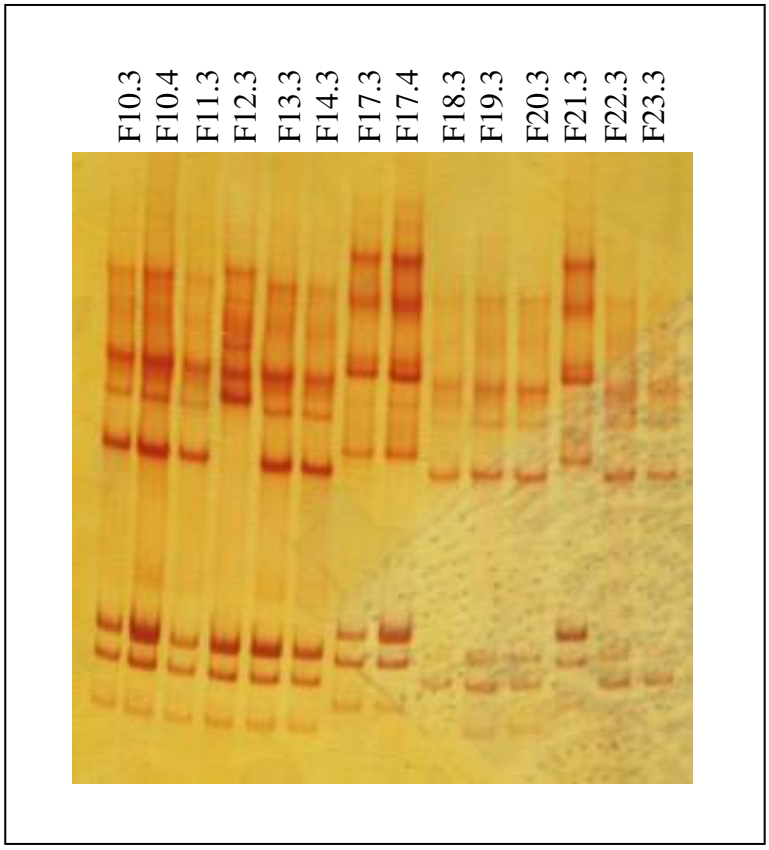

Figure 5.24. SSCP gel for screening of fragment 1 of the *GJA12* gene.

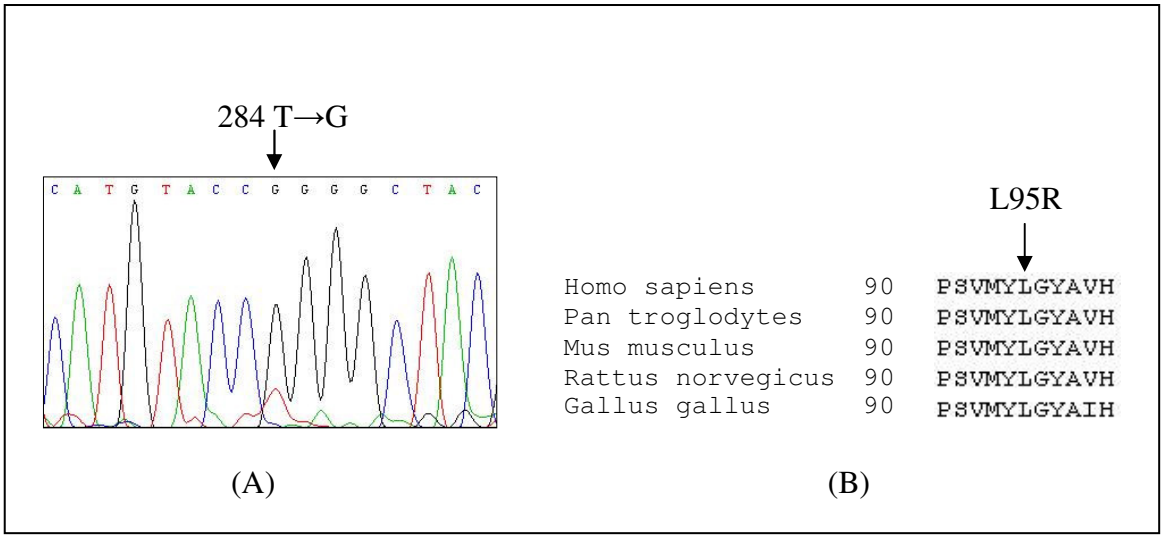

Figure 5.25. Chromatogram showing sequencing profile of the *GJA12* gene in patient F12.3 for the sense strand (A) and alignment of the selected region of human *GJA*12 region with orthologs of other species.

Restriction analysis performed using *Msp*I enzyme resulted in the cleavage of 284 bp PCR product into 238 and 46 bp fragments (Figure 5.26). Although consanguinity was not reported, the parents were found to be carriers of the mutation. The two unaffected siblings were negative for the mutant allele. Although the restriction digestion was partial for the patient on the gel, the homozygosity state of the patient was confirmed by sequencing both strands. The mutation was absent in 100 normal chromosomes.

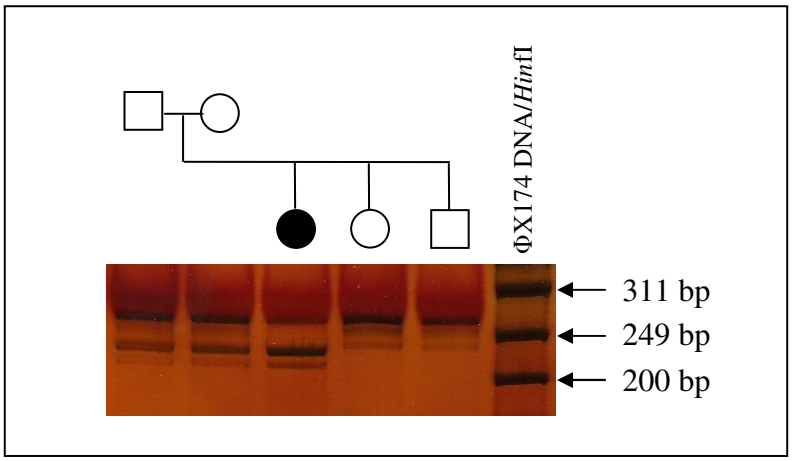

Figure 5.26. *Msp*I restriction analysis in family F12.

5.4.2.4. Families F17 and F21. The SSCP results for fragment 1 of the *GJA12* gene that is presented in Figure 5.24 revealed another altered pattern of migration for patients F17.3, F17.4 and F21.3. A 14 bp tandem duplication comprising the region between nucleotide positions 177 and 190 (177-190dup) was identified in all these cases (Figure 5.27). The insertion hypothetically results in truncation of the protein (D64fs214X) at the third transmembrane domain of the protein, leading to 213 amino acid long product. This sequence change creates an *Aci*I site; however, the restriction digestion with *Aci*I enzyme was again inconclusive. Thus, the segregation of the mutant allele in these families and the screening of the normal population were performed by separation of the alleles on 8 per cent denaturing polyacrylamide gel (Figure 5.28). PCR product of the normal allele is 284 bp in length; the mutation results in 298 bp product.

5.4.2.5. Family F23. An insertion was observed for patient F23.3 in the SSCP analysis of the fifth fragment of the *GJA12* gene (Figure 5.29). However, sequence variations could not be observed in sequencing profiles of the patient.

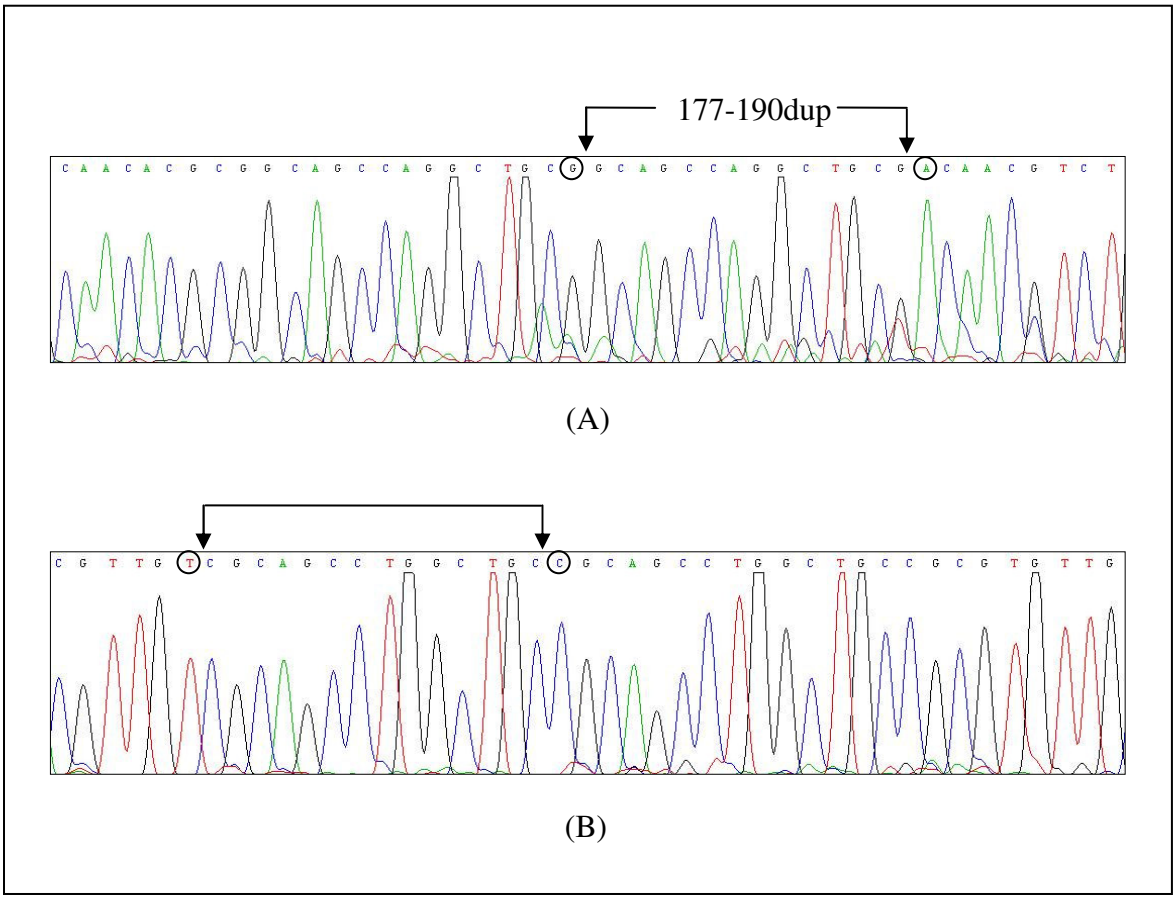

Figure 5.27. Chromatograms showing sequencing profile of the *GJA12* gene in patient F17.4 for the sense (A) and anti-sense (B) strands.

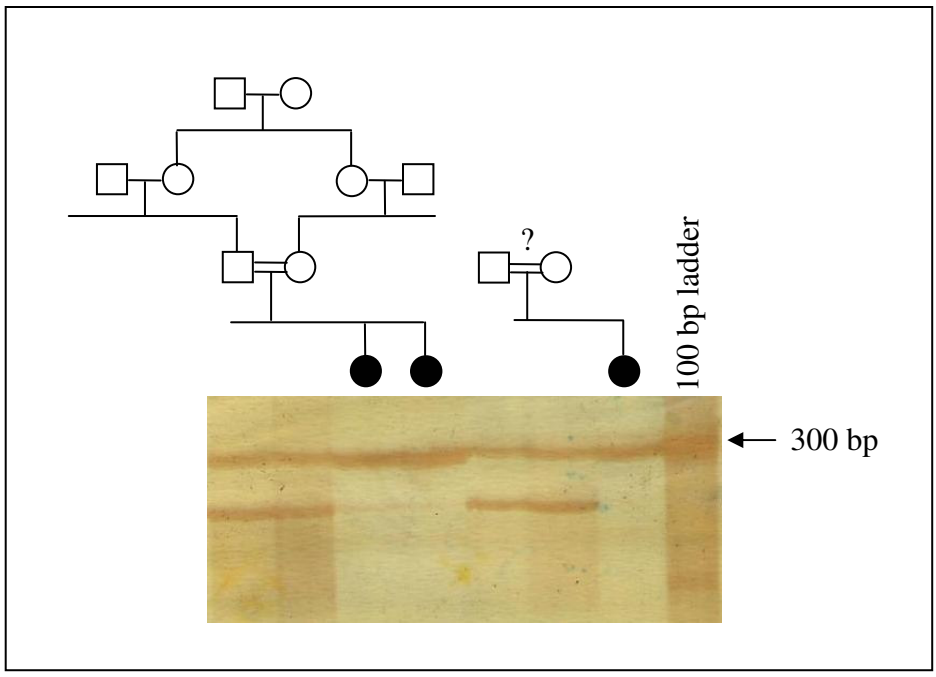

Figure 5.28. Segregation of the 177-190dup in families F17 and F21.

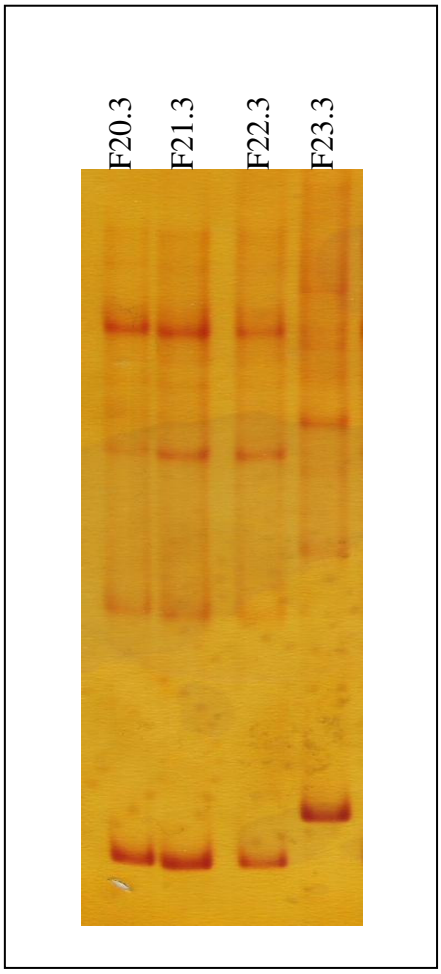

Figure 5.29. SSCP gel for screening of fragment 5 of the *GJA12* gene.

Table 5.5. List of the mutations identified in this study.

Family No	Gene	Exon	Mutation	Mutation Type	Effect on Protein	Affected Domain
F1	*GJA12*	1	546-562del	Deletion	V182fs257X	EC-2
F7	*GJA12*	1	706G→C	Missense	G236R	EC-2
F12	*GJA12*	1	284T→G	Missense	L95R	TM-2
F15	*PLP1*	5	643C→T	Missense	P215S	EC-2
F16	*PLP1*	6	695T→C	Missense	F232S	EC-2
F17	*GJA12*	1	177-190dup	Duplication	D64fs214X	TM-3
F21	*GJA12*	1	177-190dup	Duplication	D64fs214X	TM-3
F23	*GJA12*	1	?	?	?	?

In total, 12 (57 per cent) of the 21 cases were found to have pathogenic *PLP1* or *GJA12* mutations (Table 5.6).

Table 5.6. Summary of the mutations identified in the cohort of patients in this study.

Patient No	Sex	Result
F1.3	Male	546-562del in *GJA12*
F2.3	Male	546-562del in *GJA12*
F3.3	Female	546-562del in *GJA12*
F4.3	Male	*PLP1* duplication
F5.3	Male	-
F6.3	Male	-
F7.3	Male	706G→C in *GJA12*
F8.3	Male	-
F9.3	Male	*PLP1* duplication
F10.3	Male	-
F10.4	Male	-
F11.3	Male	-
F12.3	Female	284T→G in *GJA12*
F13.3	Male	-
F14.3	Male	-
F15.3	Male	643C→T in *PLP1*
F16.3	Male	695T→C in *PLP1*
F17.3	Female	177-190dup in *GJA12*
F17.4	Female	177-190dup in *GJA12*
F18.3	Male	-
F19.3	Male	*PLP1* duplication
F20.3	Male	*PLP1* duplication
F21.3	Female	177-190dup in *GJA12*
F22.3	Male	-
F23.3	Male	?

5.5. *In vitro* Analysis of the P215S and F232S Mutations in PLP1 and DM20

The effect of the two missense mutations, PLP1^{P215S} and PLP1^{F232S}, identified in our families was examined to determine the possible pathogenic mechanisms by *in vitro* analysis. The subcellular distribution of mutant PLP1s and DM20s, and the induction of the UPR pathway by these mutant proteins were examined in COS-7 cells. Statistical evaluation of the cell counts were performed using the ANOVA program of SPSS 15.0 Package.

5.5.1. Site-Directed Mutagenesis to Generate the P215S and F232S Mutations in Human *PLP1* and *DM20* cDNAs

The mutations identified in the *PLP1* gene, P215S and F232S, were generated *in vitro* by site-directed mutagenesis in the pCMV vectors containing the human *PLP1* or *DM20* cDNA. Mini-prep DNAs from eight random colonies transformed with the mutant PCR product was isolated. The PLP1^{P215S} and DM20^{P215S} constructs were digested with the *Mlu*I restriction enzyme, and the PLP1^{F232S} and DM20^{F232S} with *Sac*II for the confirmation of the presence of the mutations (Table 5.7; Figure 5.30). For further confirmation, two of those with the correct restriction pattern were then sequenced on both strands (Figure 5.31). Large scale plasmid DNA isolation was performed by CsCl density gradient centrifugation (Table 5.8; Figure 5.32).

Table 5.7. Restriction digestion analysis of the mutant human *PLP1* and *DM20* constructs.

Name of the Construct	Number of the Restriction Site		Size of the Restriction Digestion Products (bp)
	*Mlu*I	*Sac*II	
PLP1^{P215S}	2	-	5376, 671
DM20^{P215S}	2	-	5271, 671
PLP1^{F232S}	-	1	6047
DM20^{F232S}	-	1	5942

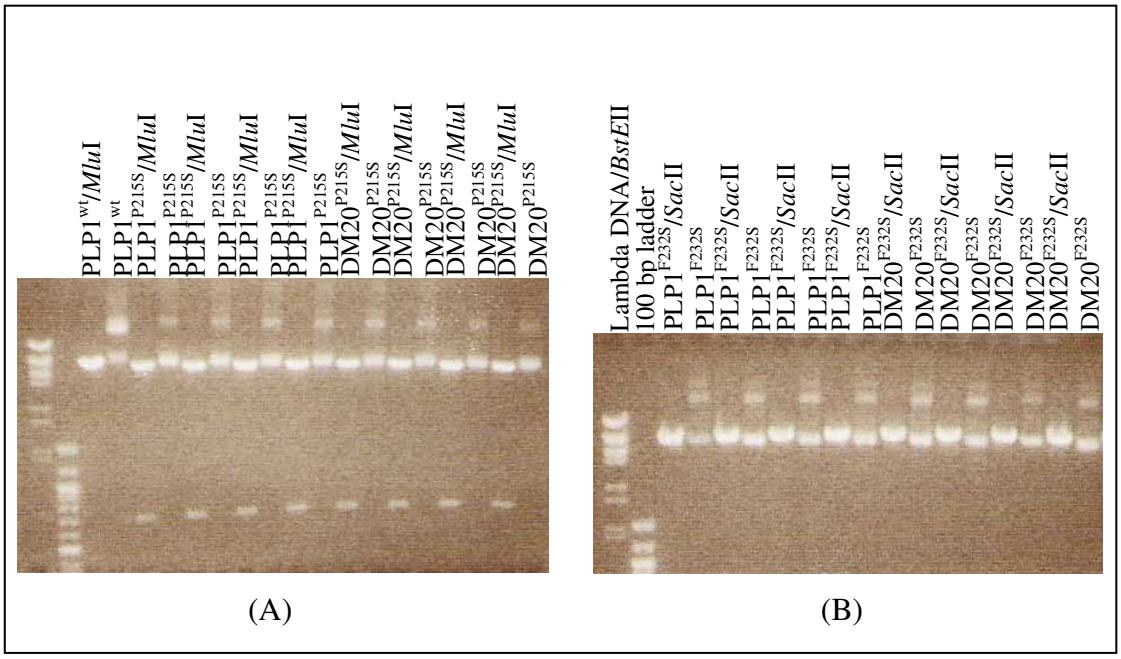

Figure 5.30. Confirmation of the P215S (A) and F232S (B) mutations generated in pCMV-hPLP1 or pCMV-hDM20 vectors by restriction digestion analysis.

5.5.2. Localization of the P215S and F232S Mutant Proteins

In order to identify the subcellular distribution of these mutant proteins, COS-7 cells transfected with the wild-type (PLP1 or DM20) or the mutant constructs ($PLP1^{P215S}$, $DM20^{P215S}$, $PLP1^{F232S}$ or $DM20^{F232S}$) were double-labeled with antibodies against PLP1 (FITC conjugated) and the rough endoplasmic reticulum marker (BiP) or lysosome-associated protein 2 (LAMP2) or golgin (Texas Red conjugated). The cells were visualized by confocal microscopy.

5.5.2.1. PLP1-BiP Double-Labeling. A nuclear rim observed in COS-7 cells transfected with the $PLP1^{wt}$ and $DM20^{wt}$ plasmids using antibodies against PLP1 revealed the synthesis of PLP1 and DM20 in the endoplasmic reticulum (Figure 5.33A; Figure 5.33B). The green fluorescent border around the edge of the cells outlines a diffuse fluorescence over the entire cell indicating that PLP1 was present in the plasma membrane. BiP staining highlighted the endoplasmic reticulum that was largely confined to the perinuclear region of the cells. PLP1 colocalizes with BiP to a small extent around the nucleus but the majority is present in vesicles. The cytoplasm appeared filled with BiP-stained endoplasmic reticulum and $PLP1^{+}$ vesicles.

Colocalization of PLP1 and BiP immunofluorescence was more apparent in cells expressing the P215S mutation than in the wild-type cells (Figure 5.33C; Figure 5.33D). This observation indicated that the mutant protein accumulated in the endoplasmic reticulum. The distribution of the mutant PLP1 also differed from that observed for wild-type protein at the level of cell surface staining; the fluorescent border at the edge of the mutant cell was absent. However, the distribution of DM20 staining was similar to that of the wild-type protein. Presence of DM20 in the plasma membrane suggested that this mutation did not interfere with the transport of DM20 to the cell surface. The F232S mutation resulted in the colocalization of both PLP1 and DM20 mutant proteins with BiP immunofluorescence which is indicative of the accumulation in the endoplasmic reticulum (Figure 5.33E; Figure 5.33F).

The cellular distribution of the transfected cells (n = 450, from three independent experiments) labeled with PLP1 and BiP antibodies are characterized in Figure 5.34.

5.5.2.2. PLP1-Golgin and PLP1-LAMP2 Double-Labelings. Normal intracellular trafficking of PLP1 gene product is through the secretory pathway to the cell surface and then into the lysosomes via the endocytotic pathway. The immunofluorescence double-labeling experiments using primary antibodies against PLP1 and Golgin or LAMP2 revealed colocalization of both fluorophores in perinuclear vesicles in cells transfected with the wild-type PLP1 or DM20 cDNA (Figure 5.35A; Figure 5.35B, Figure 5.36A; Figure 5.36B). This finding demonstrated presence of these proteins in Golgi and lysosomes as expected. However, the $PLP1^{P215S}$ and $PLP1^{F232S}$ proteins were confined to the perinuclear region and endoplasmic reticulum rather than the cell surface (Figure 5.35C; Figure 5.35E; Figure 5.36C; Figure 5.36E). The double-stained cells were negative for Golgin and LAMP2 antibodies. The immunocytochemical analysis with the same markers for the $DM20^{F232S}$ showed similar results to that of mutant PLP1s (Figure 5.35F; Figure 5.36F). On the contrary, $DM20^{P215S}$ protein was localized correctly to the plasma membrane and cytoplasm as in the wild-type DM20 (Figure 5.35D; Figure 5.36D).

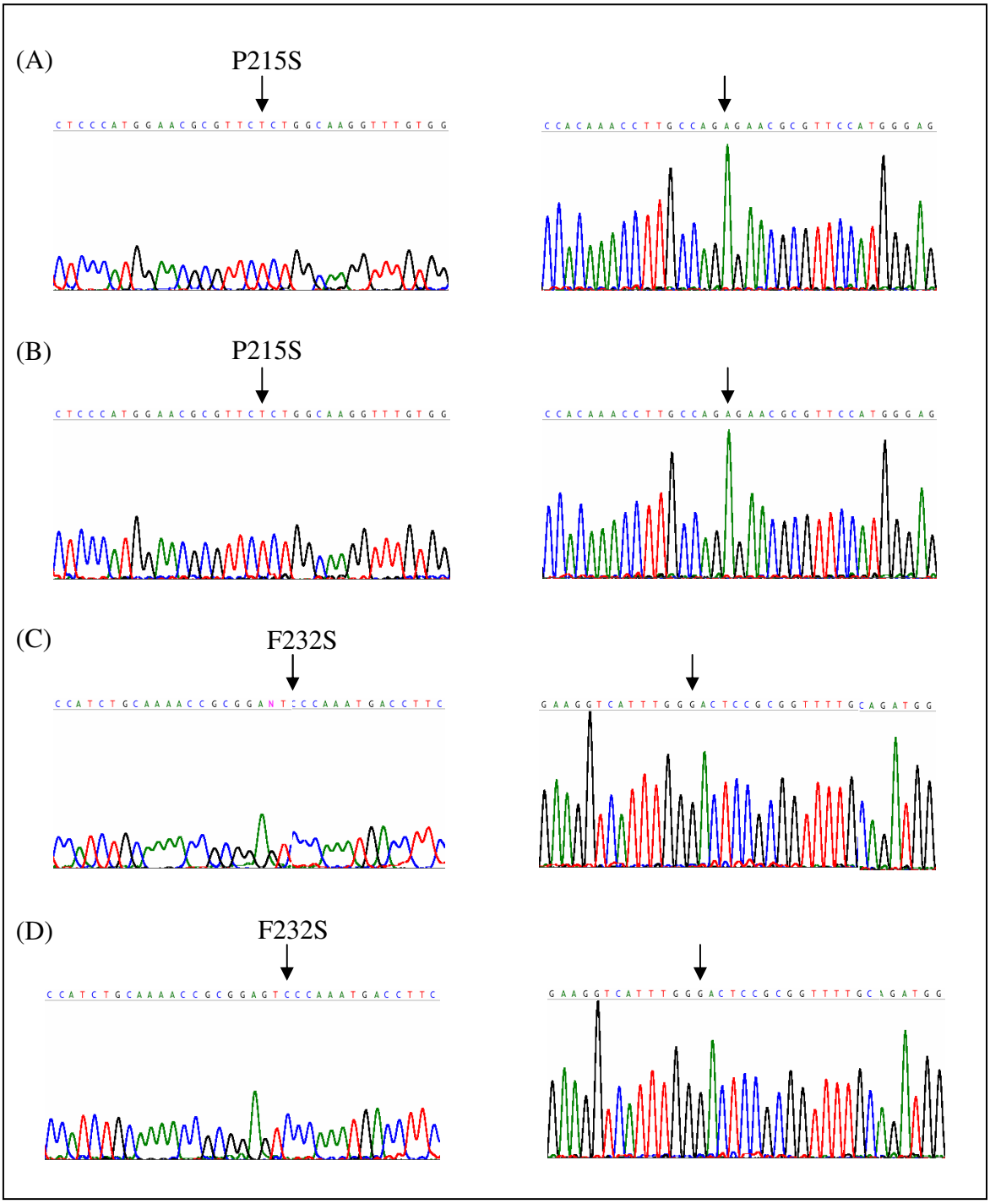

Figure 5.31. Sequencing profiles for the sense and anti-sense strands of the constructs PLP1^{P215S} (A), DM20^{P215S} (B), PLP1^{F232S} (C) and DM20^{F232S} (D).

Table 5.8. Large scale plasmid DNA isolation of mutant human *PLP1* and *DM20* constructs.

Name of the Construct	Concentration (µg/µl)
$PLP1^{P215S}$	3.6
$DM20^{P215S}$	2.7
$PLP1^{F232S}$	7.0
$DM20^{F232S}$	6.1

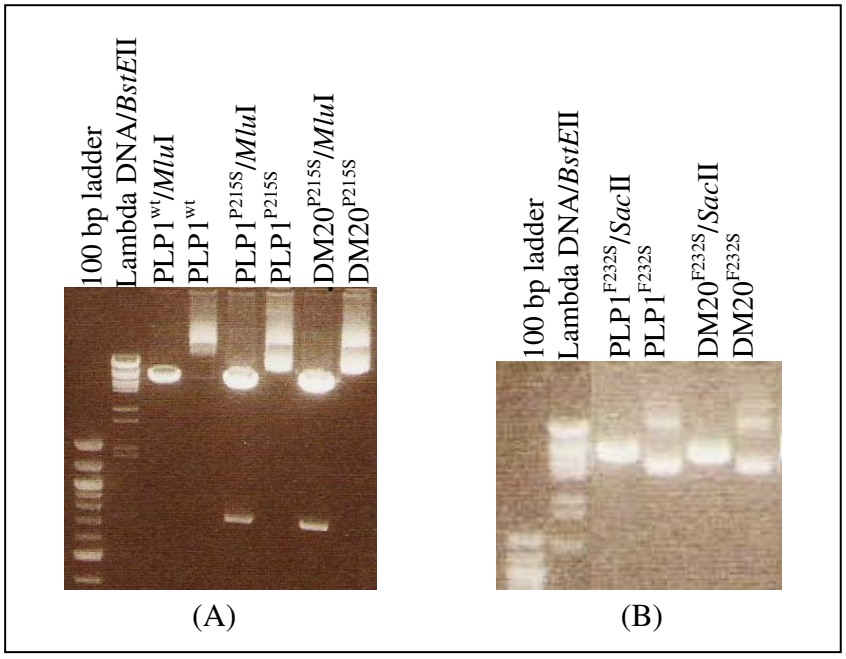

Figure 5.32. Confirmation of the P215S (A) and F232S (B) mutations in large scale isolated constructs by restriction digestion analysis.

5.5.3. UPR Induction in COS-7 Cells Expressing the Mutant PLP1 and DM20 Proteins

To determine if the UPR was induced *in vitro* by P215S and F232S mutant proteins, COS-7 cells were transfected with the wild-type PLP1/DM20 or the mutant plasmids. The untransfected cells were treated with tunicamycin as a positive control to mimic endoplasmic reticulum stress (Figure 5.37A; Figure 5.37B; Figure 5.38A; Figure 5.38B). Cells were then double-stained with the antibodies against the PLP1/DM20 and the transcription factor, CHOP, or its downstream element, ATF3.

In the transfected cells expressing the wild-type PLP1 or DM20, the localization of the protein was observed in all major compartments of the secretory and endocytic pathways as expected (Figure 5.37C; Figure 5.37D; Figure 5.38C; Figure 5.38D). CHOP or ATF3 staining was negative indicating absence of UPR induction. In cells transfected with $PLP1^{P215S}$, $PLP1^{F232S}$ or $DM20^{F232S}$ constructs, the mutant proteins were distinctively localized to the endoplasmic reticulum as previously demonstrated in Figure 5.33 (Figure 5.37E, Figure 5.37G; Figure 5.37H; Figure 5.38E, Figure 5.38G; Figure 5.38H). In addition, they expressed both CHOP and ATF3 that colocalized with the nuclear stain DAPI, as in the tunicamycin-treated cells. However, among the cells transfected with the $DM20^{P215S}$ construct, although $ATF3^{+}$ cells were observed, CHOP expression was not detected (Figure 5.37F; Figure 5.38F). The ratios for $CHOP^{+}$ or $ATF3^{+}$ cells among transfected cells are represented in Figure 5.39 and 5.40.

5.5.4. Activation of Apoptosis in COS-7 Cells Expressing the Mutant PLP1 and DM20 Proteins

To determine whether the UPR induced apoptosis in COS-7 cells expressing the P215S and F232S mutant proteins, they were double-labeled with the antibodies against PLP1 and Caspase3. The cells transfected with the wild-type PLP1 or DM20 were negative for Caspase3 indicating absence of apoptosis (Figure 5.41C; Figure 5.41D). In cells transfected with $PLP1^{P215S}$, $PLP1^{F232S}$ or $DM20^{F232S}$ constructs, the nuclei were condensed suggesting apoptosis (Figure 5.41E; Figure 5.41G; Figure 5.41H). However, the cells transfected with the $DM20^{P215S}$ construct showed no Caspase3 staining (Figure 5.41F). The ratio for $Caspase3^{+}$ cells among transfected cells are represented in Figure 5.42.

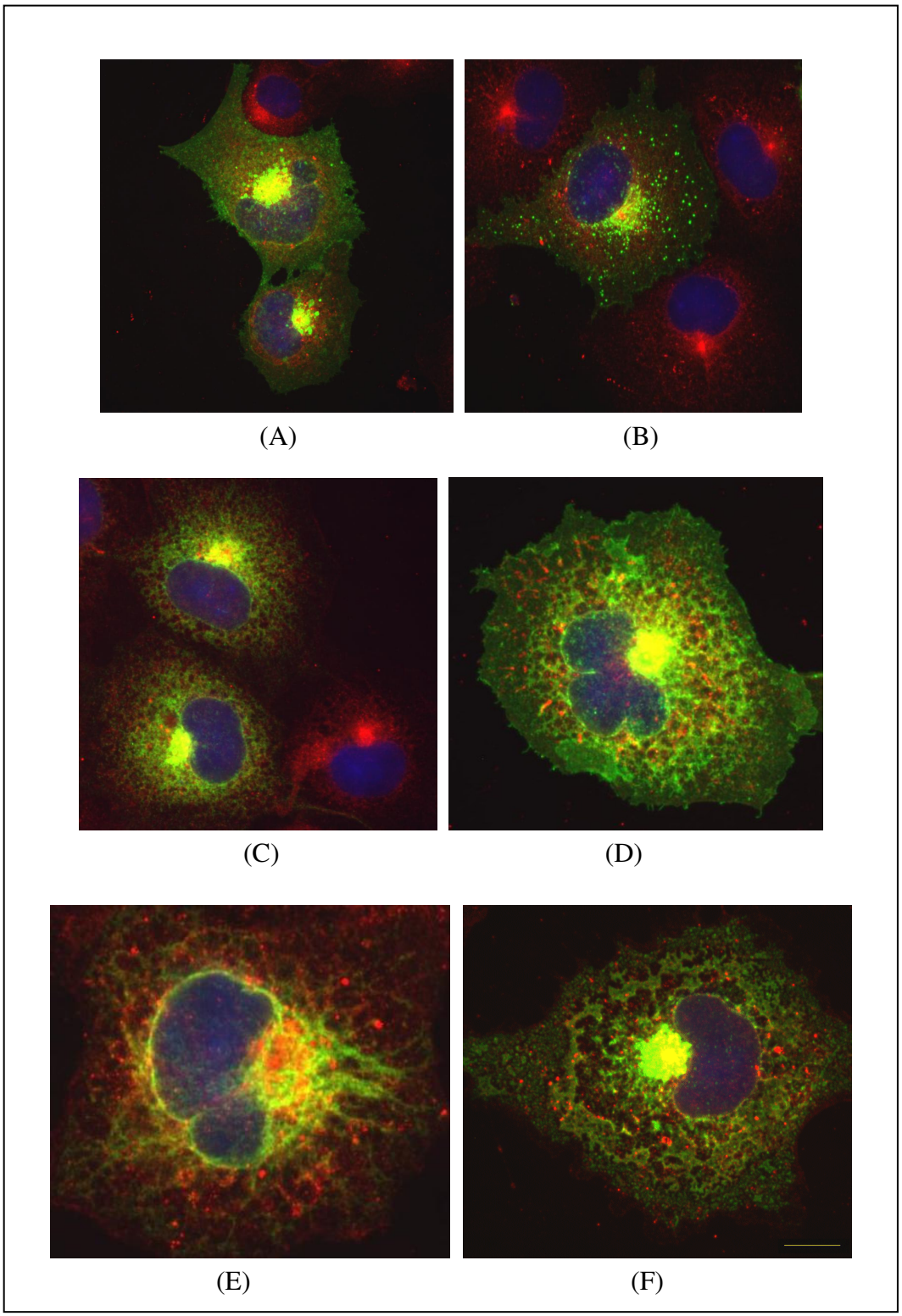

Figure 5.33. Immunofluorescence confocal images showing the distributions of PLP1 (green) and BiP (red) proteins in COS-7 cells transfected with $PLP1^{wt}$ (A), $DM20^{wt}$ (B), $PLP1^{P215S}$, (C) $DM20^{P215S}$ (D), $PLP1^{F232S}$ (E) and $DM20^{F232S}$(F). Scale bar, 15 μm; X 400.

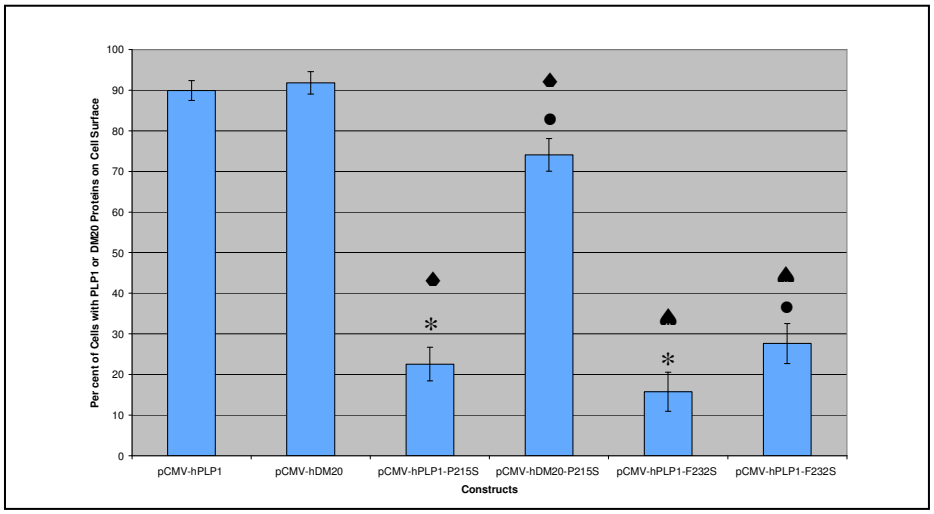

Figure 5.34. Histogram showing the cells with PLP1 or DM20 proteins on cell surface as a proportion of transfected cells. * compared to $PLP1^{wt}$ ($p < 0.001$), • compared to $DM20^{wt}$ ($p < 0.001$), ♦ compared to each other ($p < 0.001$) and ♠ compared to each other ($p= 0.052$).

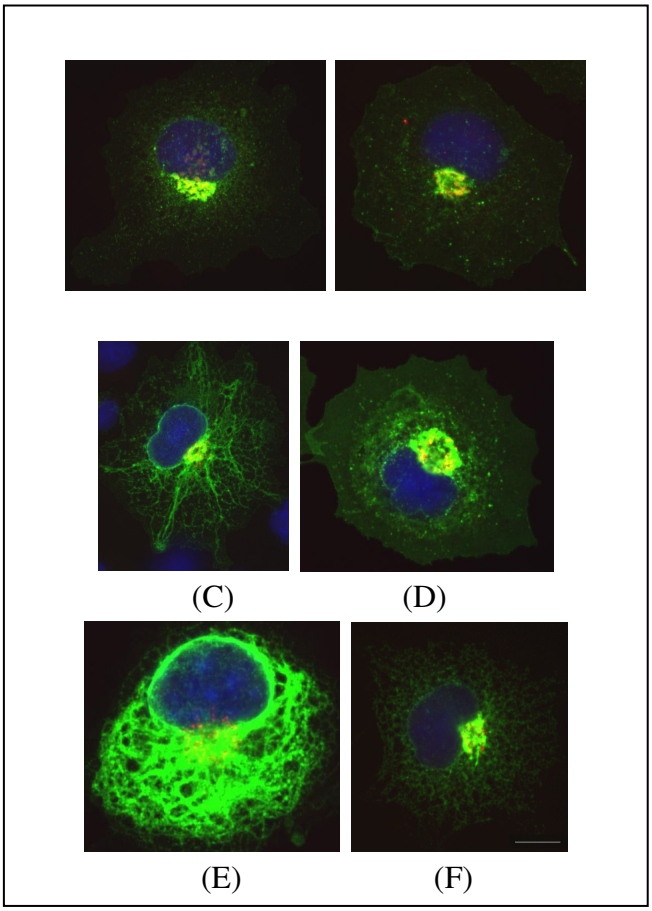

Figure 5.35. Immunofluorescence confocal images showing the distributions of PLP1 (green) and Golgin (red) proteins in COS-7 cells transfected with $PLP1^{wt}$ (A), $DM20^{wt}$ (B), $PLP1^{P215S}$, (C) $DM20^{P215S}$ (D), $PLP1^{F232S}$ (E) and $DM20^{F232S}$(F). Scale bar, 15 μm; X 400.

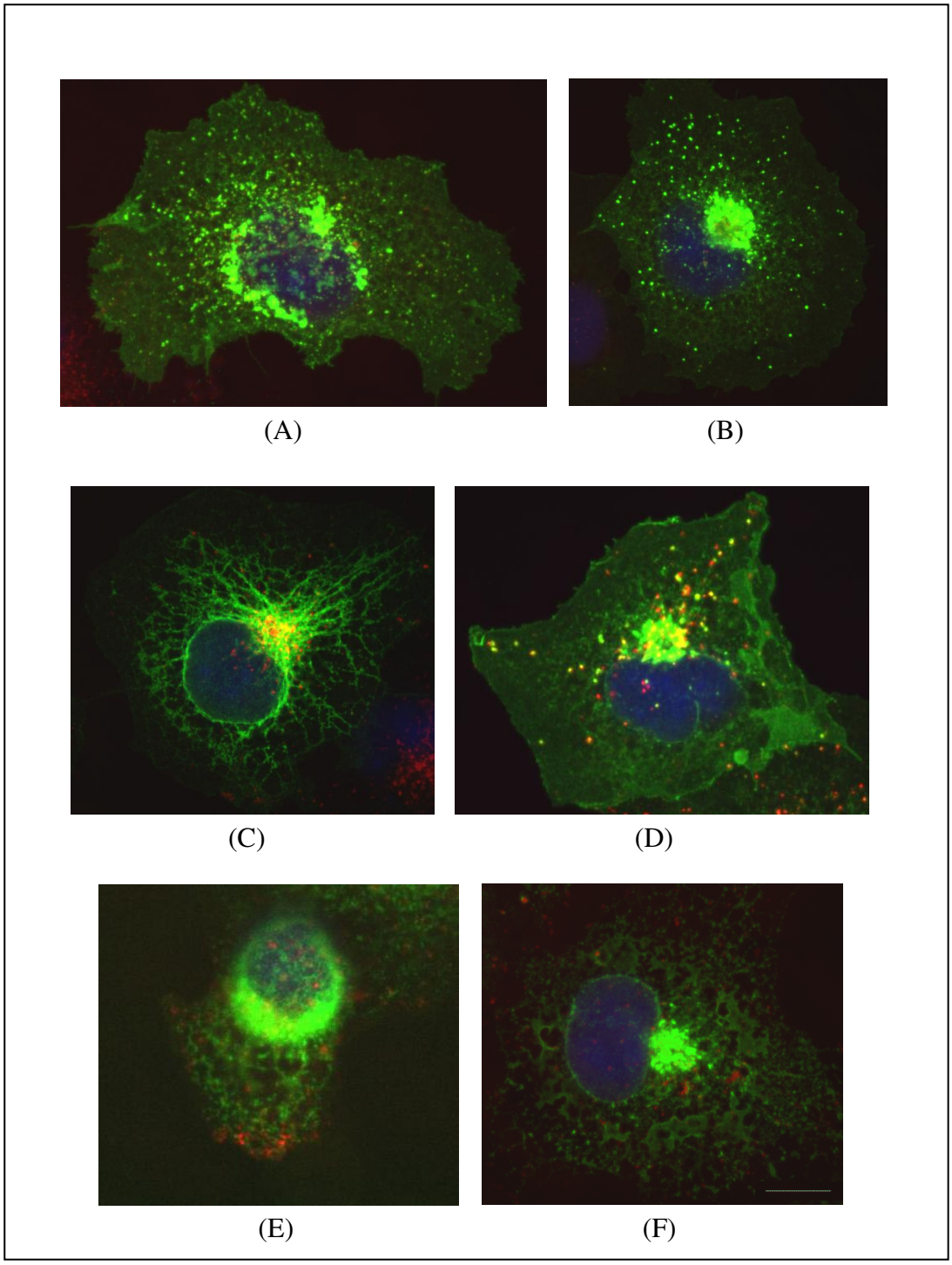

Figure 5.36. Immunofluorescence confocal images showing the distributions of PLP1 (green) and LAMP2 (red) proteins in COS-7 cells transfected with $PLP1^{wt}$ (A), $DM20^{wt}$ (B), $PLP1^{P215S}$, (C) $DM20^{P215S}$ (D), $PLP1^{F232S}$ (E) and $DM20^{F232S}$(F). Scale bar, 15 μm; X 400.

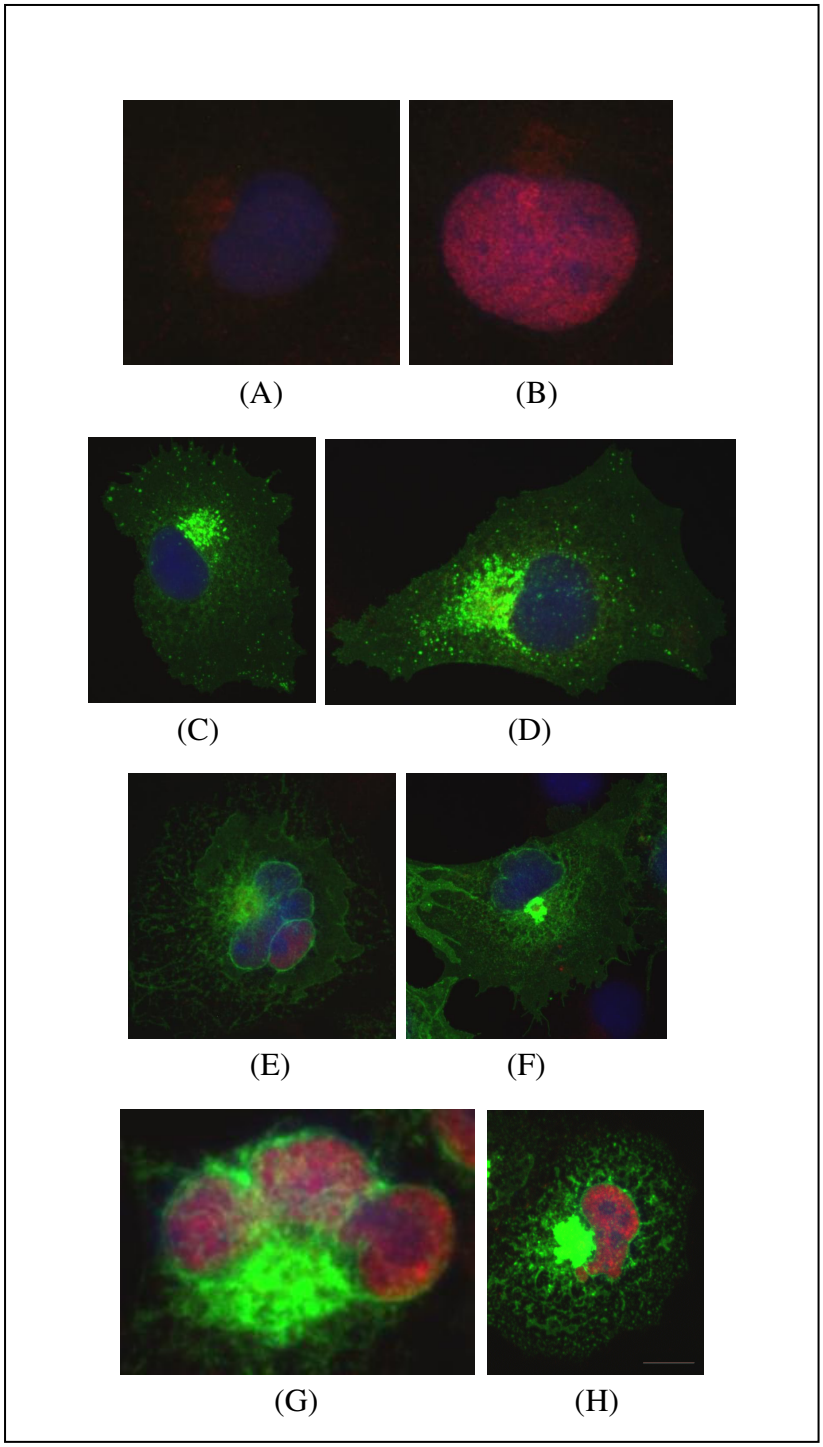

Figure 5.37. Immunofluorescence confocal images showing the distributions of CHOP (red) protein in tunicamycin-untreated (A) and -treated (B) cells and those of PLP1 (green) and CHOP (red) proteins in COS-7 cells transfected with $PLP1^{wt}$ (C), $DM20^{wt}$ (D), $PLP1^{P215S}$ (E), $DM20^{P215S}$ (F), $PLP1^{F232S}$ (G) and $DM20^{F232S}$(H). Scale bar, 15 μm; X 400.

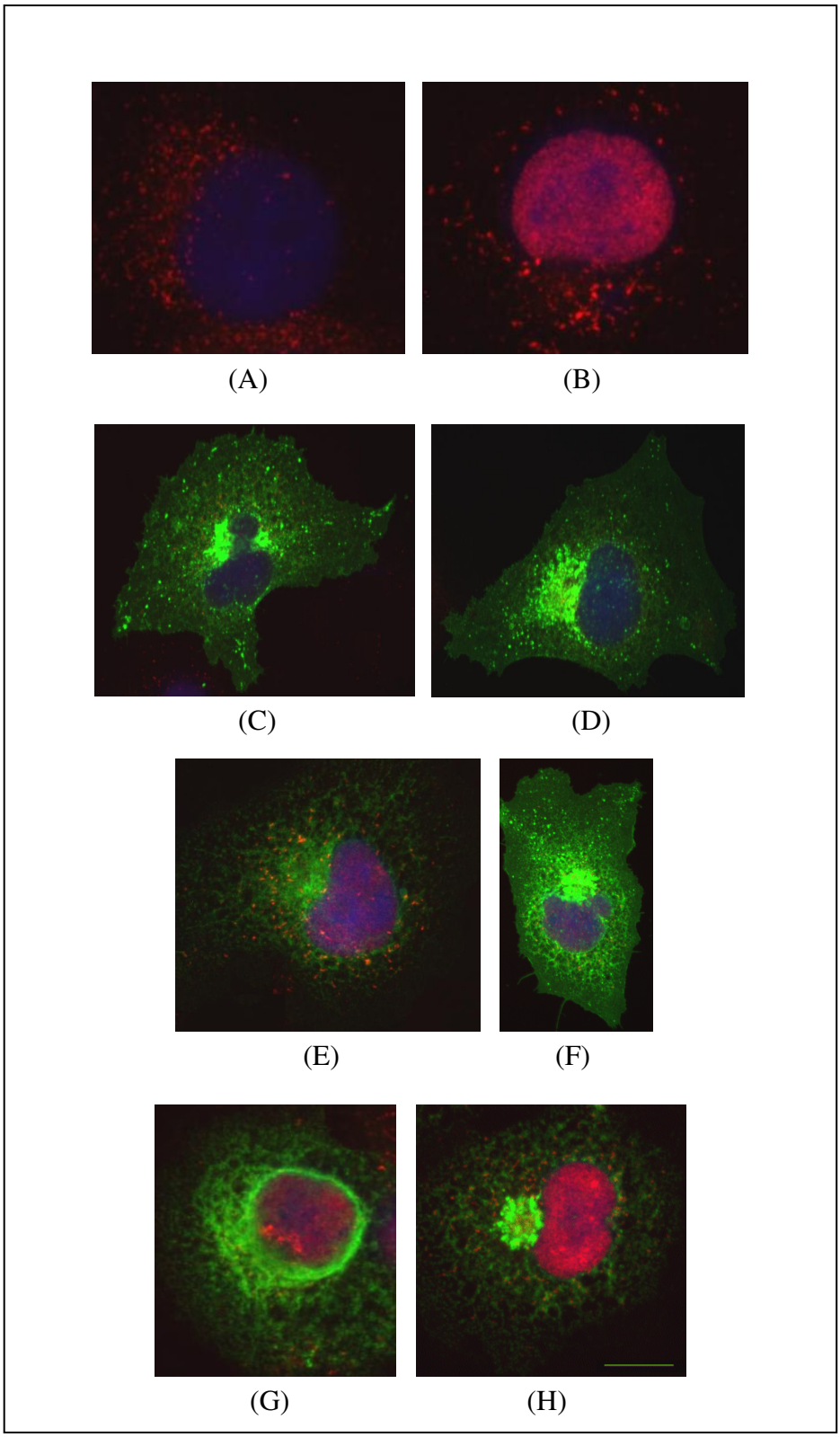

Figure 5.38. Immunofluorescence confocal images showing the distributions of ATF3 (red) protein in tunicamycin-untreated (A) and -treated (B) cells and those of PLP1 (green) and ATF3 (red) proteins in COS-7 cells transfected with $PLP1^{wt}$ (C), $DM20^{wt}$ (D), $PLP1^{P215S}$ (E), $DM20^{P215S}$ (F), $PLP1^{F232S}$ (G) and $DM20^{F232S}$(H). Scale bar, 15 μm; X 400.

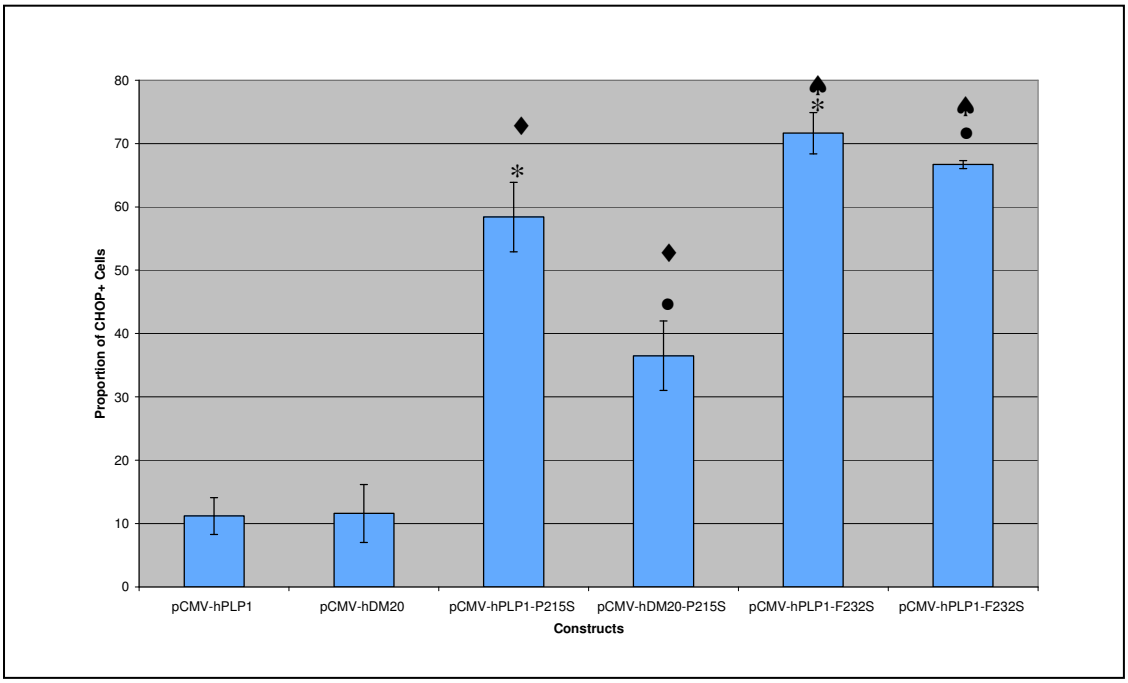

Figure 5.39. Histogram showing the CHOP^{+} cells a proportion of transfected cells. * compared to PLP1^{wt} ($p < 0.001$), • compared to DM20^{wt} ($p < 0.001$), ♦ compared to each other ($p = 0.001$) and ♠ compared to each other ($p < 0.001$).

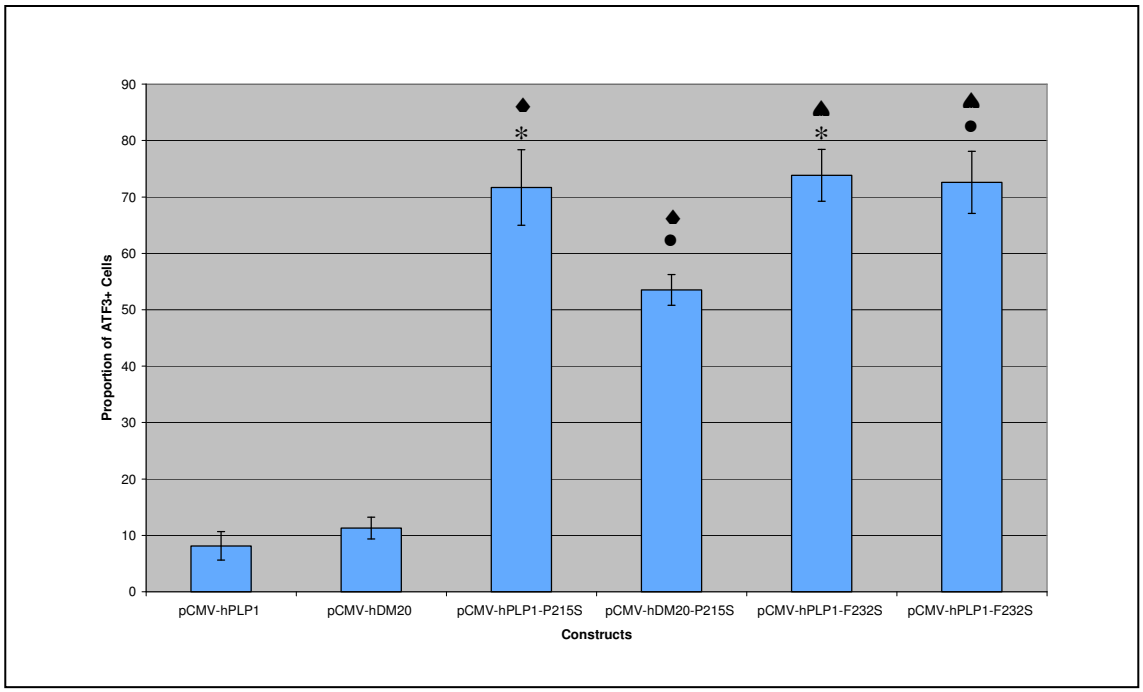

Figure 5.40. Histogram showing the ATF3^{+} cells a proportion of transfected cells. * compared to PLP1^{wt} ($p < 0.001$), • compared to DM20^{wt} ($p < 0.001$), ♦ compared to each other ($p = 0.003$) and ♠ compared to each other ($p = 1$).

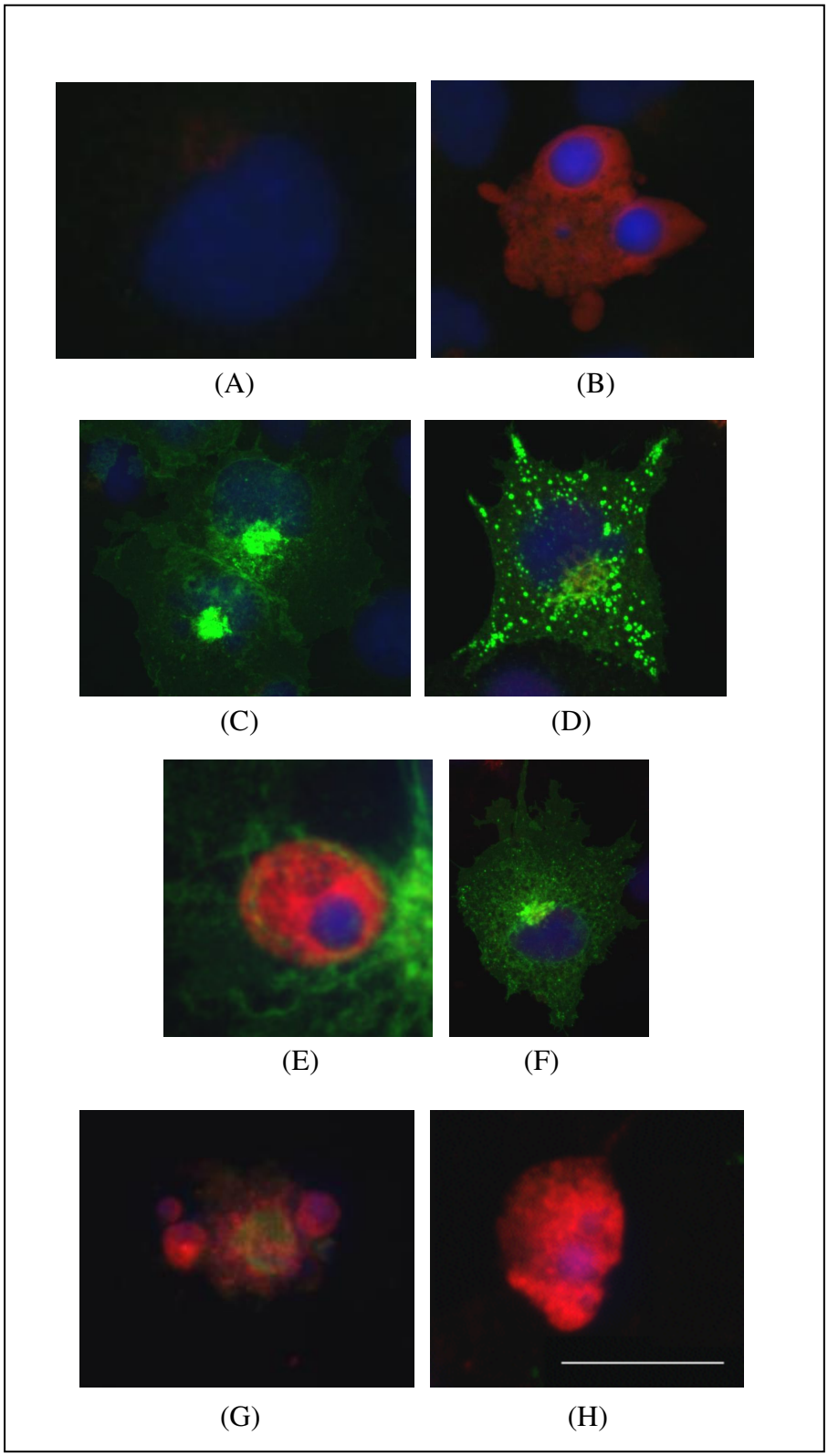

Figure 5.41. Immunofluorescence confocal images showing the distributions of Caspase3 (red) protein in tunicamycin-untreated (A) and -treated (B) cells and those of PLP1 (green) and Caspase3 (red) proteins in COS-7 cells transfected with $PLP1^{wt}$ (C), $DM20^{wt}$ (D), $PLP1^{P215S}$ (E), $DM20^{P215S}$ (F), $PLP1^{F232S}$ (G) and $DM20^{F232S}$(H). Scale bar, 15 μm; X 400.

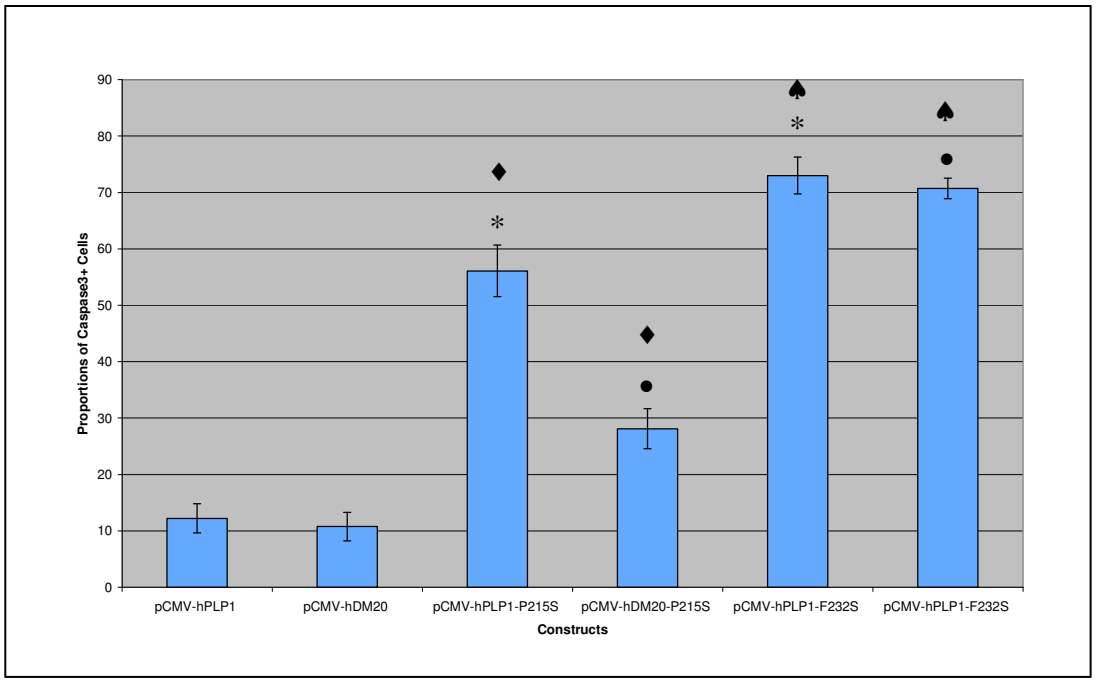

Figure 5.42. Histogram showing the Caspase3^{+} cells a proportion of transfected cells. * compared to PLP1^{wt} ($p < 0.001$), • compared to DM20^{wt} ($p < 0.001$), ♦ compared to each other ($p < 0.001$) and ♠ compared to each other ($p = 1$).

6. DISCUSSION

The application of genetic and molecular techniques in the field of neuroscience has led to remarkable advances in the elucidation of the molecular mechanisms underlying neurological diseases which, in turn, leads to understanding of the functions of the human nervous system. Identification of the defect is critical to unravel the events resulting in the pathogenesis of the disease and ultimately to develop therapies that may improve the quality of life and lifespan of the affected people. In order to shed light to the molecular basis of PMD, we initiated genetic studies for the disease in Turkey. PMD is a rare X-linked leukodystrophy characterized by hypomyelination of the CNS. It is clinically and pathologically heterogeneous, mostly caused by duplications, deletions or point mutations of the *PLP1* gene, which is on the long arm of the X chromosome. The gene encodes two proteins, the PLP1 and its alternatively spliced isoform DM20, which are the most abundant proteins of the myelin sheath in the CNS. The PMD phenotype is also associated with the mutations of the *GJA12* gene on chromosome 1q41-42.

Linkage to the *PLP1* locus on X chromosome could be performed in three of 21 families with PMD (F1, F10 and F17) since the family members were not available in the other familial cases and the disease was sporadic in the rest of families. Family F1 was a large family with three branches, all with consanguineous marriages. Three affected individuals, two of which were males and one female, were present. A common and maternally inherited haplotype was identified among the patients and in two asymptomatic sisters. This finding led to suspect linkage to *PLP1* locus in this family since females are mosaic due to X chromosome inactivation, enabling the possibility of manifesting two different phenotypes from the heterozygous genotype of a female. The two affected sisters in the second family, F17, were found to inherit different haplotypes from the asymptomatic mother, evidently ruling out the *PLP1* as the causative gene in this family. Since female patients were present in families F1 and F17, X chromosome inactivation analysis could be performed, revealing almost 100 per cent skewed inactivation in both families. The active X chromosome was inherited from the healthy father in family F1 and from the asymptomatic mother in family F17. These complementary findings, further confirmed by the lod score analysis, concluded that the genetic defects leading to PMD

phenotypes in these families were not associated with the X chromosome. Further genetic analysis in these families led to identification of novel mutations in the *GJA12* gene that is responsible for the autosomal recessive form of the disease.

A deletion of 17 bp, 546-542del, was identified in family F1. The mutation led to clinical heterogeneity among the affected individuals in the family which could be due to the presence of modifier genes, genetic background or environmental influences. Patient F1.3 is an 11-year-old boy and has congenital nystagmus, titubation, cerebellar findings and spasticity together with ankle contracture, and is not able to walk. However, patient F2.3, a 16-year-old boy, has nystagmus with age of onset at 1.5 years, moderate cerebellar findings and mild axial hypotonia. He is able to sit with support, but cannot walk. The third patient in the family, F3.3, is an 11-year-old girl with nystagmus at onset age of two months. She has severe cerebellar dysarthria, axial hypotonia and spastic paraparesis, and is not able to walk. The deletion is predicted to lead to a translational frameshift starting from amino acid residue V182 and the truncation of the protein after amino acid 256 that resides near to the end of the second extracellular domain. Lack of the fourth transmembrane domain as well as the long C-terminal intracellular tail of the Cx47 may lead to formation of a non-functional protein by disrupting its stability or membrane insertion.

In family F17, a tandem duplication of 14 bp, 177-190dup, was found to be the causative mutation. Patient F17.3 is a 16-year-old girl and her affected sister, F17.4, died at age of 14. They presented similar clinical pictures with nystagmus at onset age of one year with decrease course, severe axial hypotonia, moderate-to-severe cerebellar findings, epileptic seizures and inability to sit and walk. The duplication starting at nucleotide 177 leads to a frameshift, predicting a prematurely truncated protein (D64fs214X) which lacks the domains downstream of the third transmembrane domain. The mutation may result in dysmyelination via a similar mechanism to the one suggested in family F1.

Haplotype analysis of the third family, F10, revealed that the two affected hemizygous individuals inherited different haplotypes from the healthy mother. This finding clearly indicated that the disease phenotype was not linked to the *PLP1* locus in this family. Lod score analysis confirmed the results of haplotype analysis. Further

exclusion of *GJA12* gene mutations in the family suggests presence of other causative gene(s) in the PMD pathogenesis. Although the neurological presentations of the patients were similar to those of PMD, presence of additional clinical features in the form of cataract and prominent atrophy in the MRI findings in both prompted us to speculate that the phenotype in this family could result from another type of leukodystrophy. Linkage to another region on the X chromosome could not be tested by X chromosome inactivation analysis since both patients were males.

Since *PLP1* duplications were reported to be the most frequent causes of PMD (50 to 75 per cent), detection of the duplications and deletions was the first step in identification of the defects in our cohort of patients. Of the 21 cases analyzed in this study, four (19 per cent) were found to carry the duplication of *PLP1*, a frequency much lower than reported by others (Mimault *et al*., 1999). The low detection rate in our cohort may be in part due to the higher frequency of autosomal recessive cases, different ethnical backgrounds, limitation of the detection systems or difficulty of distinguishing different myelin disorders. The interphase FISH, which is the conventional method for the molecular diagnosis of duplications, revealed the presence of the *PLP1* duplication in seven of the patients. Although FISH is one of the most reliable techniques for the confirmation of the results, other methods, including RFLP, quantitative fluorescent multiplex PCR and quantitative real-time PCR were also used to detect the *PLP1* copy number. The RFLP results were not informative for our patients since none of the males were found to be heterozygous, and no females with dosage differences or three alleles were observed. The quantitative fluorescent multiplex PCR assay was initially tested on both the male and female controls in order to establish the method; however, it could not be used for the detection of the duplications in this study. Use of multiple primer sets might be one of the reasons of the errors observed in the results due to the spectral overlap between the fluorophores. The problem could be solved by labeling the primer sets using fluorophores with different emission wavelengths. However, the assay would have a high cost and reaction conditions should be optimized accordingly, that would take time. The quantitative real-time PCR using Light Cycler (Roche) was the method of choice for this reason. The technique confirmed the presence of the *PLP1* duplication in only four of the seven patients. Discrepancies using FISH analysis have also been reported for PMD and other disorders like Kabuki Syndrome and anxiety disorders with joint laxity (Lee *et al*.,

2006b; Hoffman *et al*., 2005; Sanlaville *et al*., 2005; Gratacos *et al*., 2001). Although the reasons for the discrepancies observed in FISH analysis remain unclear, the false-positive results could correspond to the repetitive DNA sequences within the probe or may result from other complex rearrangements such as inversions or translocations. Alternatively, artifactual duplications might be due to the asynchronous replication in lymphoblastoid cells that are prone to high level of instability. Therefore, when duplication is suspected by FISH, the increased copy number should be confirmed using other gene quantification techniques, which are sensitive, rapid and cost-effective. *PLP1* deletion was not present in any of the patients, which is not surprising since the cases with the deletion account for less than one per cent in the literature. Amplification of the *PLP1* exons further confirmed the absence of *PLP1* deletion in our PMD patients.

A variation of clinical phenotypes that has been reported for other populations was also observed in our cohort of patients with the *PLP1* duplication (Hübner *et al*., 2005). Patient F4.3 is a 14-year-old boy with congenital nystagmus that diminished about 70 per cent by age. He has a mild form of mental retardation, is able to crawl, straighten up and walk with support. Patient F9.3 is a 26-year-old male who has a mild clinical presentation with reduced nystagmus. He is able to walk, use technical equipment and communicate. F19.3 is a 4-year-old boy with prominent nystagmus and severe hypotonia. He is even not able to stand and sit, and has some autistic features. Patient F20.3 is a four-year-old boy. He has prominent nystagmus and is able to sit and walk with support. This apparent difference in the clinical pictures may be explained by the variable size of duplicated region among different families. Inclusion of other genes in the duplicated region or disruption of genes at the duplication endpoints may also affect the severity of the phenotype.

Mutation analysis of the *PLP1* gene revealed two sequence variations, accounting for approximately nine per cent of the cases in our cohort. These patients presented with the most severe PMD phenotype among all the cases included in this study. Patient F15.3, who was found to carry the $PLP1^{P215S}$ mutation, is a four-year-old boy. He had congenital nystagmus although its course had decreased. At about age of two, he had stridor, which later disappeared. He has difficulty in swallowing big pieces and sometimes disgorges while eating. He can sit and walk with support. The patient with the $PLP1^{F232S}$ mutation,

F16.3, is a five-year-old boy. Nystagmus was present since the second month after birth and continued in a decreased manner. He had congenital stridor, which had also decreased. He has difficulty in chewing and swallowing solid pieces. He has hypotonia and can sit with support.

The PLP1^{P215S} and PLP1^{F232S} mutations both affect the extracellular loop between the third and fourth transmembrane domains which is highly conserved among human, mouse, rat, dog and bovine, and has been suggested to play an important role in maintaining protein structure and function. The proline and phenylalanine amino acids are both nonpolar whereas serine is uncharged polar. The non-conservative, proline to serine and phenylalanine to serine, substitutions most probably result in the alteration of the tertiary structure of the protein or its stability by disrupting either helix geometry or side-chain packing, and induce the misfolding of both PLP1 and DM20.

In order to examine the effects of these missense mutations on the processing of PLP1 and the role of the mutant proteins in inducing the hypomyelinating disorder, the subcellular distribution of the mutant proteins and the involvement of the UPR were characterized. In contrast to the wild-type PLP1 and DM20 which reach to the cell surface, the PLP1^{P215S}, PLP1^{F232S} and DM20^{F232S} mutant proteins accumulated in the endoplasmic reticulum. However, the intracellular trafficking of DM20^{P215S} was similar to that of wild-type DM20. Expression of CHOP, ATF3 and Caspase3 in cells with PLP1^{P215S}, PLP1^{F232S} and DM20^{F232S} mutants indicated that the UPR pathway and the subsequent apoptosis were activated; however, low level of cell death was observed in DM20^{P215S} cells. These findings suggest that a common mechanism of protein misfolding may result in accumulation of the mutant proteins in the endoplasmic reticulum and this gain-of-toxic function may be the cause of cell death via activation of the UPR. The difference in the localizations of PLP1^{P215S} and DM20^{P215S} proteins indicates that P215S mutation affects the three-dimensional structure of PLP1 and DM20 significantly different and results in different levels of cell death. On the other hand, the difference between the trafficking of DM20^{P215S} and DM20^{F232S} may provide a cellular basis for the distinction between the clinical severities of the two patients. The F232S mutation causing the endoplasmic reticulum accumulation of both PLP1 and DM20 may result in a severe PMD phenotype. In contrast, the transport of DM20^{P215S} to the cell surface prompted us to speculate that the

patient with the P215S mutation would have a milder disease. Considering the cell counts, we also concluded that the greater the accumulation in the endoplasmic reticulum, the higher the involvement of the UPR and apoptosis, which may also be consistent with the variable disease severity. Interestingly, the clinical presentation of the patients does not support this suggestion since a clinical severity difference was not reported by the clinician. Since DM20 is transported to the cell surface, it is expected to compensate the lack of PLP1. However, lack of myelin in the patient F15.3 suggests that PLP1 and DM20 may have different functions in myelin.

In addition to F1 and F17 families, three different novel *GJA12* variations were found to be associated with the autosomal recessive form of the disease in families F7, F12, F21 and F23. The clinical features of *GJA12*-related PMD in our cohort were almost identical and seem to be milder than those of the patients carrying the *PLP1* duplication. All our patients with the *GJA12* mutations showed diffuse white matter in the MRI findings, and stridor and dysphagia were absent. The synthesis of aberrant and truncated proteins resulting from the homozygous missense and nonsense mutations in the *GJA12* gene may lead to the failure of functional gap junction channels. This suggests that the loss of Cx47 function may be the cause of pathogenesis observed in the patients with these mutations.

Patient F7.3, who was found to carry a heterozygous G236R substitution, is a 14-year-old boy. Nystagmus has been present since the age of one month with a reduced course, and he has mild cerebellar findings and spasticity. Hypotonia is absent and he can sit and stand with support but cannot walk. Glycine to arginine change results in the substitution of a nonpolar residue to a basic one in the second extracellular loop, adjacent to the third transmembrane domain which is a highly conserved region of the protein. The heterozygosity state of the mutation in the patient, born to non-consanguineous parents, suggests that he should be a compound heterozygote. However, no other sequence variations could be detected in the gene for this patient.

Patient F12.3, a 12-year-old girl, was shown to carry a L95R mutation in homozygous state. She has nystagmus with onset at third month and prominent dysarthria, cerebellar findings and spasticity. She is able to control her head, sit and walk with

support. The non-polar leucine is substituted with the basic arginine amino acid at position 95, which locates in the second transmembrane domain. This non-conservative change may result in the disruption of the Cx47 channels.

Patient F21.3 is a six-year-old girl with congenital nystagmus, hypotonia, severe titubation and moderate cerebellar findings. She is not able to sit and walk. Mutation analysis of the *GJA12* gene revealed that she was homozygous for the D64fs214X mutation, which was also identified in family 17. Although consanguinity was not reported, the involvement of the same mutation in these two families suggests the presence of a founder mutation. Comparison of the clinical presentations of the patients in two families revealed that F21.3 has a more severe disease phenotype, with respect to the age of onset and course of the nystagmus.

Patient F23.3, a four-year-old boy, has congenital nystagmus with decreased course. He has titubation, dysarthria and mild hypotonia, and is able to sit and walk without support. He was suspected to have an insertion according to the SSCP analysis. However, due to the high GC-content of the region of interest, the characterization of the sequence change could not be performed by sequencing analysis.

The genetic and molecular bases of PMD were investigated in the framework of this study. Our findings can be summarized as follows:

- Linkage to *PLP1* locus was excluded in three families and the causative gene mutations were identified in the *GJA12* gene in two of these families. The third family was suspected to manifest another type of leukodystrophy upon elimination of the *PLP1* and *GJA12* genes for pathogenic mutations.
- *PLP1* gene duplication was identified in four of the cases. Although different approaches were used to detect duplications, quantitative real-time PCR analysis proved to be the most reliable and time-effective.
- PMD phenotype was confirmed by identification of *PLP1* mutations in two and *GJA12* mutations in four additional families. In total, pathogenic mutations were identified in 12 (57 per cent) of 21 families suspected with PMD, 19 per cent of which were due to *PLP1* duplications, and nine and 29 per cent were due to mutations in the *PLP1* and *GJA12* genes, respectively. The distribution of the

mutations responsible for the PMD phenotype in our cohort of patients was significantly different from that reported in the literature. This difference may be due to the high number of autosomal recessive cases in our population, considering the fact that about 50 per cent of the parents have consanguineous marriages in our cohort. Absence of mutations in either *PLP1* or *GJA12* in 43 per cent of the cases analyzed suggests presence of further genetic heterogeneity in PMD.

- The results of immunocytochemical analysis for the PLP1 mutant proteins revealed that they accumulated in the endoplasmic reticulum, leading to UPR activation and subsequent apoptosis for $PLP1^{P215S}$, $PLP1^{F232S}$ and $DM20^{F232S}$ but not for the $DM20^{P215S}$. The difference in the cellular localizations of $DM20^{P215S}$ and $DM20^{F232S}$ proteins prompted us to speculate a cellular basis for the distinction between the clinical severities of the two patients with these mutations. The localization of the mutant proteins and the clinical severity were in accordance with the results of previously reported *in vitro* studies. However, our patients present similar degrees of clinical severity though $DM20^{P215S}$ reaches the cell surface and expected to compensate the lack of $PLP1^{P215S}$. This observation suggests that PLP1 and DM20 may have different roles in myelin.

7. CONCLUSION

This study contributes the genetic and molecular bases of PMD in the Turkish population and thus helps to better understand the molecular pathogenesis leading to PMD. It concludes that the autosomal recessive form of PMD is more common than the X-linked type in our population, and further genetic heterogeneity is present in PMD. Genome-wide searches in large families suitable for the linkage analysis will enable the identification of new loci and of respective genes, responsible for the PMD phenotype. Analysis of the PLP1 mutant proteins by *in vitro* assays led to the suggestion that PLP1 and DM20 may have different roles in myelin. Further *in vitro* and *in vivo* analyses of novel mutations in the *PLP1* and *GJA12* genes will aid to characterize the molecular mechanisms causing the disease and, also to improve our knowledge of proteolipid and gap junction proteins.

APPENDIX: ELECTROPHEROGRAMS OF CONTROLS IN THE QUANTITATIVE FLOURESCENT MULTIPLEX PCR

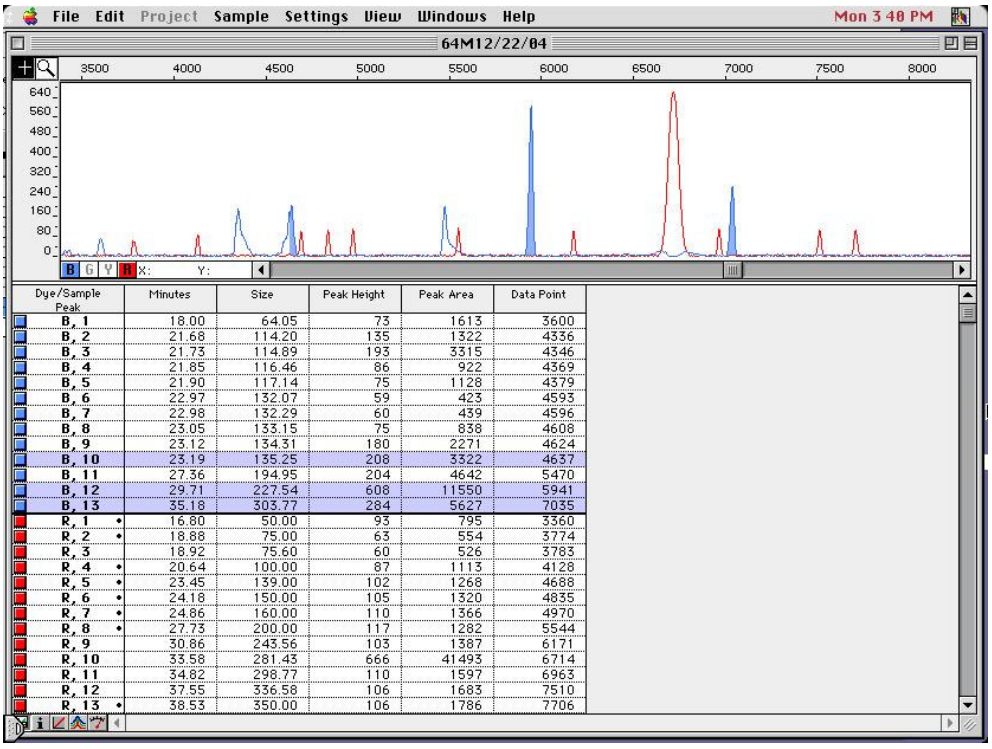

Dye/Sample Peak	Minutes	Size	Peak Height	Peak Area	Data Point
B, 1	18.00	64.05	73	1613	3600
B, 2	21.68	114.20	135	1322	4336
B, 3	21.73	114.89	193	3315	4346
B, 4	21.85	116.46	86	922	4369
B, 5	21.90	117.14	75	1128	4379
B, 6	22.97	132.07	59	423	4593
B, 7	22.98	132.29	60	439	4596
B, 8	23.05	133.15	75	838	4608
B, 9	23.12	134.31	180	2271	4624
B, 10	23.19	135.25	208	3322	4637
B, 11	27.36	194.95	204	4642	5470
B, 12	29.71	227.54	608	11550	5941
B, 13	35.18	303.77	284	5627	7035
R, 1 •	16.80	50.00	93	795	3360
R, 2 •	18.88	75.00	63	554	3774
R, 3	18.92	75.60	60	526	3783
R, 4 •	20.64	100.00	87	1113	4128
R, 5 •	23.45	139.00	102	1268	4688
R, 6 •	24.18	150.00	105	1320	4835
R, 7 •	24.86	160.00	110	1366	4970
R, 8 •	27.73	200.00	117	1282	5544
R, 9	30.86	243.56	103	1387	6171
R, 10	33.58	281.43	666	41493	6714
R, 11	34.82	298.77	110	1597	6963
R, 12	37.55	336.58	106	1683	7510
R, 13 •	38.53	350.00	106	1786	7706

Figure A.1. Electropherogram of male control 1.

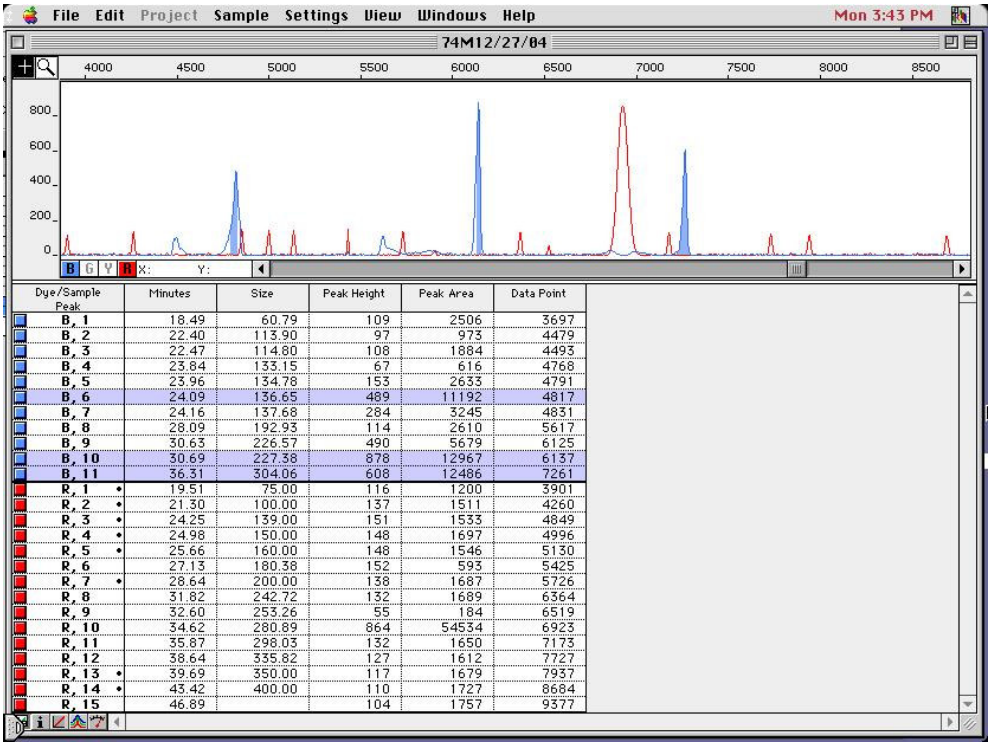

Dye/Sample Peak	Minutes	Size	Peak Height	Peak Area	Data Point
B, 1	18.49	60.79	109	2506	3697
B, 2	22.40	113.90	97	973	4479
B, 3	22.47	114.80	108	1884	4493
B, 4	23.84	133.15	67	616	4768
B, 5	23.96	134.78	153	2633	4791
B, 6	24.09	136.65	489	11192	4817
B, 7	24.16	137.68	284	3245	4831
B, 8	28.09	192.93	114	2610	5617
B, 9	30.63	226.57	490	5679	6125
B, 10	30.69	227.38	878	12967	6137
B, 11	36.31	304.06	608	12486	7261
R, 1 •	19.51	75.00	116	1200	3901
R, 2 •	21.30	100.00	137	1511	4260
R, 3 •	24.25	139.00	151	1533	4849
R, 4 •	24.98	150.00	148	1697	4996
R, 5 •	25.66	160.00	148	1546	5130
R, 6	27.13	180.38	152	593	5425
R, 7 •	28.64	200.00	138	1687	5726
R, 8	31.82	242.72	132	1689	6364
R, 9	32.60	253.26	55	184	6519
R, 10	34.62	280.89	864	54534	6923
R, 11	35.87	298.03	132	1650	7173
R, 12	38.64	335.82	127	1612	7727
R, 13 •	39.69	350.00	117	1679	7937
R, 14 •	43.42	400.00	110	1727	8684
R, 15	46.89		104	1757	9377

Figure A.2. Electropherogram of male control 2.

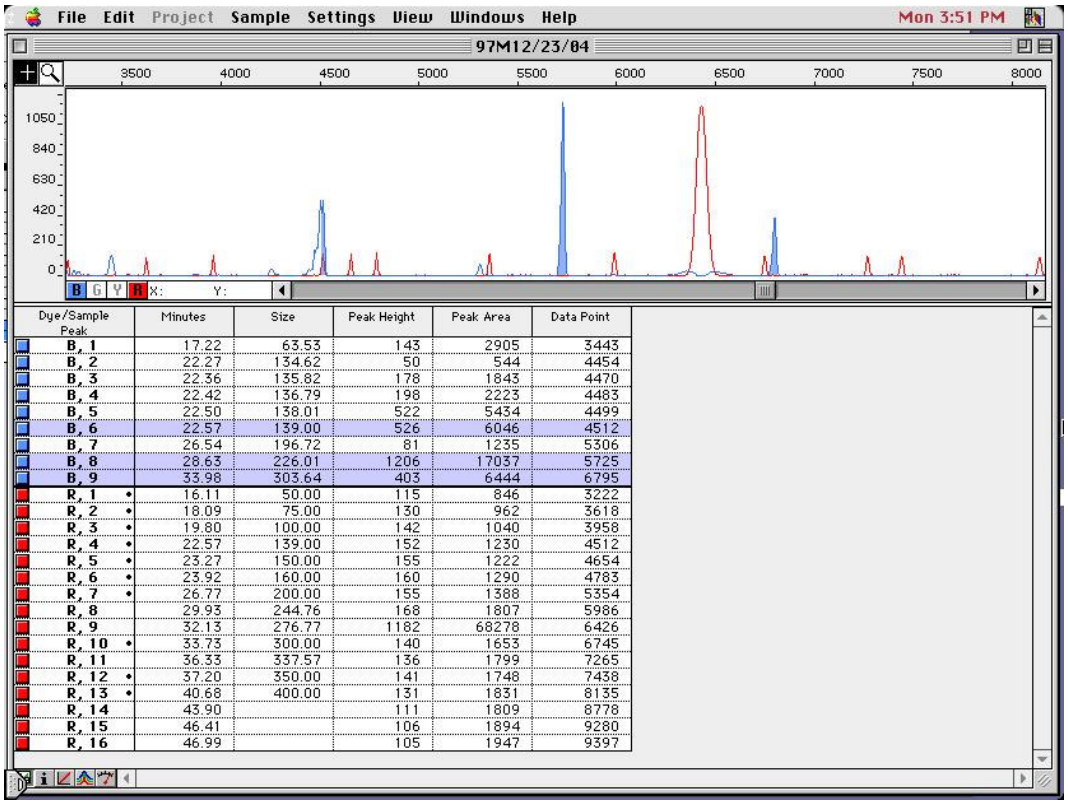

Dye/Sample Peak	Minutes	Size	Peak Height	Peak Area	Data Point
B, 1	17.22	63.53	143	2905	3443
B, 2	22.27	134.62	50	544	4454
B, 3	22.36	135.82	178	1843	4470
B, 4	22.42	136.79	198	2223	4483
B, 5	22.50	138.01	522	5434	4499
B, 6	22.57	139.00	526	6046	4512
B, 7	26.54	196.72	81	1235	5306
B, 8	28.63	226.01	1206	17037	5725
B, 9	33.98	303.64	403	6444	6795
R, 1 •	16.11	50.00	115	846	3222
R, 2 •	18.09	75.00	130	962	3618
R, 3 •	19.80	100.00	142	1040	3958
R, 4 •	22.57	139.00	152	1230	4512
R, 5 •	23.27	150.00	155	1222	4654
R, 6 •	23.92	160.00	160	1290	4783
R, 7 •	26.77	200.00	155	1388	5354
R, 8	29.93	244.76	168	1807	5986
R, 9	32.13	276.77	1182	68278	6426
R, 10 •	33.73	300.00	140	1653	6745
R, 11	36.33	337.57	136	1799	7265
R, 12 •	37.20	350.00	141	1748	7438
R, 13 •	40.68	400.00	131	1831	8135
R, 14	43.90		111	1809	8778
R, 15	46.41		106	1894	9280
R, 16	46.99		105	1947	9397

Figure A.3. Electropherogram of male control 3.

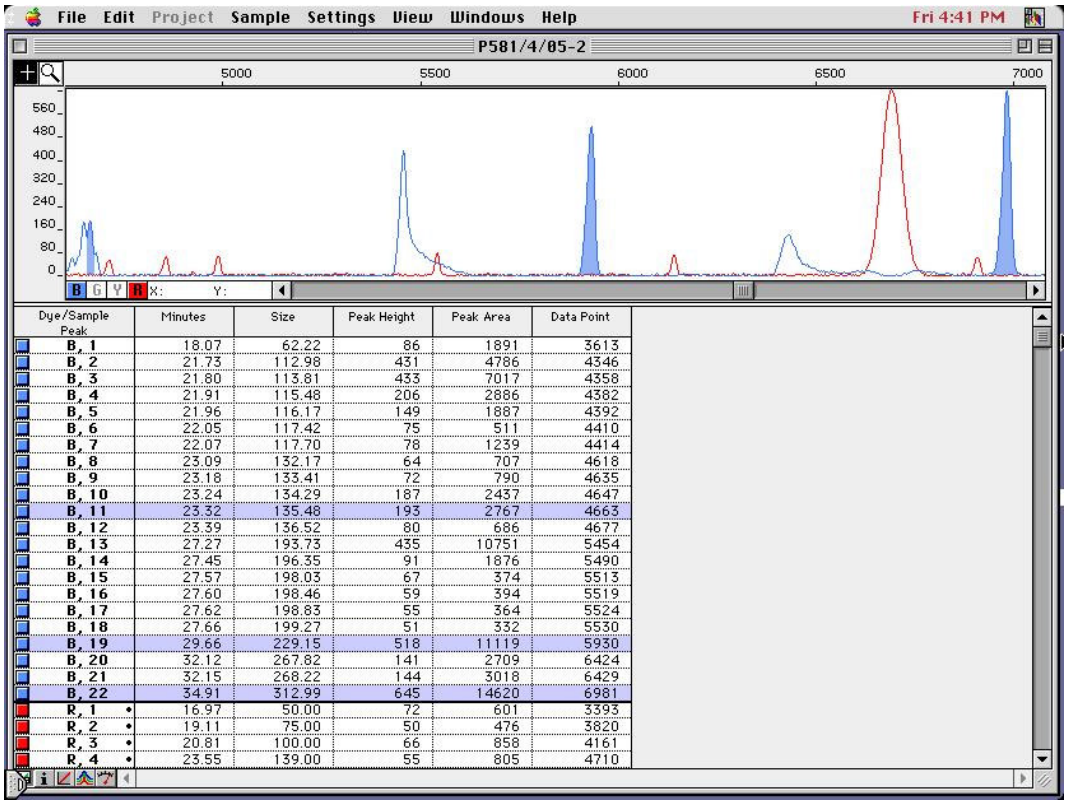

Dye/Sample Peak	Minutes	Size	Peak Height	Peak Area	Data Point
B, 1	18.07	62.22	86	1891	3613
B, 2	21.73	112.98	431	4786	4346
B, 3	21.80	113.81	433	7017	4358
B, 4	21.91	115.48	206	2886	4382
B, 5	21.96	116.17	149	1887	4392
B, 6	22.05	117.42	75	511	4410
B, 7	22.07	117.70	78	1239	4414
B, 8	23.09	132.17	64	707	4618
B, 9	23.18	133.41	72	790	4635
B, 10	23.24	134.29	187	2437	4647
B, 11	23.32	135.48	193	2767	4663
B, 12	23.39	136.52	80	686	4677
B, 13	27.27	193.73	435	10751	5454
B, 14	27.45	196.35	91	1876	5490
B, 15	27.57	198.03	67	374	5513
B, 16	27.60	198.46	59	394	5519
B, 17	27.62	198.83	55	364	5524
B, 18	27.66	199.27	51	332	5530
B, 19	29.66	229.15	518	11119	5930
B, 20	32.12	267.82	141	2709	6424
B, 21	32.15	268.22	144	3018	6429
B, 22	34.91	312.99	645	14620	6981
R, 1 •	16.97	50.00	72	601	3393
R, 2 •	19.11	75.00	50	476	3820
R, 3 •	20.81	100.00	66	858	4161
R, 4 •	23.55	139.00	55	805	4710

Figure A.4. Electropherogram of male control 4.

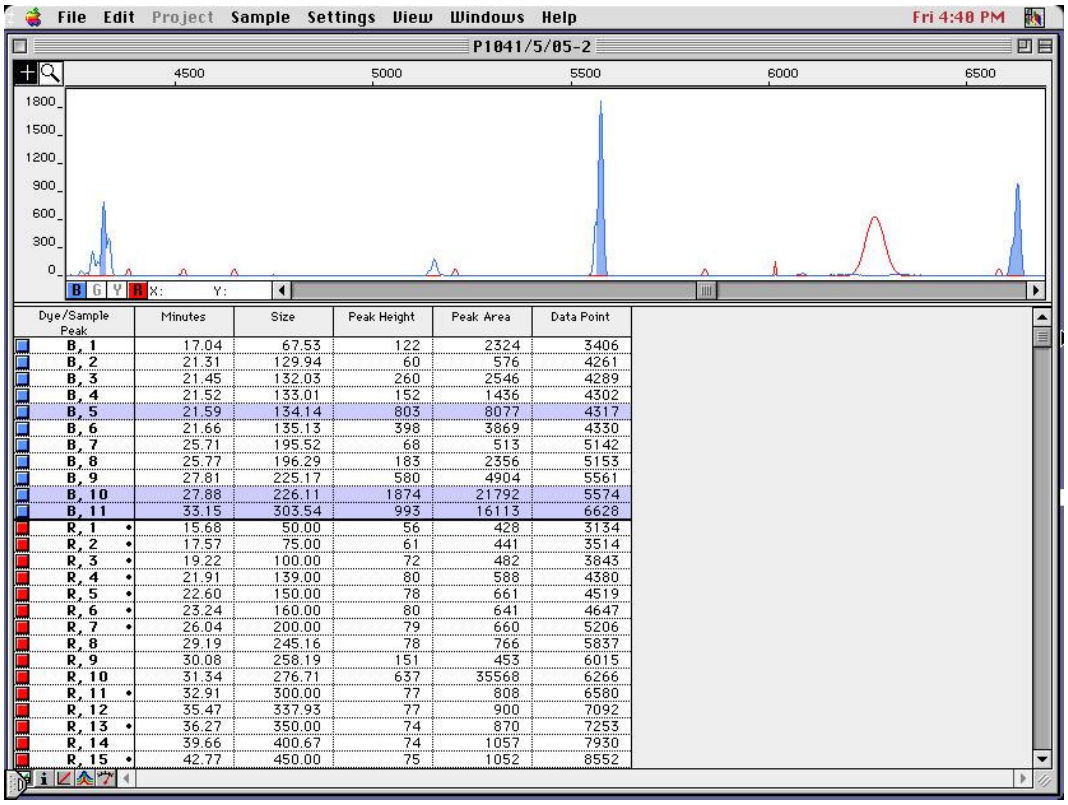

Dye/Sample Peak	Minutes	Size	Peak Height	Peak Area	Data Point
B, 1	17.04	67.53	122	2324	3406
B, 2	21.31	129.94	60	576	4261
B, 3	21.45	132.03	260	2546	4289
B, 4	21.52	133.01	152	1436	4302
B, 5	21.59	134.14	803	8077	4317
B, 6	21.66	135.13	398	3869	4330
B, 7	25.71	195.52	68	513	5142
B, 8	25.77	196.29	183	2356	5153
B, 9	27.81	225.17	580	4904	5561
B, 10	27.88	226.11	1874	21792	5574
B, 11	33.15	303.54	993	16113	6628
R, 1 •	15.68	50.00	56	428	3134
R, 2 •	17.57	75.00	61	441	3514
R, 3 •	19.22	100.00	72	482	3843
R, 4 •	21.91	139.00	80	588	4380
R, 5 •	22.60	150.00	78	661	4519
R, 6 •	23.24	160.00	80	641	4647
R, 7 •	26.04	200.00	79	660	5206
R, 8	29.19	245.16	78	766	5837
R, 9	30.08	258.19	151	453	6015
R, 10	31.34	276.71	637	35568	6266
R, 11 •	32.91	300.00	77	808	6580
R, 12	35.47	337.93	77	900	7092
R, 13 •	36.27	350.00	74	870	7253
R, 14	39.66	400.67	74	1057	7930
R, 15 •	42.77	450.00	75	1052	8552

Figure A.5. Electropherogram of male control 5.

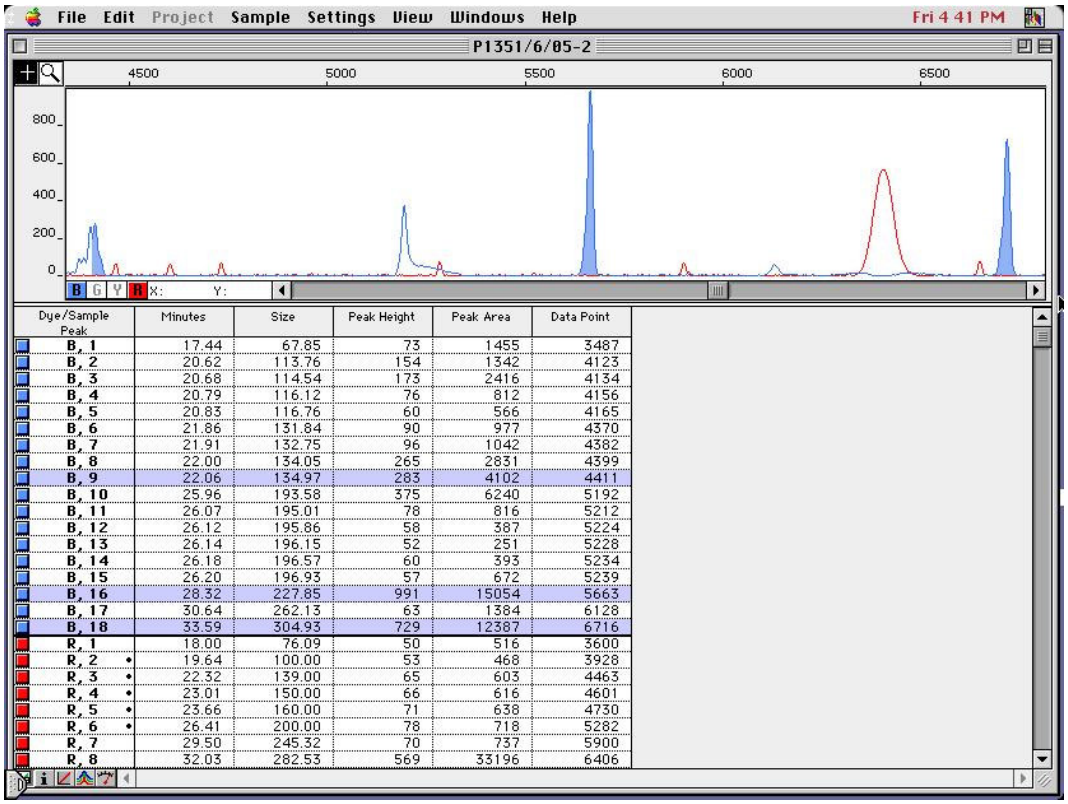

Dye/Sample Peak	Minutes	Size	Peak Height	Peak Area	Data Point
B, 1	17.44	67.85	73	1455	3487
B, 2	20.62	113.76	154	1342	4123
B, 3	20.68	114.54	173	2416	4134
B, 4	20.79	116.12	76	812	4156
B, 5	20.83	116.76	60	566	4165
B, 6	21.86	131.84	90	977	4370
B, 7	21.91	132.75	96	1042	4382
B, 8	22.00	134.05	265	2831	4399
B, 9	22.06	134.97	283	4102	4411
B, 10	25.96	193.58	375	6240	5192
B, 11	26.07	195.01	78	816	5212
B, 12	26.12	195.86	58	387	5224
B, 13	26.14	196.15	52	251	5228
B, 14	26.18	196.57	60	393	5234
B, 15	26.20	196.93	57	672	5239
B, 16	28.32	227.85	991	15054	5663
B, 17	30.64	262.13	63	1384	6128
B, 18	33.59	304.93	729	12387	6716
R, 1	18.00	76.09	50	516	3600
R, 2 •	19.64	100.00	53	468	3928
R, 3 •	22.32	139.00	65	603	4463
R, 4 •	23.01	150.00	66	616	4601
R, 5 •	23.66	160.00	71	638	4730
R, 6 •	26.41	200.00	78	718	5282
R, 7	29.50	245.32	70	737	5900
R, 8	32.03	282.53	569	33196	6406

Figure A.6. Electropherogram of male control 6.

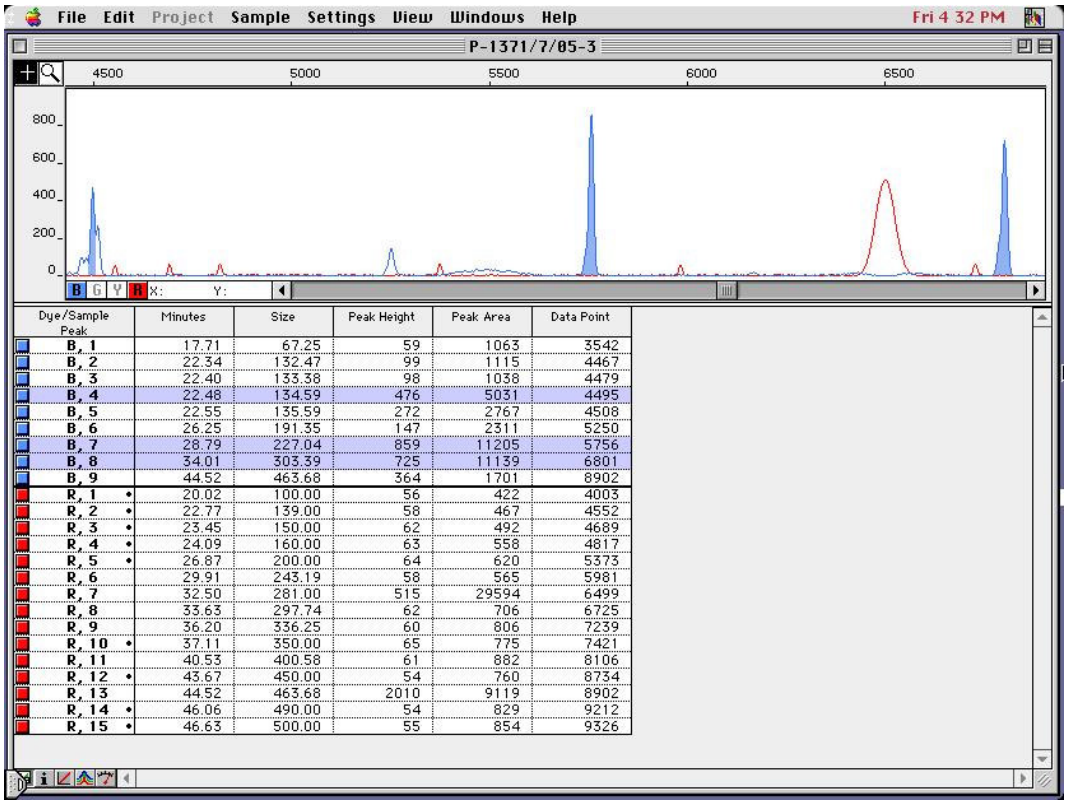

Dye/Sample Peak	Minutes	Size	Peak Height	Peak Area	Data Point
B, 1	17.71	67.25	59	1063	3542
B, 2	22.34	132.47	99	1115	4467
B, 3	22.40	133.38	98	1038	4479
B, 4	22.48	134.59	476	5031	4495
B, 5	22.55	135.59	272	2767	4508
B, 6	26.25	191.35	147	2311	5250
B, 7	28.79	227.04	859	11205	5756
B, 8	34.01	303.39	725	11139	6801
B, 9	44.52	463.68	364	1701	8902
R, 1 •	20.02	100.00	56	422	4003
R, 2 •	22.77	139.00	58	467	4552
R, 3 •	23.45	150.00	62	492	4689
R, 4 •	24.09	160.00	63	558	4817
R, 5 •	26.87	200.00	64	620	5373
R, 6	29.91	243.19	58	565	5981
R, 7	32.50	281.00	515	29594	6499
R, 8	33.63	297.74	62	706	6725
R, 9	36.20	336.25	60	806	7239
R, 10 •	37.11	350.00	65	775	7421
R, 11	40.53	400.58	61	882	8106
R, 12 •	43.67	450.00	54	760	8734
R, 13	44.52	463.68	2010	9119	8902
R, 14 •	46.06	490.00	54	829	9212
R, 15 •	46.63	500.00	55	854	9326

Figure A.7. Electropherogram of male control 7.

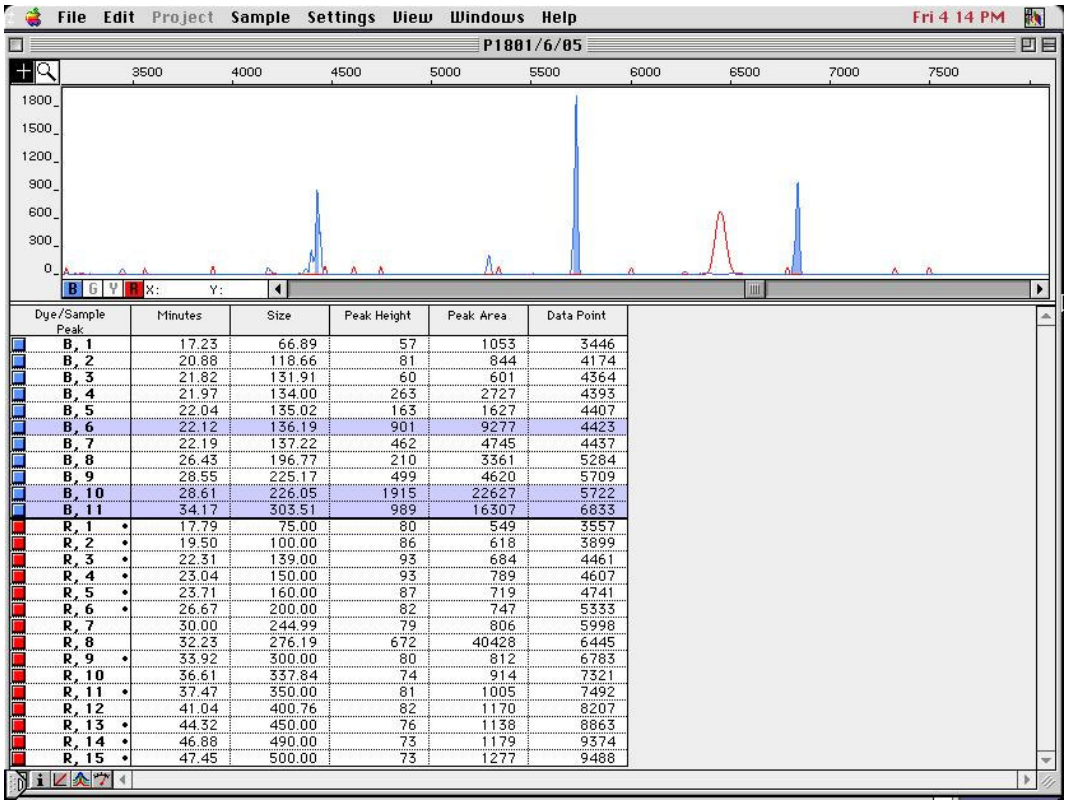

Dye/Sample Peak	Minutes	Size	Peak Height	Peak Area	Data Point
B, 1	17.23	66.89	57	1053	3446
B, 2	20.88	118.66	81	844	4174
B, 3	21.82	131.91	60	601	4364
B, 4	21.97	134.00	263	2727	4393
B, 5	22.04	135.02	163	1627	4407
B, 6	22.12	136.19	901	9277	4423
B, 7	22.19	137.22	462	4745	4437
B, 8	26.43	196.77	210	3361	5284
B, 9	28.55	225.17	499	4620	5709
B, 10	28.61	226.05	1915	22627	5722
B, 11	34.17	303.51	989	16307	6833
R, 1 •	17.79	75.00	80	549	3557
R, 2 •	19.50	100.00	86	618	3899
R, 3 •	22.31	139.00	93	684	4461
R, 4 •	23.04	150.00	93	789	4607
R, 5 •	23.71	160.00	87	719	4741
R, 6 •	26.67	200.00	82	747	5333
R, 7	30.00	244.99	79	806	5998
R, 8	32.23	276.19	672	40428	6445
R, 9 •	33.92	300.00	80	812	6783
R, 10	36.61	337.84	74	914	7321
R, 11 •	37.47	350.00	81	1005	7492
R, 12	41.04	400.76	82	1170	8207
R, 13 •	44.32	450.00	76	1138	8863
R, 14 •	46.88	490.00	73	1179	9374
R, 15 •	47.45	500.00	73	1277	9488

Figure A.8. Electropherogram of male control 8.

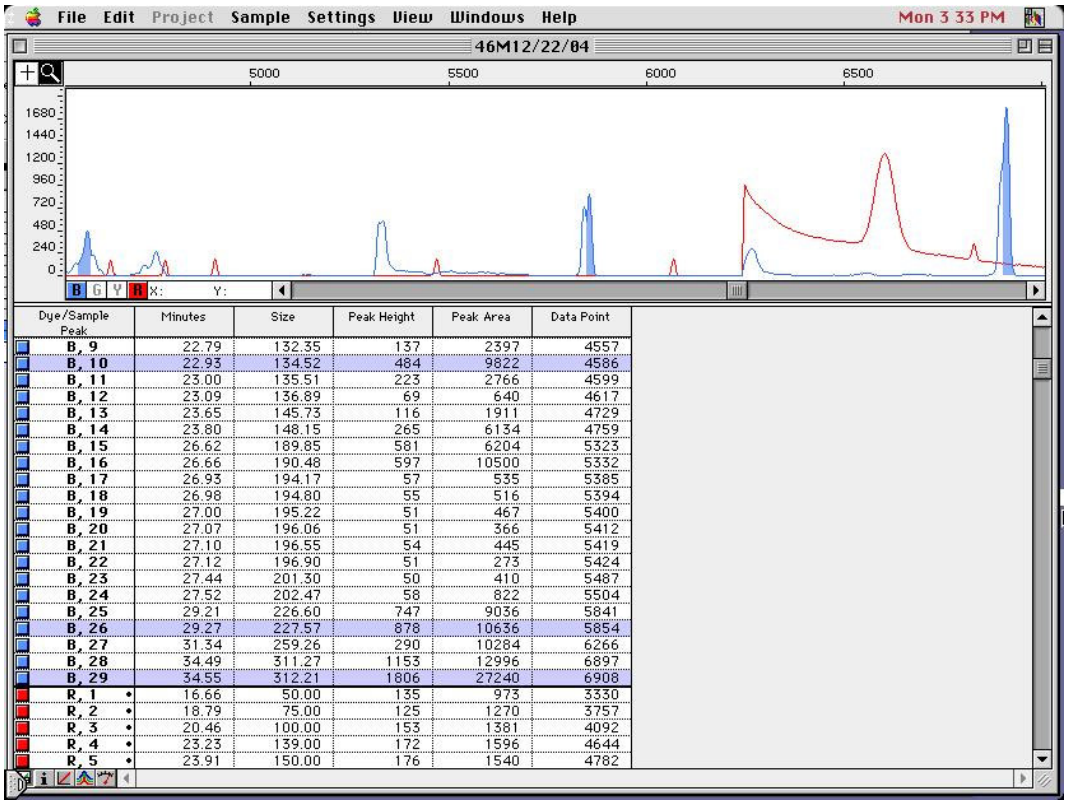

Dye/Sample Peak	Minutes	Size	Peak Height	Peak Area	Data Point
B, 9	22.79	132.35	137	2397	4557
B, 10	22.93	134.52	484	9822	4586
B, 11	23.00	135.51	223	2766	4599
B, 12	23.09	136.89	69	640	4617
B, 13	23.65	145.73	116	1911	4729
B, 14	23.80	148.15	265	6134	4759
B, 15	26.62	189.85	581	6204	5323
B, 16	26.66	190.48	597	10500	5332
B, 17	26.93	194.17	57	535	5385
B, 18	26.98	194.80	55	516	5394
B, 19	27.00	195.22	51	467	5400
B, 20	27.07	196.06	51	366	5412
B, 21	27.10	196.55	54	445	5419
B, 22	27.12	196.90	51	273	5424
B, 23	27.44	201.30	50	410	5487
B, 24	27.52	202.47	58	822	5504
B, 25	29.21	226.60	747	9036	5841
B, 26	29.27	227.57	878	10636	5854
B, 27	31.34	259.26	290	10284	6266
B, 28	34.49	311.27	1153	12996	6897
B, 29	34.55	312.21	1806	27240	6908
R, 1 •	16.66	50.00	135	973	3330
R, 2 •	18.79	75.00	125	1270	3757
R, 3 •	20.46	100.00	153	1381	4092
R, 4 •	23.23	139.00	172	1596	4644
R, 5 •	23.91	150.00	176	1540	4782

Figure A.9. Electropherogram of female control 1.

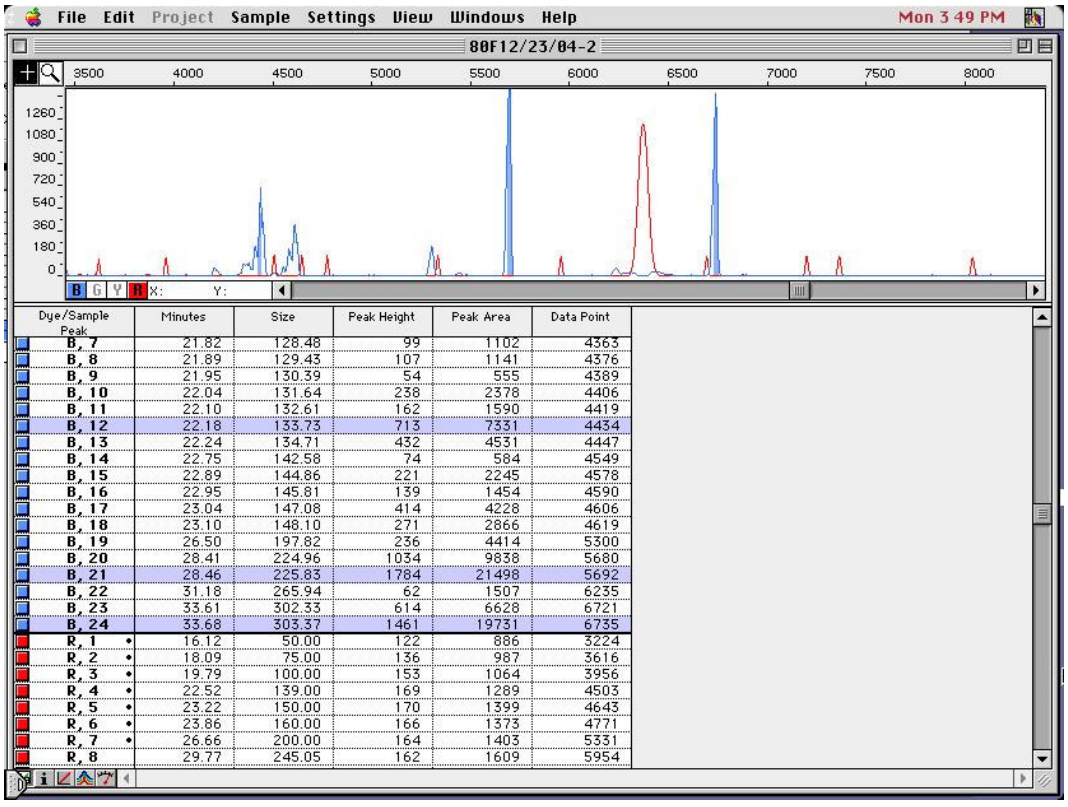

Dye/Sample Peak	Minutes	Size	Peak Height	Peak Area	Data Point
B, 7	21.82	128.48	99	1102	4363
B, 8	21.89	129.43	107	1141	4376
B, 9	21.95	130.39	54	555	4389
B, 10	22.04	131.64	238	2378	4406
B, 11	22.10	132.61	162	1590	4419
B, 12	22.18	133.73	713	7331	4434
B, 13	22.24	134.71	432	4531	4447
B, 14	22.75	142.58	74	584	4549
B, 15	22.89	144.86	221	2245	4578
B, 16	22.95	145.81	139	1454	4590
B, 17	23.04	147.08	414	4228	4606
B, 18	23.10	148.10	271	2866	4619
B, 19	26.50	197.82	236	4414	5300
B, 20	28.41	224.96	1034	9838	5680
B, 21	28.46	225.83	1784	21498	5692
B, 22	31.18	265.94	62	1507	6235
B, 23	33.61	302.33	614	6628	6721
B, 24	33.68	303.37	1461	19731	6735
R, 1 •	16.12	50.00	122	886	3224
R, 2 •	18.09	75.00	136	987	3616
R, 3 •	19.79	100.00	153	1064	3956
R, 4 •	22.52	139.00	169	1289	4503
R, 5 •	23.22	150.00	170	1399	4643
R, 6 •	23.86	160.00	166	1373	4771
R, 7 •	26.66	200.00	164	1403	5331
R, 8	29.77	245.05	162	1609	5954

Figure A.10. Electropherogram of female control 2.

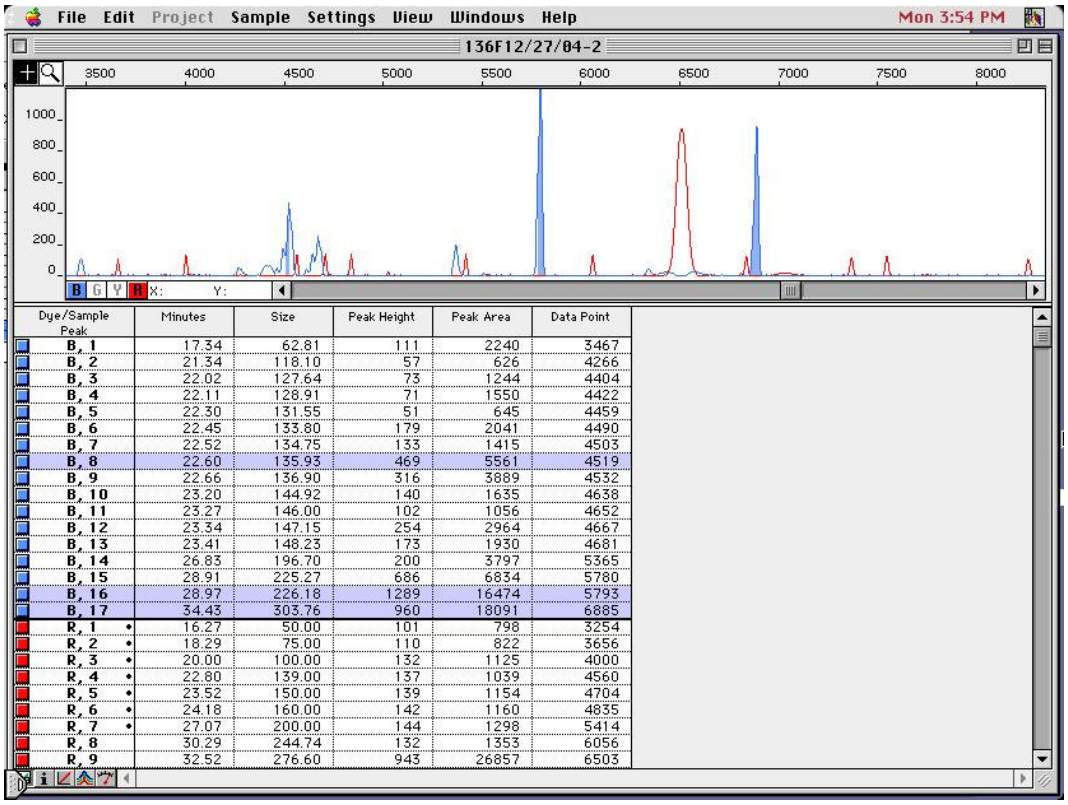

Dye/Sample Peak	Minutes	Size	Peak Height	Peak Area	Data Point
B, 1	17.34	62.81	111	2240	3467
B, 2	21.34	118.10	57	626	4266
B, 3	22.02	127.64	73	1244	4404
B, 4	22.11	128.91	71	1550	4422
B, 5	22.30	131.55	51	645	4459
B, 6	22.45	133.80	179	2041	4490
B, 7	22.52	134.75	133	1415	4503
B, 8	22.60	135.93	469	5561	4519
B, 9	22.66	136.90	316	3889	4532
B, 10	23.20	144.92	140	1635	4638
B, 11	23.27	146.00	102	1056	4652
B, 12	23.34	147.15	254	2964	4667
B, 13	23.41	148.23	173	1930	4681
B, 14	26.83	196.70	200	3797	5365
B, 15	28.91	225.27	686	6834	5780
B, 16	28.97	226.18	1289	16474	5793
B, 17	34.43	303.76	960	18091	6885
R, 1 •	16.27	50.00	101	798	3254
R, 2 •	18.29	75.00	110	822	3656
R, 3 •	20.00	100.00	132	1125	4000
R, 4 •	22.80	139.00	137	1039	4560
R, 5 •	23.52	150.00	139	1154	4704
R, 6 •	24.18	160.00	142	1160	4835
R, 7 •	27.07	200.00	144	1298	5414
R, 8	30.29	244.74	132	1353	6056
R, 9	32.52	276.60	943	26857	6503

Figure A.11. Electropherogram of female control 3.

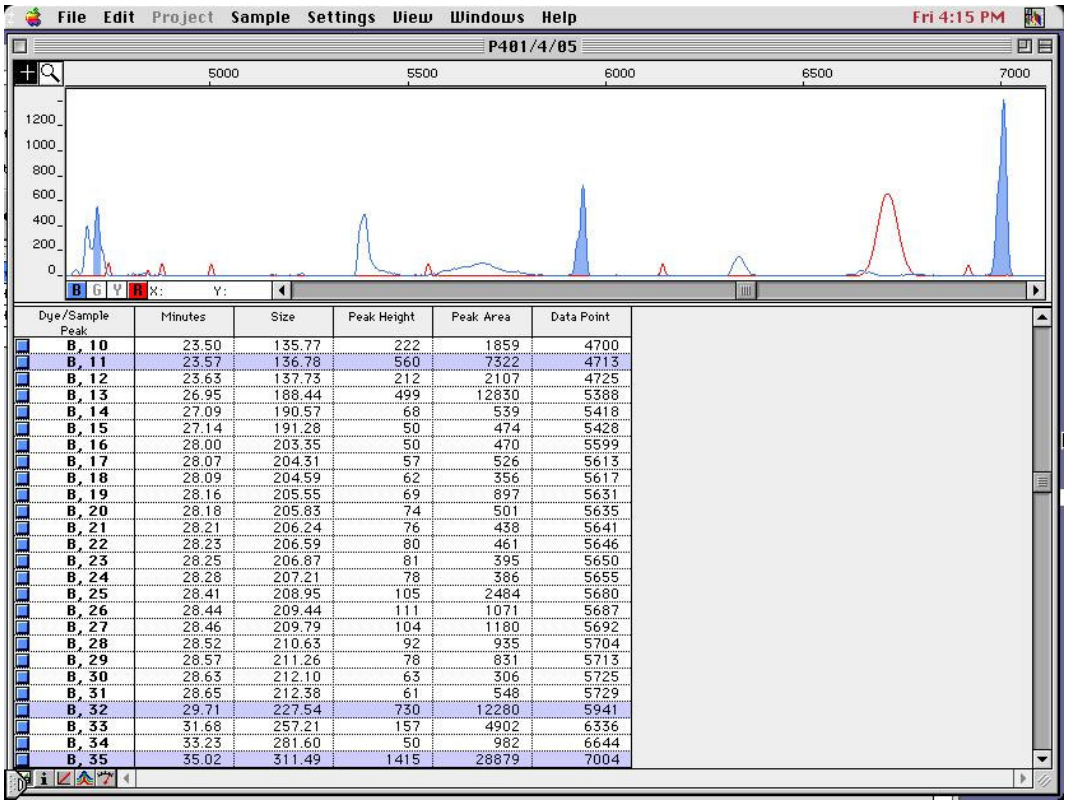

Dye/Sample Peak	Minutes	Size	Peak Height	Peak Area	Data Point
B, 10	23.50	135.77	222	1859	4700
B, 11	23.57	136.78	560	7322	4713
B, 12	23.63	137.73	212	2107	4725
B, 13	26.95	188.44	499	12830	5388
B, 14	27.09	190.57	68	539	5418
B, 15	27.14	191.28	50	474	5428
B, 16	28.00	203.35	50	470	5599
B, 17	28.07	204.31	57	526	5613
B, 18	28.09	204.59	62	356	5617
B, 19	28.16	205.55	69	897	5631
B, 20	28.18	205.83	74	501	5635
B, 21	28.21	206.24	76	438	5641
B, 22	28.23	206.59	80	461	5646
B, 23	28.25	206.87	81	395	5650
B, 24	28.28	207.21	78	386	5655
B, 25	28.41	208.95	105	2484	5680
B, 26	28.44	209.44	111	1071	5687
B, 27	28.46	209.79	104	1180	5692
B, 28	28.52	210.63	92	935	5704
B, 29	28.57	211.26	78	831	5713
B, 30	28.63	212.10	63	306	5725
B, 31	28.65	212.38	61	548	5729
B, 32	29.71	227.54	730	12280	5941
B, 33	31.68	257.21	157	4902	6336
B, 34	33.23	281.60	50	982	6644
B, 35	35.02	311.49	1415	28879	7004

Figure A.12. Electropherogram of female control 4.

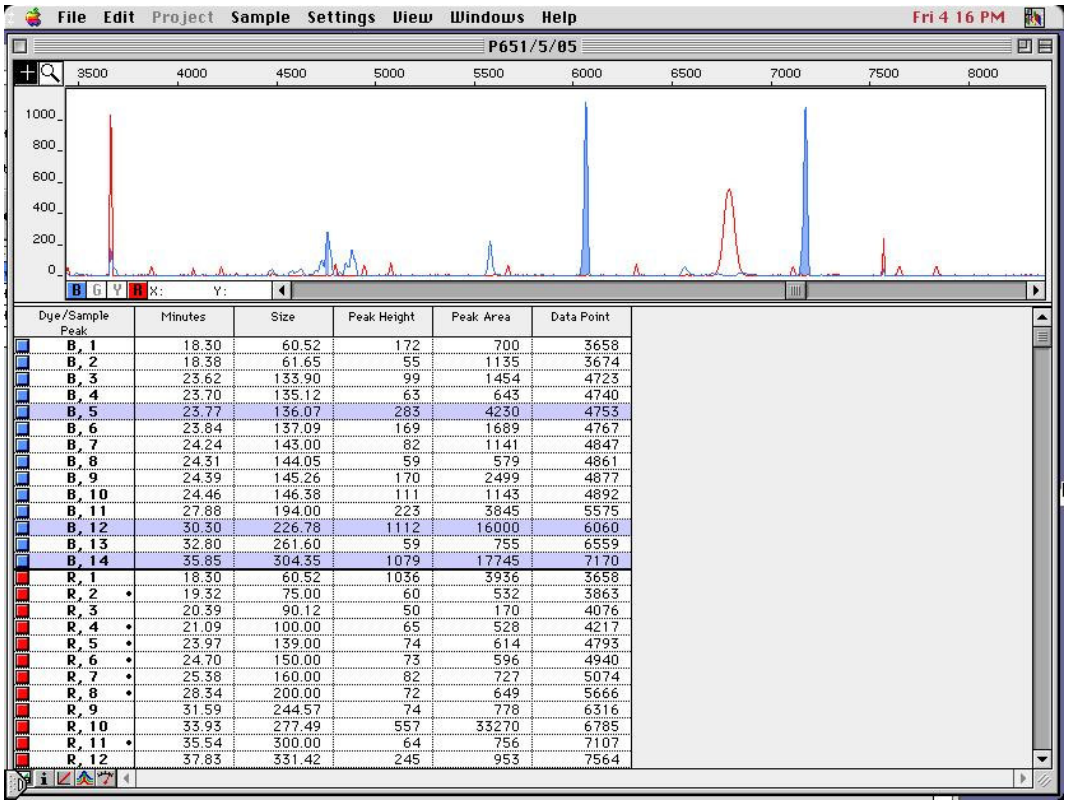

Dye/Sample Peak	Minutes	Size	Peak Height	Peak Area	Data Point
B, 1	18.30	60.52	172	700	3658
B, 2	18.38	61.65	55	1135	3674
B, 3	23.62	133.90	99	1454	4723
B, 4	23.70	135.12	63	643	4740
B, 5	23.77	136.07	283	4230	4753
B, 6	23.84	137.09	169	1689	4767
B, 7	24.24	143.00	82	1141	4847
B, 8	24.31	144.05	59	579	4861
B, 9	24.39	145.26	170	2499	4877
B, 10	24.46	146.38	111	1143	4892
B, 11	27.88	194.00	223	3845	5575
B, 12	30.30	226.78	1112	16000	6060
B, 13	32.80	261.60	59	755	6559
B, 14	35.85	304.35	1079	17745	7170
R, 1	18.30	60.52	1036	3936	3658
R, 2 •	19.32	75.00	60	532	3863
R, 3	20.39	90.12	50	170	4076
R, 4 •	21.09	100.00	65	528	4217
R, 5 •	23.97	139.00	74	614	4793
R, 6 •	24.70	150.00	73	596	4940
R, 7 •	25.38	160.00	82	727	5074
R, 8 •	28.34	200.00	72	649	5666
R, 9	31.59	244.57	74	778	6316
R, 10	33.93	277.49	557	33270	6785
R, 11 •	35.54	300.00	64	756	7107
R, 12	37.83	331.42	245	953	7564

Figure A.13. Electropherogram of female control 5.

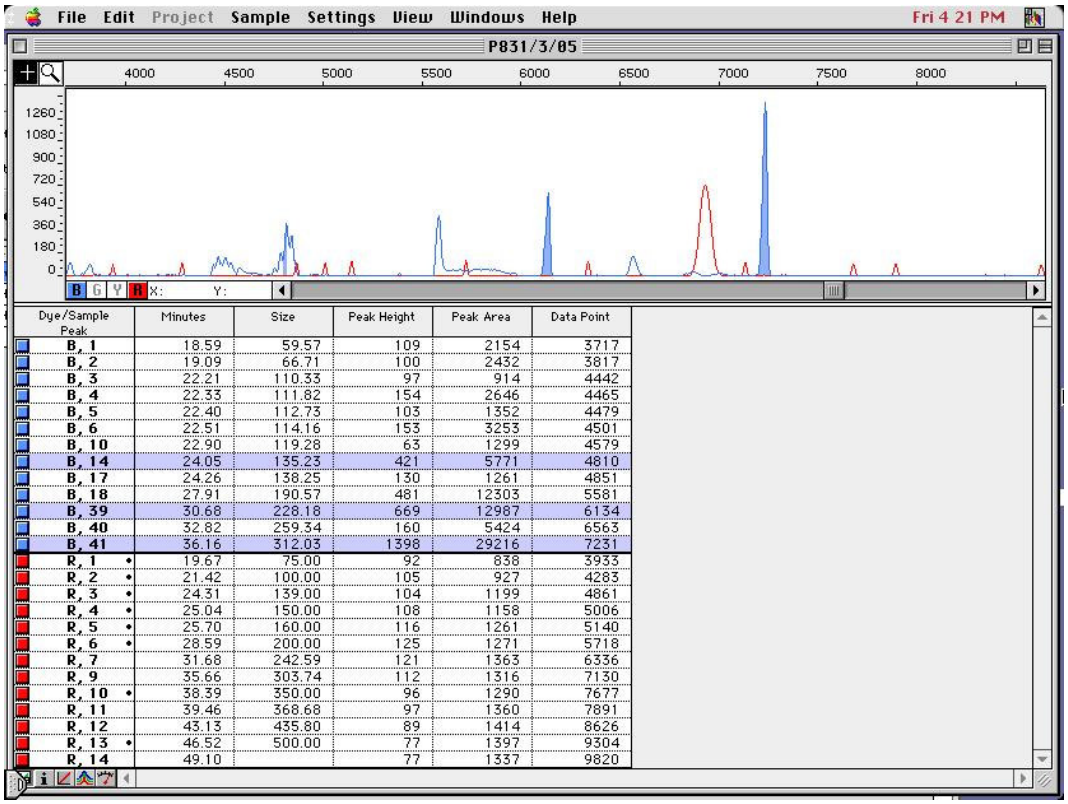

Dye/Sample Peak	Minutes	Size	Peak Height	Peak Area	Data Point
B, 1	18.59	59.57	109	2154	3717
B, 2	19.09	66.71	100	2432	3817
B, 3	22.21	110.33	97	914	4442
B, 4	22.33	111.82	154	2646	4465
B, 5	22.40	112.73	103	1352	4479
B, 6	22.51	114.16	153	3253	4501
B, 10	22.90	119.28	63	1299	4579
B, 14	24.05	135.23	421	5771	4810
B, 17	24.26	138.25	130	1261	4851
B, 18	27.91	190.57	481	12303	5581
B, 39	30.68	228.18	669	12987	6134
B, 40	32.82	259.34	160	5424	6563
B, 41	36.16	312.03	1398	29216	7231
R, 1 •	19.67	75.00	92	838	3933
R, 2 •	21.42	100.00	105	927	4283
R, 3 •	24.31	139.00	104	1199	4861
R, 4 •	25.04	150.00	108	1158	5006
R, 5 •	25.70	160.00	116	1261	5140
R, 6 •	28.59	200.00	125	1271	5718
R, 7	31.68	242.59	121	1363	6336
R, 9	35.66	303.74	112	1316	7130
R, 10 •	38.39	350.00	96	1290	7677
R, 11	39.46	368.68	97	1360	7891
R, 12	43.13	435.80	89	1414	8626
R, 13 •	46.52	500.00	77	1397	9304
R, 14	49.10		77	1337	9820

Figure A.14. Electropherogram of female control 6.

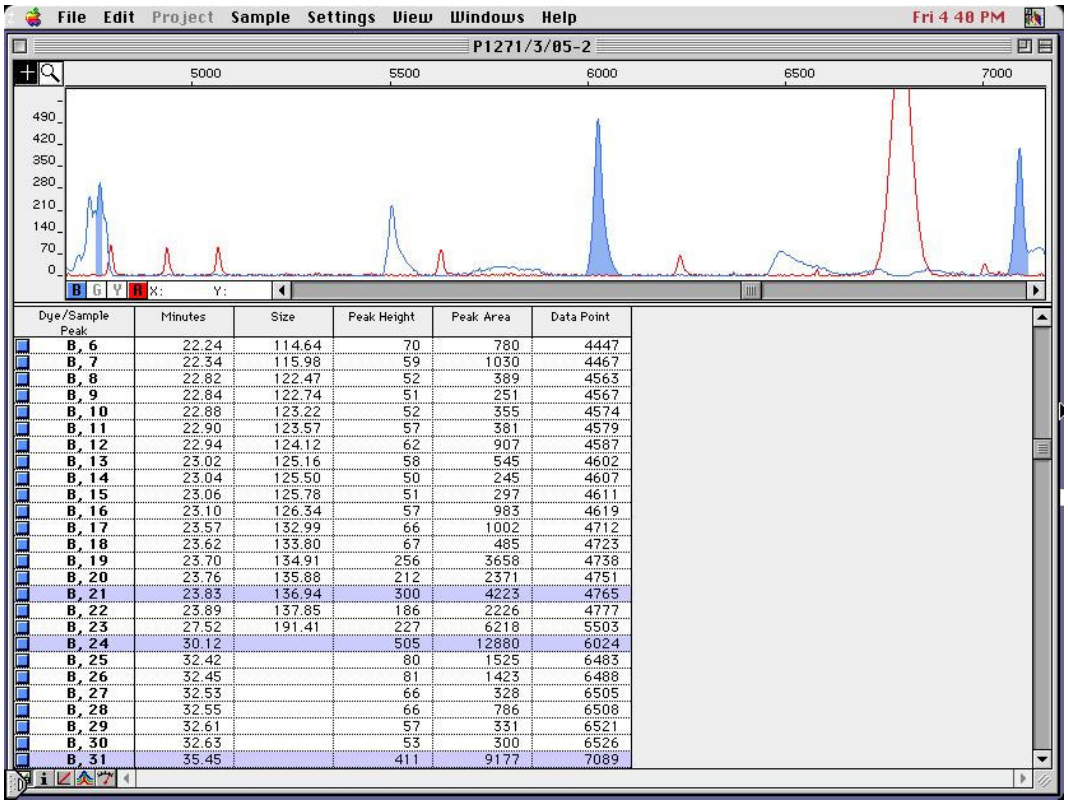

Dye/Sample Peak	Minutes	Size	Peak Height	Peak Area	Data Point
B, 6	22.24	114.64	70	780	4447
B, 7	22.34	115.98	59	1030	4467
B, 8	22.82	122.47	52	389	4563
B, 9	22.84	122.74	51	251	4567
B, 10	22.88	123.22	52	355	4574
B, 11	22.90	123.57	57	381	4579
B, 12	22.94	124.12	62	907	4587
B, 13	23.02	125.16	58	545	4602
B, 14	23.04	125.50	50	245	4607
B, 15	23.06	125.78	51	297	4611
B, 16	23.10	126.34	57	983	4619
B, 17	23.57	132.99	66	1002	4712
B, 18	23.62	133.80	67	485	4723
B, 19	23.70	134.91	256	3658	4738
B, 20	23.76	135.88	212	2371	4751
B, 21	23.83	136.94	300	4223	4765
B, 22	23.89	137.85	186	2226	4777
B, 23	27.52	191.41	227	6218	5503
B, 24	30.12		505	12880	6024
B, 25	32.42		80	1525	6483
B, 26	32.45		81	1423	6488
B, 27	32.53		66	328	6505
B, 28	32.55		66	786	6508
B, 29	32.61		57	331	6521
B, 30	32.63		53	300	6526
B, 31	35.45		411	9177	7089

Figure A.15. Electropherogram of female control 7.

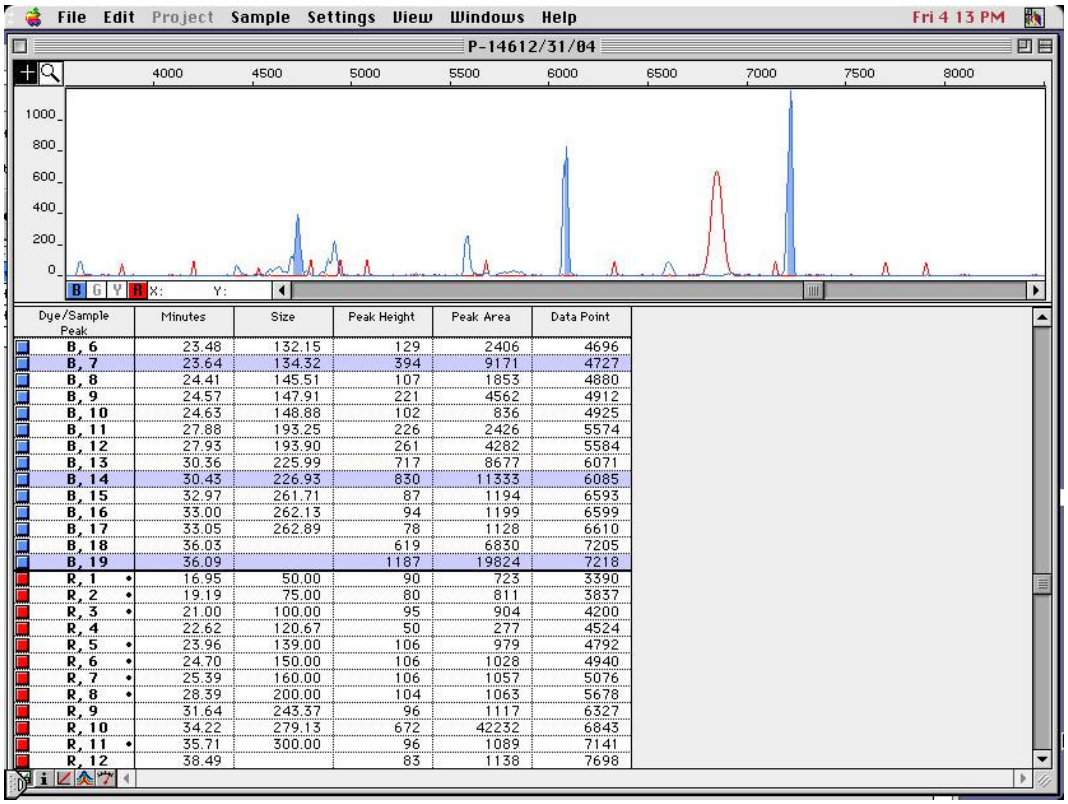

Dye/Sample Peak	Minutes	Size	Peak Height	Peak Area	Data Point
B, 6	23.48	132.15	129	2406	4696
B, 7	23.64	134.32	394	9171	4727
B, 8	24.41	145.51	107	1853	4880
B, 9	24.57	147.91	221	4562	4912
B, 10	24.63	148.88	102	836	4925
B, 11	27.88	193.25	226	2426	5574
B, 12	27.93	193.90	261	4282	5584
B, 13	30.36	225.99	717	8677	6071
B, 14	30.43	226.93	830	11333	6085
B, 15	32.97	261.71	87	1194	6593
B, 16	33.00	262.13	94	1199	6599
B, 17	33.05	262.89	78	1128	6610
B, 18	36.03		619	6830	7205
B, 19	36.09		1187	19824	7218
R, 1 •	16.95	50.00	90	723	3390
R, 2 •	19.19	75.00	80	811	3837
R, 3 •	21.00	100.00	95	904	4200
R, 4	22.62	120.67	50	277	4524
R, 5 •	23.96	139.00	106	979	4792
R, 6 •	24.70	150.00	106	1028	4940
R, 7 •	25.39	160.00	106	1057	5076
R, 8 •	28.39	200.00	104	1063	5678
R, 9	31.64	243.37	96	1117	6327
R, 10	34.22	279.13	672	42232	6843
R, 11 •	35.71	300.00	96	1089	7141
R, 12	38.49		83	1138	7698

Figure A.16. Electropherogram of female control 8.

REFERENCES

Bandtlow, C. E. and M. E. Schwab, 2000, "NI-35/250/Nogo-A: A Neurite Growth Inhibitor Restricting Structural Plasticity and Regeneration of Nerve Fibers in the Adult Vertebrate CNS", *Glia*, Vol. 29, pp. 175-181.

Baumann, N. and D. Pham-Dinh, 2001, "Biology of Oligodendrocyte and Myelin in the Mammalian Central Nervous System", *Physiological Reviews*, Vol. 81, pp.871-927.

Baumgartner, B. G. and B. Brenig, 1996, "Isolation and Characterization of the Porcine Proteolipid Protein (PLP) Gene", *Journal of Animal Breeding and Genetics*, Vol. 113, pp. 311-321.

Berger, J., H. W. Moser and S. Forss-Petter, 2001, "Leukodysrophies: Recent Developments in Genetics, Molecular Biology, Pathogenesis and Treatment", *Current Opinion in Neurology*, Vol. 14, pp. 305-312.

Bergoffen, J., S. S. Scherer, S. Wang, M. O. Scott, L. J. Bone, D. L. Paul, K. Chen, M. W. Lensch, P. F. Chance and K. H. Fischbeck, 1993, "Connexin Mutations in X-Linked Charcot-Marie-Tooth Disease", *Science*, Vol. 262, pp. 2039-2042.

Bizzozero, O. A., J. F. McGarry and M. B. Lees, 1987, "Autoacylation of Myelin Proteolipid Protein with Acyl Coenzyme A", *The Journal of Biological Chemistry*, Vol. 262, pp. 13550-13557.

Blight, A., 1998, "Containing Plasticity: Neurite Inhibitory Factors of Myelin", *Nature Neuroscience*, Vol. 1, pp. 87-88.

Boison, D. and W. Stoffel, 1989, "Myelin-Deficient Rat: A Point Mutation in Exon III (A→C, Thr75→Pro) of the Myelin Proteolipid Protein Causes Dysmyelination and Oligodendrocyte Death", *EMBO Journal*, Vol. 8, pp. 3295-3302.

Boison, D. and W. Stoffel, 1994, "Disruption of the Compacted Myelin Sheath of Axons of the Central Nervous System in Proteolipid Protein-Deficient Mice", *Proceedings of the National Academy of Sciences of the United States of America*, Vol. 91, pp. 11709-11713.

Boison, D., H. Büssow, D. D'Urso, H. W. Müller and W. Stoffel, 1995, "Adhesive Properties of Proteolipid Protein are Responsible for the Compaction of CNS Myelin Sheaths", *The Journal of Neuroscience*, Vol. 15, pp. 5502-5513.

Boucher, S. E., M. A. Cypher, L. R. Carlock and R. P. Skoff, 2002, "Proteolipid Protein Gene Modulates Viability and Phenotype of Neurons", *The Journal of Neuroscience*, Vol. 22, pp. 1772-1783.

Boulloche, J. and J. Aicardi, 1986, "Pelizaeus-Merzbacher Disease: Clinical and Nosological Study", *Journal of Child Neurology*, Vol. 1, pp. 233-239.

Buckle, V. J., J. H. Edwards, E. P. Evans, J. A. Jonasson, M. F. Lyon, J. Peters and A. G. Searle, 1985, "Comparative Maps of Human and Mouse X Chromosomes", *Cytogenetics and Cell Genetics*, Vol. 40, pp. 594-595.

Bugiani, M., S. Al Shahwan, E. Lamantea, A. Bizzi, E. Bakhsh, I. Moroni, M. R. Balestrini, G. Uziel and M. Zeviani, 2006, "GJA12 Mutations in Children with Recessive Hypomyelinating Leukoencephalopathy", *Neurology*, Vol. 67, pp. 273-279.

Bunge, M. B., R. P. Bunge and G. D. Pappas, 1962, "Electron Microscopic Demonstration of the Connections between Glia and Myelin Sheath in the Developing Mammalian Central Nervous System", *The Journal of Cell Biology*, Vol. 12, pp. 448–459.

Bunge, R. P., 1968, "Glial Cells and the Central Myelin Sheath", *Physiological Reviews*, Vol. 48, pp. 197-210.

Butt, A. M. and B. Ransom, 1989, "Visualization of Oligodendrocytes and Astrocytes in the Intact Rat Optic Nerve by Intracellular Injection of Lucifer Yellow and Horseradish Peroxidase", *Glia*, Vol. 2, pp. 470-475.

Cailloux, F., F. Gauthier-Barichard, C. Mimault, V. Isabelle, V. Courtois, G. Giraud, B. Dastugue and O. Boespflug-Tanguy, 2000, "Genotype-Phenotype Correlation in Inherited Brain Myelination Defects due to Proteolipid Protein Gene Mutations", *European Journal of Human Genetics*, Vol. 8, pp. 837-845.

Calfon, M., H. Zeng, F. Urano, J. H. Till, S. R. Hubbard, H. P. Harding, S. G. Clark and D. Ron, 2002, "IRE1 Couples Endoplasmic Reticulum Load to Secretory Capacity by Processing the XBP-1 mRNA", *Nature*, Vol. 415, pp. 92-96.

Campagnoni, A. T. and W. B. Macklin, 1988, "Cellular and Molecular Aspects of Myelin Protein Gene Expression", *Molecular Neurobiology*, Vol. 2, pp. 41-89.

Campagnoni, C. W., B. Garbay, P. Micevych, T. Pribyl, K. Kampf, V. W. Handley and A. T. Campagnoni, 1992, "DM20 mRNA Splice Product of the Myelin Proteolipid Protein Gene is Expressed in the Murine Heart", *Journal of Neuroscience Research*, Vol. 33, pp. 148-155.

Campagnoni, A. T. and R. P. Skoff, 2001, "The Pathobiology of Myelin Mutants Reveal Novel Biological Functions of the MBP and PLP Genes", *Brain Pathology*, Vol. 11, pp. 74-91.

Cremers, F. P., R. A. Pfeiffer, T. J. van de Pol, M. H. Hofker, T. A. Kruse, B. Wieringa and H. H. Ropers, 1987, "An Interstitial Duplication of the X Chromosome in a Male Allows Physical Fine Mapping of Probes from the Xq13-q22 Region", *Human Genetics*, Vol. 77, pp. 23-27.

Cremers, F. P., T. J. van de Pol, B. Wieringa, M. H. Hofker, P. L. Pearson, R. A. Pfeiffer, M. Mikkelsen, A. Tabor and H. H. Ropers, 1988, "Molecular Analysis of Male-

Viable Deletions and Duplications Allows Ordering of 52 DNA probes on Proximal Xq", *American Journal of Human Genetics*, Vol. 43, pp. 452-461.

Curtis, R., J. Cohen, J. Fok-Seang, M. R. Hanley, N. A. Gregson, R. Reynolds and G. P. Wilkin, 1988, "Development of Macroglial Cells in Rat cerebellum. I. Use of Antibodies to Follow Early in vivo Development and Migration of Oligodendrocytes", *Journal of Neurocytology*, Vol. 17, pp. 43-54.

Dautigny, A., P. M. Alliel, L. d'Auriol, D. Pham-Dinh, J. L. Nussbaum and F. Galibert, 1985, "Molecular Cloning and Nucleotide Sequence of a cDNA Clone Coding for Rat Brain Myelin Proteolipid", *FEBS Letters*, Vol. 188, pp. 33-36.

Diehl, H. J., M. Schaich, R. M. Budzinski and W. Stoffel, 1986, "Individual Exons Encode the Integral Membrane Domains of Human Myelin Proteolipid Protein", *Proceedings of the National Academy of Sciences of the United States of America*, Vol. 83, pp. 9807-9811.

Ellis, D. and S. Malcolm, 1994, "Proteolipid Protein Gene Dosage Effect in Pelizaeus-Merzbacher Disease", *Nature Genetics*, Vol. 6, pp. 333-334.

Folch, J. and M. Lees, 1951, "Proteolipides, a New Type of Tissue Lipoproteins; Their Isolation from Brain", *The Journal of Biological Chemistry*, Vol. 191, pp. 807-817.

Forman, M. S., V. M. Lee and J. Q. Trojanowski, 2003, "Unfolding Pathways in Neurodegenerative Disease", *Trends in Neurosciences*, Vol. 26, pp. 407-410.

Fujimoto, K., B. I. Roots, R. M. Burton and H. C. Agrawal, 1976, "Morphological and Biochemical Characterization of Light and Heavy Myelin Isolated from Developing Rat Brain", *Biochimica et Biophysica Acta*, Vol. 426, pp. 659-668.

Garbern, J., F. Cambi, M. Shy and J. Kamholz, 1999, "The Molecular Pathogenesis of Pelizaeus-Merzbacher Disease", *Archives of Neurology*, Vol. 56, pp. 1210-1214.

Garbern, J. and G. Hobson, 2002, "Prenatal Diagnosis of Pelizaeus-Merzbacher Disease", *Prenatal Diagnosis*, Vol. 22, pp. 1033-1035.

Garbern, J., K. M. Krajewski and G. M. Hobson, 2006, *PLP-Related Disorders*, http://www.geneclinics.org/profiles/pmd

Garbern, J. Y., 2007, "Pelizaeus-Merzbacher Disease: Genetic and Cellular Pathogenesis", *Cellular and Molecular Life Sciences,* Vol. 64, pp. 50-65.

Gardinier, M. V., W. B. Macklin, A. J. Diniak and P. L. Deininger, 1986, "Characterization of Myelin Proteolipid mRNAs in Normal and Jimpy Mice", *Molecular and Cellular Biology*, Vol. 6, pp. 3755-3762.

Gencic, S. and L. D. Hudson, 1990, "Conservative Amino Acid Substitution in the Myelin Proteolipid Protein of jimpy^{msd} Mice", *The Journal of Neuroscience*, Vol. 10, pp. 117-124.

Gow, A., 1997, "Redefining the Lipophilin Family of Proteolipid Proteins", *Journal of Neuroscience Research*, Vol. 50, pp. 659-664.

Gow, A., A. Gragerov, A. Gard, D. R. Colman and R. A. Lazzarini, 1997, "Conservation of Topology, but not Conformation, of the Proteolipid Proteins of the Myelin Sheath", *The Journal of Neuroscience*, Vol. 17, pp. 181-189.

Gow, A., C. M. Southwood and R. A. Lazzarini, 1998, "Disrupted Proteolipid Protein Trafficking Results in Oligodendrocyte Apoptosis in an Animal Model of Pelizaeus-Merzbacher Disease", *The Journal of Cell Biology*, Vol. 140, pp. 925-934.

Gratacos, M., M. Nadal, R. Martin-Santos, M.A. Pujana, J. Gago, B. Peral, L. Armengol, I. Ponsa, R. Miro, A. Bulbena and X. Estivill, 2001, "A Polymorphic Genomic Duplication on Human Chromosome 15 is a Susceptibility Factor for Panic and Phobic Disorders", *Cell*, Vol. 106, pp. 367-379.

Griffiths, I. R., P. Dickinson and P. Montague, 1995, "Expression of the Proteolipid Protein Gene in Glial Cells of the Post-Natal Peripheral Nervous System of Rodents", *Neuropathology and Applied Neurobiology*, Vol. 21, pp. 97-110.

Griffiths, I., M. Klugmann, T. Anderson, C. Thomson, D. Vouyiouklis and K. A. Nave, 1998a, "Current Concepts of PLP and Its Role in the Nervous System", *Microscopy Research and Technique*, Vol. 41, pp. 344-358.

Griffiths, I., M. Klugmann, T. Anderson, D. Yool, C. Thomson, M. H. Schwab, A. Schneider, F. Zimmermann, M. McCulloch, N. Nadon and K. A. Nave, 1998b, "Axonal Swellings and Degeneration in Mice Lacking the Major Proteolipid of Myelin", *Science*, Vol. 280, pp. 1610-1613.

Gudz, T. I., T. E. Schneider, T. A. Haas and W. B. Macklin, 2002, "Myelin Proteolipid Protein Forms a Complex with Integrins and May Participate in Integrin Receptor Signaling in Oligodendrocytes", *The Journal of Neuroscience*, Vol. 22, pp. 7398-7407.

Harding, H. P., I. Novoa, Y. Zhang, H. Zeng, R. Wek, M. Schapira and D. Ron, 2000, "Regulated Translation Initiation Controls Stress-Induced Gene Expression in Mammalian Cells", *Molecular Cell*, Vol. 6, pp. 1099-1108.

Hardy, R. and R. Reynolds, 1991, "Proliferation and Differentiation Potential of Rat Forebrain Oligodendroglial Progenitors both in vitro and in vivo", *Development*, Vol. 111, pp. 1061-1080.

Heim, P., M. Claussen, B. Hoffmann, E. Conzelmann, J. Gärtner, K. Harzer, D. H. Hunneman, W. Köhler, G. Kurlemann and A. Kohlschütter, 1997, "Leukodystrophy Incidence in Germany", *American Journal of Medical Genetics*, Vol. 71, pp. 475-478.

Helynck, G., B. Luu, J. L. Nussbaum, D. Picken, G. Skalidis, E. Trifilieff, A. Van Dorsselaer, P. Seta, R. Sandeaux, C. Gavach, F. Heitz, D. Simon and G. Spach, 1983,

"Brain Proteolipids. Isolation, Purification and Effect on Ionic Permeability of Membranes", *European Journal of Biochemistry*, Vol. 133, pp. 689-695.

Hobson, G. M., A. P. Davis, N. C. Stowell, E. H. Kolodny, E. A. Sistermans, I. F. de Coo, V. L. Funanage and H. G. Marks, 2000, "Mutations in Noncoding Regions of the Proteolipid Protein Gene in Pelizaeus-Merzbacher Disease", *Neurology*, Vol. 55, pp. 1089-1096.

Hodes, M. E., V. M. Pratt and S. R. Dlouhy, 1993, "Genetics of Pelizaeus-Merzbacher Disease", *Developmental Neuroscience*, Vol. 15, pp. 383-394.

Hodes, M. E., W. E. DeMyer, V. M. Pratt, M. K. Edwards, and S. R. Dlouhy, 1995, "Girls with Signs of Pelizaeus-Merzbacher Disease Heterozygous for a Mutation in Exon 2 of the Proteolipid Protein Gene", *American Journal of Human Genetics*, Vol. 55, pp. 397-401.

Hodes, M. E., C. A. Blank, V. M. Pratt, J. Morales, J. Napier and S. R. Dlouhy, 1997, "Nonsense Mutation in Exon 3 of the Proteolipid Protein Gene (PLP) in a Family with an Unusual Form of Pelizaeus-Merzbacher Disease", *American Journal of Medical Genetics*, Vol. 69, pp. 121-125.

Hodes, M. E., K. Woodward, N. B. Spinner, B. S. Emanuel, A. Enrico-Simon, J. Kamholz, D. Stambolian, E. H. Zackai, V. M. Pratt, I. T. Thomas, K. Crandall, S. R. Dlouhy and S. Malcolm, 2000, "Additional Copies of the Proteolipid Protein Gene Causing Pelizaeus-Merzbacher Disease Arise by Separate Integration into the X Chromosome", *American Journal of Human Genetics*, Vol. 67, pp. 14-22.

Hoffman, J. D., Y. Zhang, J. Greshock, K. L. Ciprero, B. S. Emanuel, E. H. Zackai, B. L. Weber and J. E. Ming, 2005, "Array Based CGH and FISH Fail to Confirm Duplication of 8p22-p23.1 in Association with Kabuki Syndrome" *Journal of Medical Genetics*, Vol. 42, pp. 49–53.

Hübner, C.A., U. Orth, A. Senning, C. Steglich, A. Kohlschutter, R. Korinthenberg and A. Gal, 2005, "Seventeen Novel PLP1 Mutations in Patients with Pelizaeus-Merzbacher Disease", *Human Mutation*, Vol. 25, pp. 321-322.

Hudson, L. D. and N. L. Nadon, 1992, "Amino Acid Substitution in Proteolipid Protein that Cause Dysmyelination", in R. E. Martenson (ed.), *Myelin: Biology and Chemistry*, pp. 677-702, CRC Press, Boca Raton.

Hudson, L. D., N. Ko and J. G. Kim, 1996, "Control of Myelin Gene Expression", in K. R. Jessen and W. D. Richardson (eds.), *Glial Cell Development: Basic Principles and Clinical Relevance*, pp. 101-121, Bios Scientific Publishers, Oxford.

Hudson, L. D., J. G. Kim, C. Wiese, D. L. Yao, X. Liu, H. D. Webster, D. V. Agoston and R. Armstrong, 1997, "Transcriptional Controls in the Oligodendrocyte Lineage", in G. Jeserich, H. H. Althaus, C. Richter-Landsberg and R. Heumann (eds.), *Molecular Signalling and Regulation in Glial Cells: A Key to Remyelination and Functional Repair*, pp. 182-190, Springer-Verlag, Berlin.

Hudson, L. D., 2001, "Pelizaeus-Merzbacher Disease and Allelic Disorder X-Linked Spastic Paraplegia Type 2", in C. R. Scriver, A. L. Beaudet, W. S. Sly and D. Walle (eds.), *The Metabolic and Molecular Basis of Inherited Diseases*, pp. 5789-5798, McGraw-Hill, New York.

Ikenaka, K., T. Kagawa and K. Mikoshiba, 1992, "Selective Expression of DM-20, an Alternatively Spliced Myelin Proteolipid Protein Gene Product, in Developing Nervous System and in Nonglial Cells", *The Journal of Neurochemistry*, Vol. 58, pp. 2248-2253.

Inoue, K., H. Osaka, N. Sugiyama, C. Kawanishi, H. Onishi, A. Nezu, K. Kimura, Y. Yamada and K. Kosaka, 1996, "A Duplicated PLP Gene Causing Pelizaeus-Merzbacher Disease Detected by Comparative Multiplex PCR", *American Journal of Human Genetics,* Vol. 58, pp. 32-39.

Inoue, K., H. Osaka, K. Imaizumi, A. Nezu, J. Takanashi, J. Arii, K. Murayama, J. Ono, Y. Kikawa, T. Mito, L. G. Shaffer and J. R. Lupski, 1999, "Proteolipid Protein Gene Duplications Causing Pelizaeus-Merzbacher Disease: Molecular Mechanism and Phenotypic Manifestations", *Annals of Neurology*, Vol. 45, pp. 624-632.

Inoue, K., H. Tanaka, F. Scaglia, A. Araki, L. G. Shaffer and J. R. Lupski, 2001, "Compensating for Central Nervous System Dysmyelination: Females with a Proteolipid Protein Gene Duplication and Sustained Clinical Improvement", *Annals of Neurology*, Vol. 50, pp. 747-754.

Inoue, K., H. Osaka, V. C. Thurston, J. T. Clarke, A. Yoneyama, L. Rosenbarker, T. D. Bird, M. E. Hodes, L. G. Shaffer and J. R. Lupski, 2002, "Genomic Rearrangements Resulting in PLP1 Deletion Occur by Nonhomologous End Joining and Cause Different Dysmyelinating Phenotypes in Males and Females", *American Journal of Human Genetics*, Vol. 71, pp. 838-853.

Inoue, K., 2005, "PLP1-Related Inherited Dysmyelinating Disorders: Pelizaeus-Merzbacher Disease and Spastic Paraplegia Type 2", *Neurogenetics*, Vol. 1, pp. 1-16.

Kagawa, T., K. Ikenaka, Y. Inoue, S. Kuriyama, T. Tsujii, J. Nakao, K. Nakajima, J. Aruga, H. Okano and K. Mikoshiba, 1994, "Glial Cell Degeneration and Hypomyelination Caused by Overexpression of Myelin Proteolipid Protein Gene", *Neuron*, Vol. 13, pp. 427-442.

Kaufman, R. J., 1999, "Stress Signaling from the Lumen of the Endoplasmic Reticulum: Coordination of Gene Transcriptional and Translational Controls", *Genes & Development*, Vol. 13, pp. 1211-1233.

Kitagawa, K., M. P. Sinoway, C. Yang, R. M. Gould and D. R. Colman, 1993, "A Proteolipid Protein Gene Family: Expression in Sharks and Rays and Possible Evolution from an Ancestral Gene Encoding a Pore-Forming Polypeptide", *Neuron*, Vol. 11, pp. 433-448.

Klugmann, M., M. H. Schwab, A. Pulhofer, A. Schneider, F. Zimmermann, I. R. Griffiths and K. A. Nave, 1997, "Assembly of CNS Myelin in the Absence of Proteolipid Protein", *Neuron,* Vol. 18, pp. 59-70.

Kronquist, K. E., B. F. Crandall, W. B. Macklin and A. T. Campagnoni, 1987, "Expression of Myelin Proteins in the Developing Human Spinal Cord: Cloning and Sequencing of Human Proteolipid Protein cDNA", *Journal of Neuroscience Research*, Vol. 18, pp. 395-401.

Lee, J. A., K. Inoue, S. W. Cheung, C. A. Shaw, P. Stankiewicz and J. R. Lupski, 2006a, "Role of Genomic Architecture in PLP1 Duplication Causing Pelizaeus-Merzbacher Disease", *Human Molecular Genetics*, Vol. 15, pp. 2250-2265.

Lee, J. A., R. E. Madrid, K. Sperle, C. M. Ritterson, G. M. Hobson, J. Garbern, J. R. Lupski and K. Inoue, 2006b, "Spastic Paraplegia Type 2 Associated with Axonal Neuropathy and Apparent PLP1 Position Effect", *Annals of Neurology*, Vol. 59, pp. 398-403.

Lees, M. B. and O. A. Bizzozero, 1991, "Structure and Acylation of Proteolipid Protein", in R. E. Martenson (ed.), *Myelin: Biology and Chemistry*, pp. 237-255, CRC Press, Boca Raton.

Levin, M., 2002, "Isolation and Community: A Review of the Role of Gap-Junctional Communication in Embryonic Patterning", *The Journal of Membrane Biology*, Vol. 185, pp. 177-192.

Lubetzki, C., C. Demerens and B. Zalc, 1997, "Signaux Axonaux et mye´ Linogene` se Dans le Syste`me Nerveux Central", *Me´decine/Sciences,* Vol. 13, pp. 1097-1105.

Lupski, J. R., 1998, "Charcot-Marie-Tooth Disease: Lessons in Genetic Mechanisms", *Molecular Medicine*, Vol. 4, pp. 3-11.

Matsuda, Y., H. Koito and H. Yamamoto, 1997, "Induction of Myelin-Associated Glycoprotein Expression through Neuron-Oligodendrocyte Contact", *Developmental Brain Research*, Vol. 100, pp. 110-116.

Mattei, M. G., P. M. Alliel, A. Dautigny, E. Passage, D. Pham-Dinh, J. F. Mattei, and P. Jolles, 1986, "The Gene Encoding for the Major Brain Proteolipid (PLP) Maps on the q-22 band of the Human X Chromosome", *Human Genetics*, Vol. 72, pp. 352-353.

McPhilemy, K., L. S. Mitchell, I. R. Griffiths, S. Morrison, A. W. Deary, I. Sommer and P. G. E. Kennedy, 1990, "Effect of Optic Nerve Transection upon Myelin Protein Gene Expression by Oligodendrocytes: Evidence for Axonal Influences on Gene Expression", *Journal of Neurocytology*, Vol. 19, pp. 494-503.

Menichella, D. M,, D. A. Goodenough, E. Sirkowski, S. S. Scherer and D. L. Paul, 2003, "Connexins are Critical for Normal Myelination in the CNS", *The Journal of Neuroscience*, Vol. 23, pp. 5963-5973.

Merzbacher L., 1910, "Eine Eigenarige Familiar-Hereditare Erkrankungsform (Aplasia Axialis Extra-Corticalis Congenital)", *Zeitschrift für die gesamte Neurologie und Psychiatrie*, Vol. 3, pp. 1-138.

Milner, R. J., C. Lai, K. A. Nave, D. Lenoir, J. Ogata and G. Sutcliffe, 1985, "Nucleotide Sequences of Two mRNAs for Rat Brain Myelin Proteolipid Protein", *Cell*, Vol. 42, pp. 931-939.

Mimault, C., G. Giraud, V. Courtois, F. Cailloux, J. Y. Boire, B. Dastugue and O. Boespflug-Tanguy, 1999, "Proteolipoprotein Gene Analysis in 82 Patients with Sporadic Pelizaeus-Merzbacher Disease: Duplications, the Major Cause of the Disease, Originate More Frequently in Male Germ Cells, but Point Mutations do not", *American Journal of Human Genetics*, Vol. 65, pp. 360-369.

Montague, P. and I. R. Griffiths, 1997, "Molecular Biology of the Glia: Components of Myelin-PLP and Minor Myelin Proteins", in W. C. Russell (ed.), *Molecular Biology of Multiple Sclerosis*, pp. 55-69, J.Wiley & Sons, Chichester.

Morell, P., R. H. Quarles and W. T. Norton, 1994, "Myelin Formation, Structure and Biochemistry", in G. J. Siegel, B. W. Agranoff, R. W. Albers and P. B. Molinoff (eds.), *Basic Neurochemistry*, pp. 117-143, Raven, New York.

Nadon, N. L., I. D. Duncan and L. D. Hudson, 1990, "A Point Mutation in the Proteolipid Protein Gene of the Shaking Pup Interrupts Oligodendrocyte Development", *Development*, Vol. 110, pp. 529-537.

Nagy, J. I. and J. E. Rash, 2003, "Astrocyte and Oligodendrocyte Connexins of the Glial Syncytium in Relation to Astrocyte Anatomical Domains and Spatial Buffering", *Cell Communication & Adhesion*, Vol. 10, pp. 401-406.

Nagy, J. I., A. V. Ionescu, B. D. Lynn and J. E. Rash, 2003, "Coupling of Astrocyte Connexins Cx26, Cx30, Cx43 to Oligodendrocyte Cx29, Cx32, Cx47: Implications from Normal and Connexin32 Knockout Mice", *Glia*, Vol. 44, pp. 205-218.

Naismith, A. L., E. Hoffman-Chudzik, L. C. Tsui and J. R. Riordan, 1985, "Study of the Expression of Myelin Proteolipid Protein (Lipophilin) Using a Cloned Complementary DNA", *Nucleic Acids Research*, Vol. 13, pp. 7413-7425.

Nance, M. A., S. Boyadjiev, V. M. Pratt, S. Taylor, M. E. Hodes and S. R. Dlouhy, 1996, "Adult-Onset Neurodegenerative Disorder due to Proteolipid Protein Gene Mutation in the Mother of a Man with Pelizaeus-Merzbacher Disease", *Neurology*, Vol. 47, pp. 1333-1335.

Nave, K. A., C. Lai, F. E. Bloom and R. J. Milner, 1987, "Splice Site Selection in the Proteolipid Protein (PLP) Gene Transcript and Primary Structure of the DM20 Protein of Central Nervous System Myelin", *Proceedings of the National Academy of Sciences of the United States of America*, Vol. 84, pp. 5665-5669.

Nave, K. A. and G. Lemke, 1991, "Induction of the Myelin Proteolipid Protein (PLP) Gene in C6 Glioblastoma Cells: Functional Analysis of the PLP Promoter", *The Journal of Neuroscience,* Vol. 11, pp. 3060-3069.

Nishitoh, H., A. Matsuzawa, K. Tobiume, K. Saegusa, K. Takeda, K. Inoue, S. Hori, A. Kakizuka and H. Ichijo, 2002, "ASK1 is Essential for Endoplasmic Reticulum Stress-Induced Neuronal Cell Death Triggered by Expanded Polyglutamine Repeats", *Genes & Development*, Vol. 16, pp. 1345-1355.

Odermatt, B., K. Wellershaus, A. Wallraff, G. Seifert, J. Degen, C. Euwens, B. Fuss, H. Bussow, K. Schilling, C. Steinhauser and K. Willecke, 2003, "Connexin 47 (Cx47)-Deficient Mice with Enhanced Green Fluorescent Protein Reporter gene Reveal Predominant Oligodendrocytic Expression of Cx47 and Display Vacuolized Myelin in the CNS", *The Journal of Neuroscience*, Vol. 23, pp. 4549-4559.

Patil, C. and P. Walter, 2001, "Intracellular Signaling from the Endoplasmic Reticulum to the Nucleus: the Unfolded Protein Response in Yeast and Mammals", *Current Opinion in Cell Biology,* Vol. 13, pp. 349-355.

Pelizaeus, F., 1885, "Ueber Eine Eigentumliche Form Spastischer Lähmung mit Cerebralerscheinungen auf Hereditärer Grundlage (Multiple Sklerose)", *Archiv für Psychiatrie und Nervenkrankheiten*, Vol. 16, pp. 698-710.

Peters, A., 1964, "Observations on the Connections between Myelin Sheaths and Glial Cells of the Optic Nerve of Young Rats", *Journal of Anatomy,* Vol. 98, pp. 125–134.

Peters, A., S. L. Palay and H. deF. Webster (eds.), 1991, *The Fine Structure of the Nervous System: The Neuron and the Supporting Cells*, Oxford University Press, Oxford.

Pfeiffer, S. E., A. E. Warrington and R. Bansal, 1993, "The Oligodendrocyte and its Many Cellular Processes", *Trends in Cell Biology*, Vol. 3, pp. 191-197.

Pham-Dinh, D., 1998, “Les Cellules Gliales”, in D. Tritsch, D. Chesnoy-Marchais and A. Feltz (eds.), *Physiologie du Neurone*, pp. 31-90, Initiatives Sante´ Press, France.

Pribyl, T. M., C. Campagnoni, K. Kampf, V. W. Handley and A. T. Campagnoni, 1996, “The Major Myelin Protein Genes are Expressed in the Human Thymus”, *Journal of Neuroscience Research*, Vol. 45, pp. 812-819.

Raskind, W. H., C. A. Williams, L. D. Hudson and T. D. Bird, 1991, “Complete Deletion of the Proteolipid Protein Gene (PLP) in a Family with X-Linked Pelizaeus-Merzbacher Disease”, *American Journal of Human Genetics*, Vol. 49, pp. 1355-1360.

Readhead, C., A. Schneider, I. Griffiths and K. A. Nave, 1994, “Premature Arrest of Myelin Formation in Transgenic Mice with Increased Proteolipid Protein Gene Dosage”, *Neuron*, Vol. 12, pp. 583-595.

Salviati, L., E. Trevisson, M. C. Baldoin, I. Toldo, S. Sartori, M. Calderone, R. Tenconi and A. Laverda, 2007, “A Novel Deletion in the GJA12 Gene Causes Pelizaeus-Merzbacher-Like Disease”, *Neurogenetics*, Vol. 8, pp. 57-60.

Sanchez, I., L. Hassinger, P. A. Paskevich, H. D. Shine and R. A. Nixon, 1996, “Oligodendroglia Regulate the Regional Expansion of Axon Caliber and Local Accumulation of Neurofilaments during Development Independently of Myelin Formation”, *The Journal of Neuroscience,* Vol. 16, pp. 5095-5105.

Sanlaville, D., D. Genevieve, C. Bernardin, J. Amiel, C. Baumann, M. C. de Blois, V. Cormier-Daire, B. Gerard, M. Gerard, M. Le Merrer, P. Parent, F. Prieur, M. Prieur, O. Raoul, A. Toutain, A. Verloes, G. Viot, S. Romana, A. Munnich, S. Lyonnet, M. Vekemans and C. Turleau, 2005, “ Failure to Detect an 8p22-8p23.1 Duplication in Patients with Kabuki (Niikawa-Kuroki) Syndrome”, *European Journal of Human Genetics*, Vol. 13, pp. 690-693.

Saugier-Veber, P., A. Munnich, D. Bonneau, J. M. Rozet, M. Le Merrer, R. Gil and O. Boespflug-Tanguy, 1994, "X-linked Spastic Paraplegia and Pelizaeus-Merzbacher Disease are Allelic Disorders at the Proteolipid Protein Locus", *Nature Genetics*, Vol. 6, pp. 257-262.

Schindler, P., B. Luu, O. Sorokine, E. Trifilieff and A. Van Dorsselaer, 1990, "Developmental Study of Proteolipids in Bovine Brain: A Novel Proteolipid and DM-20 Appear before Proteolipid Protein (PLP) during Myelination", *Journal of Neurochemistry*, Vol. 55, pp. 2079-2085.

Schneider, A., P. Montague, I. R. Griffiths, M. L. Fanarraga, P. G. E. Kennedy, P. J. Brophy and K. A. Nave, 1992, "Uncoupling of Hypomyelination and Glial Cell Death by a Mutation in the Proteolipid Protein Gene", *Nature*, Vol. 358, pp. 758-761.

Schneider, A., H. Lander, G. Schulz, H. Wolburg, K. A. Nave, J. B. Schulz and M. Simons, 2005, "Palmitoylation is a Sorting Determinant for Transport to the Myelin Membrane", *Journal of Cell Science*, Vol. 118, pp. 2415-2423.

Seitelberger, F., 1970, "Pelizaeus-Merzbacher Disease", in P. Vinken and G. Bruyn (eds.), *Handbook of Clinical Neurology. Leucodystrophies and Poliodystrophies*, pp. 150-202, North-Holland Publishing Company, Amsterdam.

Seitelberger, F., 1995, "Neuropathology and Genetics of Pelizaeus-Merzbacher Disease", *Brain Pathology*, Vol. 5, pp. 267-273.

Shy, M. E., G. Hobson, M. Jain, O. Boespflug-Tanguy, J. Garbern, K. Sperle, W. Li, A. Gow, D. Rodriguez, E. Bertini, P. Mancias, K. Krajewski, R. Lewis and J. Kamholz, 2003, "Schwann Cell Expression of PLP1 but not DM 20 is Necessary to Prevent Neuropathy", *Annals of Neurology*, Vol. 53, pp. 354-365.

Simons, M., E. M. Kramer, C. Thiele, W. Stoffel and J. Trotter, 2000, "Assembly of Myelin by Association of Proteolipid Protein with Cholesterol- and

Galactosylceramide-Rich Membrane Domains", *The Journal of Cell Biology*, Vol. 151, pp. 143-154.

Simons, M., E. M. Kramer, P. Macchi, S. Rathke-Hartlieb, J. Trotter, K. A. Nave and J. B. Schulz, 2002, "Overexpression of the Myelin Proteolipid Protein in Endosomes/Lysosomes: Implications for Pelizaeus-Merzbacher Disease", *The Journal of Cell Biology*, Vol. 157, pp. 327-336.

Sistermans, E. A., I. J. de Wijs, R. F. de Coo, L. M. Smit, F. H. Menko and B. A. van Oost, 1996, "A (G-to-A) Mutation in the Initiation Codon of the Proteolipid Protein Gene Causing a Relatively Mild form of Pelizaeus-Merzbacher Disease in a Dutch Family", *Human Genetics*, Vol. 97, pp. 337-339.

Sivakumar, K., N. Sambuughin, B. Selenge, J. W. Nagle, D. Baasanjav, L. D. Hudson and L. G. Goldfarb, 1999, "Novel Exon 3B Proteolipid Protein Gene Mutation Causing Late-Onset Spastic Paraplegia Type 2 with Variable Penetrance in Female Family Members", *Annals of Neurology*, Vol. 45, pp. 60-683.

Skalidis, G., E. Trifilieff and B. Luu, 1986, "Selective Extraction of the DM-20 Brain Proteolipid", *Journal of Neurochemistry*, Vol. 46, pp. 297-299.

Söhl, G., S. Maxeiner and K. Willecke, 2005, "Expression and Functions of Neuronal Gap Junctions", *Nature Reviews Neuroscience*, Vol. 6, pp. 191-200.

Sorg, B. A., M. M. Smith and A. T. Campagnoni, 1987, "Developmental Expression of the Myelin Proteolipid Protein and Basic Protein mRNAs in Normal and Dysmyelinating Mutant Mice", *Journal of Neurochemistry*, Vol. 49, pp. 1146-1154.

Spörkel, O., T. Uschkureit, H. Büssow and W. Stoffel, 2002, "Oligodendrocytes Expressing Exclusively the DM20 Isoform of the Proteolipid Protein Gene: Myelination and Development", *Glia*, Vol. 37, pp. 19-30.

Stecca, B., C. M. Southwood, A. Gragerov, K. A. Kelley, V. L. Friedrich and A. Gow, 2000, "The Evolution of Lipophilin Genes from Invertebrates to Tetrapods: DM-20 cannot Replace Proteolipid Protein in CNS Myelin", *The Journal of Neuroscience*, Vol. 20, pp. 4002-4010.

Southwood, C. and A. Gow, 2001, "Molecular Pathways of Oligodendrocyte Apoptosis Revealed by Mutations in the Proteolipid Protein Gene", *Microscopy Research and Technique*, Vol. 52, pp. 700-708.

Southwood, C., M., J. Garbern, W. Jiang and A. Gow, 2002, "The Unfolded Protein Response Modulates Disease Severity in Pelizaeus-Merzbacher Disease", *Neuron,* Vol. 36, pp. 585-596.

Swanton, E., S. High and P. Woodman, 2003, "Role of Calnexin in the Glycan-Independent Quality Control of Proteolipid Protein", *EMBO Journal*, Vol. 22, pp. 2948-2958.

Takashima, H., M. Nakagawa, F. Umehara, K. Hirata, M. Suehara, H. Mayumi, K. Yoshishige, W. Matsuyama, M. Saito, M. Jonosono, K. Arimura and M. Osame, 2003, "Gap Junction Protein Beta 1 (GJB1) Mutations and Central Nervous System Symptoms in X-Linked Charcot-Marie-Tooth Disease", *Acta Neurologica Scandinavica*, Vol. 107, pp. 31-37.

Timsit, S. G., L. Bally-Cuif, D. R. Colman and B. Zalc, 1992, "DM-20 mRNA is Expressed during the Embryonic Development of the Nervous System of the Mouse", *Journal of Neurochemistry*, Vol. 58, pp. 1172-1175.

Timsit, S., S. Martinez, B. Allinquant, F. Peyron, L. Puelles and B. Zalc, 1995, "Oligodendrocytes Originate in a Restricted Zone of the Embryonic Ventral Neural Tube Defined by DM-20 mRNA Expression", *The Journal of Neuroscience*, Vol. 15, pp. 1012-1024.

Tosic, M., M. Dolivo, K. Domanska-Janik and J. M. Matthieu, 1994, "Paralytic Tremor (pt): A New Allele of the Proteolipid Protein Gene in Rabbits", *Journal of Neurochemistry*, Vol. 63, pp. 2210-2216.

Uhlenberg, B., M. Schuelke, F. Rüschendorf, N. Ruf, A. M. Kaindl, M. Henneke, H. Thiele, G. Stoltenburg-Didinger, F. Aksu, H. Topaloğlu, P. Nürnberg, C. Hübner, B. Weschke and J. Gärtner, 2004, "Mutations in the Gene Encoding Gap Junction Protein Alpha 12 (Connexin 46.6) Cause Pelizaeus-Merzbacher-Like Disease", *American Journal of Human Genetics*, Vol. 75, pp. 251-260.

Urano, F., X. Wang, A. Bertolotti, Y. Zhang, P. Chung, H. P. Harding and D. Ron, 2000, "Coupling of Stress in the ER to Activation of JNK Protein Kinases by Transmembrane Protein Kinase IRE1", *Science*, Vol. 287, pp. 664-666.

Weimbs, T. and W. Stoffel, 1992, "Proteolipd Protein (PLP) of CNS Myelin: Positions of Free, Disulfide-Bonded, and Fatty Acid Thioester-linked Cysteine Residues and Implications for the Membrane Topology of PLP", *Biochemistry*, Vol. 31, pp. 12289-12296.

Wight, P. A. and A. Dobretsova, 1997, "The First Intron of the Myelin Proteolipid Protein Gene Confers Cell Type-specific Expression by a Transcriptional Repression Mechanism in Non-Expressing Cell Types", *Gene*, Vol. 201, pp. 111-117.

Wight, P. A., A. Dobretsova and W. B. Macklin, 1997, "Regulation of Murine Myelin Proteolipid Protein Gene Expression", *Journal of Neuroscience Research*, Vol. 50, pp. 917-927.

Willard, H. F. and J. R. Riordan, 1985, "Assignment of the Gene for Myelin Proteolipid Protein to the X Chromosome: Implications for X-linked Myelin Disorders", *Science*, Vol. 230, pp. 940-942.

Willecke, K., J. Eiberger, J. Degen, D. Eckardt, A. Romualdi, M. Güldenagel, U. Deutsch and G. Söhl, 2002, "Structural and Functional Diversity of Connexin Genes in the Mouse and Human Genome", *Biological Chemistry*, Vol. 383, pp. 725-737.

Woodward, K., E. Kendall, D. Vetrie and S. Malcolm, 1998, "Pelizaeus-Merzbacher Disease: Identification of Xq22 Proteolipid Protein Duplications and Characterization of Breakpoints by Interphase FISH", *American Journal of Human Genetics*, Vol. 63, pp. 207-217.

Woodward, K., and S. Malcolm, 1999, "Proteolipid Protein Gene Pelizaeus-Merzbacher Disease in Humans and Neurodegeneration in Mice", *Trends in Genetics*, Vol. 15, pp. 125-128.

Woodward, K., K. Kirtland, S. Dloughy, W. Raskind, T. Bird, S. Malcolm and D. Abeliovich, 2000, "X-inactivation in Carriers of Pelizaeus-Merzbacher Disease: Skewed in Carriers of a Duplication and Random in Carriers of Point Mutation", *European Journal of Human Genetics*, Vol. 8, pp. 449-454.

Woodward and Malcolm, 2001; "CNS Myelination and PLP Gene Dosage", *Pharmacogenomics*, Vol. 2, pp. 263-72.

Woodward, K., M. Cundall, R. Palmer, R. Surtees, R. M. Winter and S. Malcolm, 2003, "Complex Chromosomal Rearrangement and Associated Counseling Issues in a Family with Pelizaeus-Merzbacher Disease", *American Journal of Medical Genetics*, Vol. 118, pp. 15-24.

Ye, J., R. B. Rawson, R. Komuro, X. Chen, U. P. Davé, R. Prywes, M. S. Brown and J. L. Goldstein, 2000, "ER Stress Induces Cleavage of Membrane-Bound ATF6 by the Same Proteases that Process SREBPs", *Molecular Cell*, Vol. 6, pp. 1355-1364.

Yamaguchi, Y., K. Ikenaka, M. Niinobe, H. Yamada and K. Mikoshiba, 1996, "Myelin Proteolipid Protein (PLP), but not DM-20, is an Inositol Hexakisphosphate-Binding Protein", *The Journal of Biological Chemistry*, Vol. 271, pp. 27838-27846.

Yoneda, T., K. Imaizumi, K. Oono, D. Yui, F. Gomi, T. Katayama and M. Tohyama, 2001, "Activation of Caspase-12, an Endoplastic Reticulum (ER) Resident Caspase, through Tumor Necrosis Factor Receptor-Associated Factor 2-Dependent Mechanism in Response to the ER Stress", *The Journal of Biological Chemistry*, Vol. 276, pp. 13935-13940.

Yool, D. A., J. M. Edgar, P. Montague and S. Malcolm, S., 2000, "The Proteolipid Protein Gene and Myelin Disorders in Man and Animal Models", *Human Molecular Genetics*, Vol. 9, pp. 987-992.

Yoshida, H., K. Haze, H. Yanagi, T. Yura and K. Mori, 1998, "Identification of the Cis-Acting Endoplasmic Reticulum Stress Response Element Responsible for Transcriptional Induction of Mammalian Glucose-Regulated Pproteins. Involvement of Basic Leucine Zipper Transcription Factors", *The Journal of Biological Chemistry*, Vol. 273, pp. 33741-33749.

Yoshida, H., T. Matsui, A. Yamamoto, T. Okada and K. Mori, 2001, "XBP1 mRNA is Induced by ATF6 and Spliced by IRE1 in Response to ER Stress to Produce a Highly Active Transcription Factor", *Cell*, Vol. 107, pp. 881-891.

Zeman, W., W. Demyer and H. F. Falls, 1964, "Pelizaeus- Merzbacher Disease: A study in Nosology", *Journal of Neuropathology and Experimental Neurology*, Vol. 23, pp. 334-354.

Ziereisen, F., B. Dan, F. Christiaens, P. Deltenre, R. Boutemy and C. Christophe, 2000, "Connatal Pelizaeus-Merzbacher Disease in two Girls", *Pediatric Radiology*, Vol. 30, pp. 435-438.